Mathematical Modeling, Numerical Simulation and Multi-Objective Optimization of Fused Deposition Modeling (FDM)

THESIS

Submitted in partial fulfilment

of the requirements for the degree of

DOCTOR OF PHILOSOPHY

by

PAVAN KUMAR G

(ID No. 2009PHXF447H)

Under the Supervision of

Prof. Srinivasa Prakash Regalla

BITS Pilani

Pilani | Dubai | Goa | Hyderabad

BIRLA INSTITUTE OF TECHNOLOGY AND SCIENCE, PILANI

2015

Mathematical Modeling, Numerical Simulation and Multi-Objective Optimization of Fused Deposition Modeling (FDM)

THESIS

Submitted in partial fulfilment

of the requirements for the degree of

DOCTOR OF PHILOSOPHY

by

PAVAN KUMAR G

(ID No. 2009PHXF447H)

Under the Supervision of

Prof. Srinivasa Prakash Regalla

BITS Pilani

Pilani | Dubai | Goa | Hyderabad

BIRLA INSTITUTE OF TECHNOLOGY AND SCIENCE, PILANI

2015

BIRLA INSTITUTE OF TECHNOLOGY AND SCIENCE, PILANI

CERTIFICATE

This is to certify that the thesis entitled **"Mathematical Modeling, Numerical Simulation and Multi-Objective Optimization of Fused Deposition Modeling (FDM)"** and submitted by **Pavan Kumar G** ID No 2009PHXF447H, for award of Ph.D. of the Institute embodies original work done by him under my supervision.

Prof. SRINIVASA PRAKASH REGALLA

Professor

Department of Mechanical Engineering,

BITS-Pilani, Hyderabad Campus,

Shameerpet Mandal, Ranga Reddy District,

Hyderabad- 500078, Andhra Pradesh

Date:

Dedicated to my beloved Parents

Acknowledgements

Accomplishment of this doctoral thesis was not possible without the support of several people directly and indirectly. It's my honor to express my sincere gratitude to all them. First of all, I am extremely grateful to my guide, Prof. Srinivasa Prakash Regalla, for his invaluable guidance and scholarly inputs consistently throughout the thesis. To put in short, I would have never imagined to have done my Ph.D. without him as a guide.

I am thankful to Prof. B. N. Jain, Vice-Chancellor, Prof. V. S. Rao, Director, BITS-Pilani, Hyderabad Campus for providing me this opportunity to pursue the on-campus Ph.D. of this institute.

I thank my doctoral advising committee members, Prof. Y. V. Daseswara Rao, HOD (Department of Mechanical Engineering) and Prof. M. Srinivas for providing suggestions during the entire thesis and sparing their valuable time in providing useful comments for my draft thesis.

Dr. S. D. Deshmukh (Associate Dean, SWD) and Dr. K. Pranav Narayan (Chief Warden) have always shown their compassion on me as a warden, without their support, it would have been tough time handling the hostel activities along with the thesis work. Thanks to them for all that cordial relationship. Special mention of my sincere gratitude to Dr. Anupam Bhattacharya and Dr. G. Ramakrishnan of department of Chemistry and Dr. Purnima of Chemical Engineering department for enriching my knowledge in polymer chemistry. Words feel short to thank Dr. A. Ramesh Babu, department of Chemical Engineering, for all his pieces of

advice and his timely help in facilitating some of the core research journal publications. Special mention of Prof. Sethuramaiah for all his kind advice in the field of tribology.

It's my pleasure to thank the department faculty colleagues and the workshop team with a special mention of Prof. Amit Kumar Gupta for key inputs in the area of multi-objective optimization and Prof. N. S. K. Reddy in allowing me to use the tribology lab in carrying out the experiments. I would be grateful to Dr. K. Venkata Ratnam, Dr. Jalaiah and Dr. C. P. Kiran for encouraging me in bringing out this thesis effectively in LaTeX.

My thesis wouldn't have come so effectively if I fall short mentioning the contributions of Mr. K. Suresh, Mr. K. Nitin and Mr. S. M. Hussaini, who stood with me during tough times with all their valuable and encouraging words.

I extend my thanks to our lab technicians Mr. Srinivas, of materials testing lab for helping me in conducting the experiments, Mr. Suryanarayana of CPDR lab for manufacturing the specimens in uPrint machine and Mr. Jagadeshwar Reddy for conducting wear tests in tribology lab. Thanks are also due to all my colleagues at BITS Pilani, Hyderabad Campus, for their whole hearted support and cooperation during the course of this work.

Last but not the least, my wife Suneetha and my sons Dakshesh and Badrinath for all their sacrifices, understanding and active cooperation throughout the course of my doctoral thesis enabling me to spend my time efficiently.

Pavan Kumar G

Abstract

Additive manufacturing (AM) technologies enables the manufacturing of parts or products directly from 3D CAD models. In distinction to the traditional methods of manufacturing where in the raw material is fabricated to the final product based on subtractive principles, these AM processes are based on additive principle for the part manufacturing. As the name implies, different AM processes use different methodologies of adding up the material to form the final product. Advantages like manufacturing complex geometries, zero tooling along with no human intervention, manufacturing in single set-up etc., are few of them. During the last decade, AM has attracted huge attention in various industries ranging from manufacturing, medical, automotive concept development etc., in developing products to meet the expectations of both the designers as well as manufacturers. Fused deposition modeling (FDM) is one among those most popular AM technologies where in the filaments are added one beside other forming a layer, and then layer upon layer to build the final product. Besides the simplicity of operation like ability to fabricate parts with locally controlled properties with varied materials, FDM has resulted in manufacturing parts not only for prototyping but also functional parts. Besides the merits of using FDM process, it faces challenges related to strength, dimensional accuracy, surface finish etc. With this motivation, it is mandatory to first understand the challenges that the process faces, identify the root cause, analyze and attempt to address the shortcomings so as to improve the part quality.

The aim of this thesis is to understand the part evolution due to neck formation between the adjacent cylindrical filaments in FDM machine. Strength contributed by the neck growth due to different orientations of the material deposition have been estimated and validated. The investigation has been extended in studying volumetric shrinkage as affected by different orientations along with material build as process parameter. Based on the responses of the process parameters, a multi-objective problem has been solved in arriving at an optimal parameter solution set that could maximize strength and minimize volumetric shrinkage. The study of mechanical properties has been extended to understand the effect of process parameters on tribological properties like wear and coefficient of friction.

A mathematical modeling technique was adopted using the principles of sintering operation. This generic mathematical model is then validated using the neck formation through FEM on filaments with ABS properties using the Generalized Maxwell's of viscoelastcity and Anand's model of viscoplasticity. The theoretical strength as obtained from the mathematical model as contributed due to the neck growth has been validated by conducting experiments on specimens manufactured using FDM process. Different orientations were experimented to find the variation in neck formation between the filaments and hence its contribution to strength. Also in order to understand the effect of various process parameters on other mechanical properties, statistical techniques like design of experiments, ANOVA and response surface methodology were used to arrive at the critical parameters. Based on the ANOVA results and the critical parameters, a multi-objective problem, namely maximization of strength and minimization of volumetric shrinkage, has been formulated and solved for optimal solutions. Pareto's plot has been obtained that arrives at the optimal set of the process parameters. Parametric study using statistical techniques has been extended to study the wear rate and friction of the parts produced by FDM. Process parameters like load, sliding speed in a standard pin-on-disc set up and orientation of the part build direction using FDM

process were considered for the study. ANOVA and response surface methodology were used to understand the effect of process parameters on the selected responses. Based on the mathematical modeling it was learnt that the neck formation between the filaments is a very important factor in determining various properties. Through experimental study and statistical analysis, it was established that the mechanical properties of the part manufactured through FDM process is greatly affected by various process parameters. Based on the study it was found that part orientation plays a very important role in all the properties chosen for the study. It has been established that as angle of deposition of material along the contour in the vertical direction increases strength but the volumetric shrinkage also increases. It has also been observed that specimen manufactured at low orientation, along with high load and high operating speed results in crack formation in the specimen. Friction is the less at the lowest load either at low or high orientation in the vertical plane but the friction increases at high load with lowest orientation. It has also been established that optimum value of orientation will yield in uniform wear rate without any crack formation in the part.

From the present work, the following key conclusions can be concluded:

1. In FDM process, the time required for the two adjacent cylindrical filaments for finally coalescing completely into one single filament is not available before complete solidification and cooling to the chamber temperature occurs. Hence it can be concluded that not every pair of adjacent filaments builds the same size of the neck. In fact, some of the pairs of filaments may not build any necks at all.

2. The neck formation results in increase in strength as well as change in dimensions. From the SEM micro-graphs, it is clear that the cylindrical filaments convert into elliptical cross-section filaments after solidification.

3. From the experimental study, it can be concluded that the specimen loaded

in the building direction fractured similar to brittle fracture as in metals whereas the failure of the specimen loaded in the transverse direction, the fracture occurred over the plane at an angle roughly equal to 45^0 to the loading direction.

4. From the experimental studies, it can also be concluded that the process parameters bear a conflicting relation with the responses chosen namely strength and volumetric shrinkage.

5. From the Pareto's plot, it can be concluded that the best possible strength that can be obtained using any of the combinations is found to be 35.83 MPa. Also any improvement in the shrinkage cannot be obtained beyond 0.77 %.

6. From the tribological studies, it can be concluded that cracks are formed in the specimens when the specimens are tested at high load, high speed and low orientation angle of the part during its manufacture using FDM process.

7. For uniform wear, the layers are to be deposited vertical to the build platform of the FDM system so that the intra-layer takes the maximum load.

Contents

List of Figures

List of Tables

Chapter 1

Introduction

1.1 Introduction

The early days of industrial manufacturing following the industrial revolution saw manual prototyping, wherein the paper drawings of the products would be sent to the shop floor for a skilled machinist to make the prototype. In general the machinist used to spend several weeks of machining and allied manufacturing processes time in the realization of the final prototype. With the advent of Computer Aided Design (CAD) and the usage of computers during the early 1980's, virtual prototyping came into existence. This resulted in the birth of a new generation of manufacturing where in, a part is manufactured by reading the features of the part from a three dimensional (3D) CAD model (Chua et al. [19]). Part is manufactured by adding layer upon layer until the final part has been manufactured. This method of part generation requires no tools, fixtures, dies and more importantly does not require process planning unlike any traditional machining or manufacturing process. Such an additively generated part process uses limited time when compared to traditional method of manufacturing and creates physical prototypes directly from digital data and hence, it is termed as 'Rapid Prototyping (RP)'. From the product development context, RP term was used to define

technologies. Later, with the introduction of technology and exhaustive use of RP technology, the users have come to realize that 'Rapid Prototyping' is inadequate and does not effectively describe the latest applications of the technology. It has been realized that with the improvements in the quality of the RP products have meant that there is a much closer relation to the final product. At present, many of the RP parts are in fact directly used as end products, necessitating to rethink of the term prototyping (Zeng et al. [108], Choi and Cheung [17]). A common feature among all the RP technologies being the addition of material to manufacture the part, it lead to re-coining and standardizing of a new term for the processes, 'Additive Manufacturing (AM)' by American Society for Testing of Materials (ASTM).

1.2 Additive Manufacturing (AM)

Additive manufacturing unlike the traditional manufacturing involves manufacturing of parts by adding the raw material layer by layer. Different AM technologies have been invented, the most popular of which are stereo-lithography (STL), fused deposition modeling (FDM), selective laser sintering (SLS), layered object manufacturing (LOM), Three Dimensional Printing (3-DP) (Pham and Dimov [67], Santos et al. [80], Oxman [62], Munguía et al. [58]).

Irrespective of the type of AM technology, in general, any AM technology involves the same basic steps, from the virtual CAD description to the physical part. These steps are followed for the product that is realized during the early stages of the product development process as during this stage the part may require only rough estimate. At later stages of the process, parts may require post-processing (like sanding, surface preparation and painting etc.,) before they are used (Noorani [60], Regalla [72], Kruth et al. [44]). The following steps describe the end to end process of part manufacture using any of these technologies.

I Modeling and conversion to STL: Parts manufactured through AM technologies must first be modelled in any of the 3D CAD solid modeling software packages. The objective of solid modeling is to ensure that the model geometry is fully described including the external features. Apart from the solid modeling software, any reverse engineering equipment (e.g., laser scanning) can also be used to model the 3D parts. Almost all the AM machines accept the 3D models in a stereo-lithography (STL) file format. Once the sliced 3D solid models have been generated, the file format of the part should be in the STL format. STL file describes the external closed surfaces of the original CAD model and forms the basis for calculation of the slices.

II File transfer to AM machine and machine set-up: The STL file describing the part is now transferred to the AM machine that reads the information of the sliced 3D solid model. General machine specific settings are performed so as to correct the size, position with respect to the build orientation, amount of material to be filled, energy source, thickness of the layer, timings etc., which is specific to the machine set-up.

III Building the part: Building the part in any of the AM machine is almost an automatic process, involving formation of the successive layers. For instance in LOM, the two successive adhesive-coated laminates are glued together and then cut to shape with a knife or with the help of laser cutter. While in SLS, a laser acts as the power source to sinter a bed of powdered material. The laser thus follows the path of the points in space defined by a 3D model, binding the material together to create a solid structure. Finally in FDM, successive filaments of the semi molten material deposits one beside the other to form a layer and once the layer is completed, the next layer is deposited following the pattern set by the sliced 3D model.

IV Part removal and post-processing: As soon as the part manufacturing is

completed, the part is removed and based on the type of AM process, the part is treated and/or cleaned to remove any additional material and/or support material is present. After this the part has reached its final stage where in additional post-processing techniques like sandblasting, painting or coating may be performed based on the requirement and the part is then put to the intended use (Gibson et al. [32]).

Figure 1.1 shows the different types of AM technologies, classified based on the type of bonding present predominantly in respective technologies (Kulkarni et al. [46]).

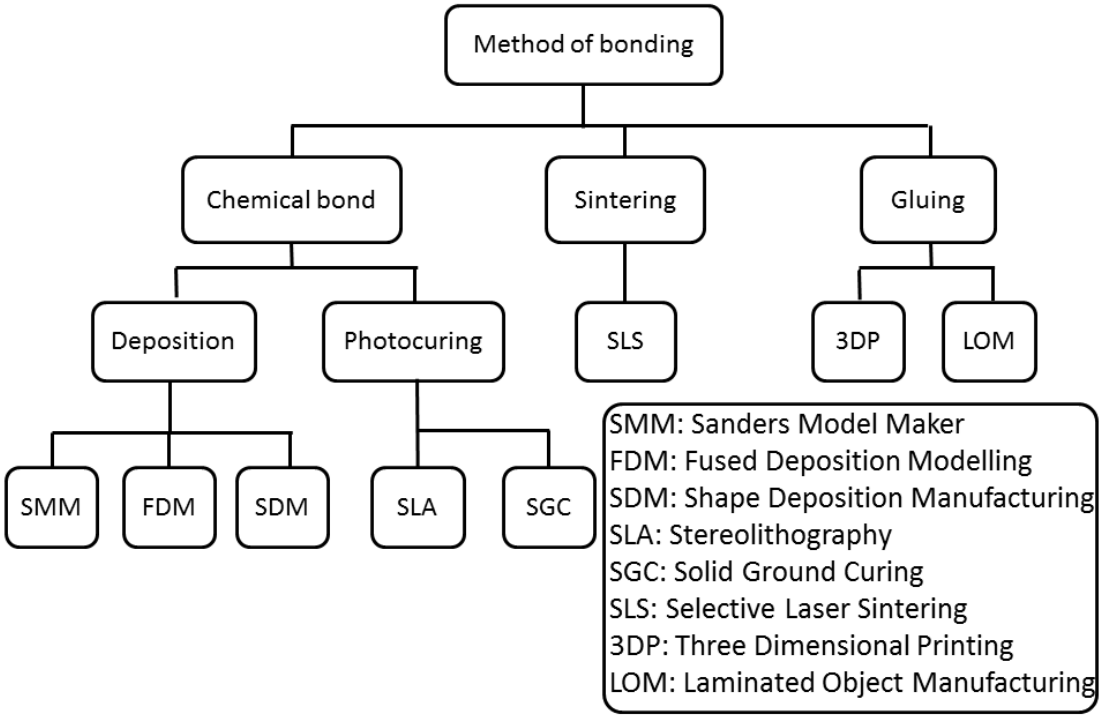

Fig. 1.1 Classification of AM technologies based on method of bonding

1.3 Fused Deposition Modeling

Among various AM process, the present thesis highlights the use of Fused Deposition Modeling (FDM) process, which is widely used in the area of AM

technology due to various advantages. FDM is owned by Stratasys™, Minnesota, USA. FDM uses Acrylonitrile Butadiene Styrene (ABS), a thermoplastic polymer, and many of its variants as the raw material to build the parts. A 3D solid model created in any of the CAD modeling software, saved in the STL format, is imported into the FDM's Insight™ software. The software generates the process plan and controls the FDM machine's hardware. The hardware for the FDM machine is represented in Figiure 1.2. The schematic consists of the model material i.e., ABS and the support material in the form of the spools. The material is fed through an extruder head, which heats the materials to the desired temperature. This semi molten heated filament is then fed through a nozzle and is deposited on to the partially constructed part. As the material is extruded in a semi-molten state, the newly deposited material fuses with adjacent material that has already been deposited. The extruder head then moves around in the x–y plane whose motion is restricted to the geometry of the slice. The extruder head also carries support material that is used whenever the part needs to support the build material. The extruder head deposits the support material through another nozzle which is adjacent to the model material nozzle. The platform holding the part then moves vertically downwards in the z-direction to begin depositing the next and a new layer on top of the previous one. After a period of time, the head will have deposited a full physical representation of the original 3D CAD model. The cooled model is then cured by treating with solvents to remove the support material.

One of the advantages of FDM machine is the ease with which the support material can be identified and removed. The support material is typically a different color than the build material so that they can be visually differentiated. Water-soluble support materials have become commercially available for very easy removal. FDM can also deposit ceramic powders mixed with a binder although an extrusion head capable of higher pressures may be necessary (Vaidyanathan

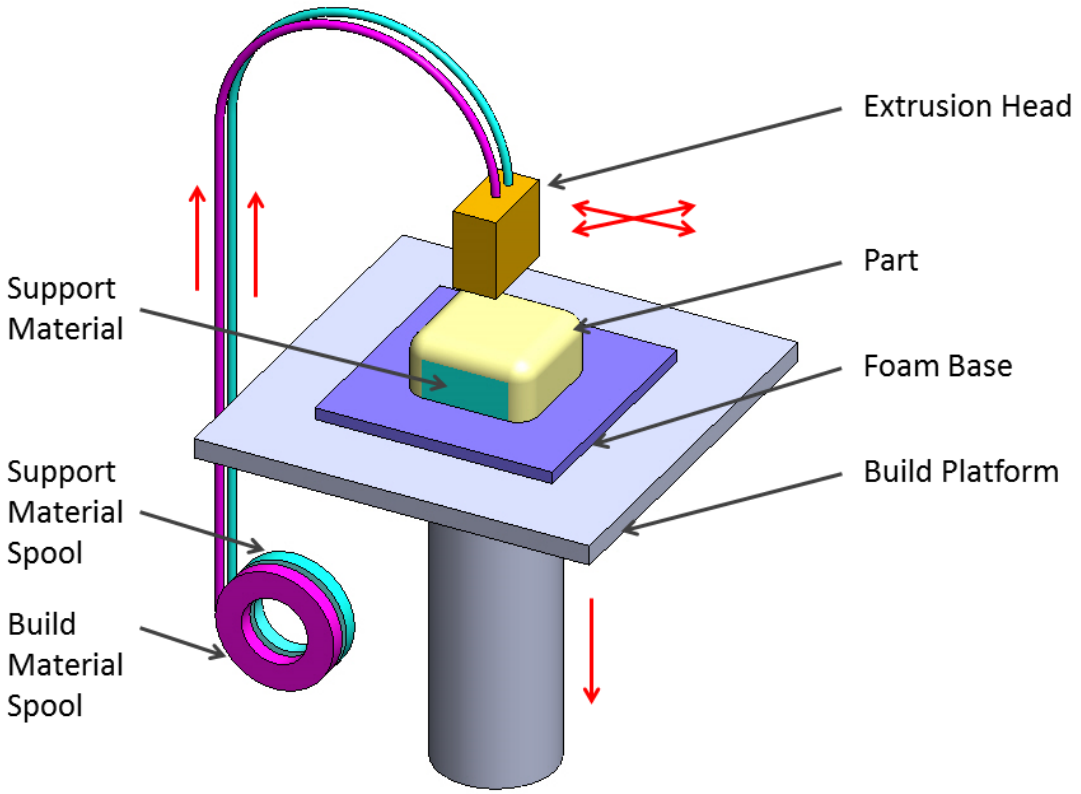

Fig. 1.2 Schematic of FDM process

et al. [101]). Metal parts can be fabricated using a metal/polymer composite as a filament. It is even possible to build metal/polymer composite tooling on a FDM system using an appropriate polymer matrix (Masood and Song [54]). FDM process has grown to become very popular due to its low cost, long lasting dimensional stability, wide range of materials, and safety. Out of all the commercially available rapid prototyping technologies, FDM process is one among the AM technologies, which does not involve hazardous fumes, carcinogenic chemicals, or messy powders. This has led to FDM process being accepted as an "office friendly 3-D printer" that can be located in the same location as the designers who use it. FDM machines are widely used as a tool in rapid investment casting (Kumar et al. [47],Chhabra and Singh [15], Singh [81], Singh [82]).

1.4 Need for the Study

Parts manufactured by FDM process are found to increase not only in the area of rapid prototyping but also as final products. Apart from products of commercial products, the end products are also used in many of the biological and biomedical applications (Pereira et al. [65],Liu et al. [53]). Manufacturing of complex parts, ease of product visualization, cost effective, time efficient manufacturing, inexpensive tools, etc., are few of those prime advantages of AM machines. Amid many advantages of AM technologies over the traditional manufacturing, with the increasing demand from the industrial and customer needs, still challenges are being faced right from the concept generation through design and manufacturing stages Brajlih et al. [12]. Among many such challenges, the following are a few of these challenges that need immediate attention (Onuh and Yusuf [61], Tromans [100], Bellini et al. [11], Lan [48], Yan et al. [107],Rochus et al. [74], Reddy et al. [71], Sreenathbabu and Karunakaran [91], Karunakaran et al. [40]).

1. As the manufactured parts are used as direct end products, based on the need of the application, a better understanding is required from the basic physics that determine the desired properties. The properties can be like strength, surface roughness, part shrinkage etc.

2. Rapid tooling and rapid casting are the prime areas FDM processed parts are extensively used in industrial applications. A very good dimensional stability of the part produced enhances the designers to release the part drawing in shorter period of time. Hence the need of the hour is better reliability and excellent accuracy.

3. With the growing need to satisfy one or more functionalities of a given product, many industrial applications require multiple functionalities/objectives to be satisfied for prototypes as well as and in final product. Hence there is

a need for multi-objective optimization for the parts to be produced.

4. Most of the AM technologies employ polymers as their raw material to manufacture the part. The materials database is limited due to many reasons like working temperature of the polymers is low, handling of polymers are comparatively easy etc. There is need for the technology to be evolved to take different types of materials that are suitable for various areas like commercial products, biological implants industrial products which also includes metals.

5. Most importantly, the AM technologies need to focus more on manufacturing products with good reliability as compared to conventional manufacturing processes.

1.5 Objectives of the Study

Parts manufactured using FDM process, like any other AM machine, display varied properties. As any other evolving technology constitutes merits and shortcomings, it is important to primarily overcome the limitations by establishing a better understanding of the process and its related process parameters that affect them. In this pursuit, the next chapter (Chapter 2) highlights the ongoing research in the area of AM and FDM process in particular that is required for current needs. In this direction, the present work attempts in understanding, analyzing and providing amicable solutions, when incorporated, make the FDM process a reliable and predictable like any other manufacturing processes.
Based on the above set benchmarks, the objectives of the current research work are highlighted as follows:

1. Filaments are the basic unit of FDM processed part. The attributes of the part manufactured are dependent of how these filaments are held together.

As the first objective, an attempt will be made to mimic the evolution of the part right from the neck growth both mathematically and through finite element simulation. Once the evolution of neck growth has been observed, the strength of the part produced will be investigated experimentally.

2. A finite element simulation of the neck growth will be attempted to understand the viscoelasticity and viscoplasticity behaviour of ABS material at elevated temperature. This preliminary investigation will be helpful in understanding the complexity of neck and bond formation between the filaments of FDM manufactured parts.

3. Since strength in the form of bulk strength and surface strength are the key design criteria towards product development a thorough analysis using robust experimental techniques like design of experiments (DOE), ANOVA and RSM shall be attempted to highlight the key process parameters that influence the properties like strength, friction and wear rate. Detailed experiments will be conducted, tested for their responses and analyzed for their parametric dependency.

4. A detailed parametric interdependence will be studied on strength and volumetric shrinkage. The process parameters affecting the two responses are investigated by conducting experiments and will be solved to optimize these objectives using RSM.

5. In order to arrive at an optimal solution set for the chosen multiple responses, a multi-objective problem will be formulated and solved using a genetic algorithm tool. Finally the optimum parameter settings in achieving a multi-objective optimization problem will be validated.

1.6 Organization of the Thesis

The present research work is presented in seven chapters as follows:

Chapter – 1: In this chapter the rationale and structure of the thesis is presented. The chapter highlights the functionality of the FDM machine along with the need for the study the process parameters. The objectives of the proposed research have been set that will be covered in the present thesis. Finally the organization and the methodology adopted in the thesis have been highlighted.

Chapter – 2: In this chapter, survey of the literature on the AM technologies in general and FDM process in particular is done in detail. The literature study starts with details of mathematical modeling and sintering operation. Later, the mechanical properties namely strength, wear rate, friction and volumetric shrinkage have been discussed in detail that are much prevalent for the current thesis. Various optimization studies along with the multi-objective optimization are detailed. Based on the literature study, the chapter concludes highlighting the research gaps that are being taken forward in the successive chapters.

Chapter – 3: In this chapter, the FDM process along with the specifications of the material used has been mentioned. In this chapter a detailed discussion on the experimental design technique that is followed in the entire thesis has been elaborated. More importantly, the manufacturing plan of the ABS polymer test specimens used for the experimental study in the present work has been explained. Test specimen preparations to estimate each of the quality responses have been discussed. Key measurement techniques involved in estimating the quality characteristics like strength, volumetric shrinkage and the tribological properties like wear rate and friction have been documented which are later used in chapters 4, 5 and 6.

Chapter – 4: In this chapter, a mathematical model for neck growth between cylindrical filaments is derived from the underlying physics of sintering operation.

Finite element simulation has been done to estimate the neck growth between the filaments using the viscoelastic and visoplasticity material models. The neck evolved from the mathematical study has been compared with that obtained from the finite element based simulation. Later, contribution of bonding between the filaments to the strength of the parts is studied. Theoretical and experimental ultimate tensile load are determined and the consequence of the strength of the parts are detailed.

Chapter – 5: In this chapter, based on the observations from the earlier chapter, strength and volumetric shrinkage have been selected for the study. FDM process setting parameters like the build interior, the horizontal build direction and the vertical build have been considered for the study of their dependency on strength and volumetric shrinkage has been attempted. Based on the observations, the multiple objectives are optimized simultaneously using a genetic algorithm. Pareto optimal solution set is obtained. The best possible strength and volumetric shrinkage has been interpreted which helps for better selection of limits for the process parameters.

Chapter – 6: In this chapter, the study has been extended to parametric study of surface strength properties of FDM processed parts. For this tribological studies are performed using Pin-on-Disc (PoD) machine. For the current study two of the PoD parameters along with one FDM process parameter are considered to understand their effect on wear rate and friction. The responses are plotted as surfaces in terms of the process parameters and their interaction effects. FDM process parameter is found to be one among the most effecting parameters and guidelines are stated for the optimum parameter settings that could result in decreased wear rate and friction.

Chapter – 7: Finally this chapter concludes providing the summary and specific contributions of the current study. Further, future scope has also been presented.

The next chapter presents the survey of literature on major areas of AM technologies with special focus on FDM process. Salient areas under due consideration towards the present research work has been highlighted.

Chapter 2

Literature Review

2.1 Introduction

Additive Manufacturing (AM) refers to manufacturing a part by adding material successively in layers. Parts manufactured through AM are prominently used in design verification, concept evaluation, design phase, testing and prototyping. Fused deposition modeling (FDM) is one such popular AM based computer-numerical-controlled (CNC) machine, distinguishes itself by manufacturing parts with complex geometries with ease in a short span of time in comparison with that of any traditional machine (Rosochowski and Matuszak [78]; Levy et al. [50]). The technology of FDM process has established itself as an industry standard for low-cost rapid prototyping of complex geometry parts. Since the prototype making involves environmental friendly pre-manufactured filaments and the technique itself involves a simple process of melting those filaments and depositing them layer by layer, still giving admirable accuracy and strength of the part. Several researchers have demonstrated the direct or indirect use of FDM processed parts in manufacturing final industrial parts, such as turbine blades from the concept of rapid tooling (Iftikhar et al. [35]) and rapid casting of certain aluminium parts using FDM processed parts as patterns (Wang et al. [104], Gill and Kaplas [33]).

With the growing utility of FDM processed parts as final products along with prototypes, there has been extensive research on various vital areas. In the current chapter an attempt has been made to brief the literature in AM with special focus on FDM process. The studies are related to mathematical modeling and sintering followed by mechanical properties like strength and volumetric shrinkage. The later sections are devoted to optimization studies followed by tribological studies like friction coefficient and wear.

2.2 Studies Related to Mathematical Modeling and Sintering

In FDM system, the raw material in the form of solid filament wire is made to pass through the extrusion head where it is heated to a semi-liquid state and deposited with a nozzle on the build platform one layer at a time. Since the chamber is maintained at a temperature lower than the melting point of the material, the deposited filaments solidify over a period of very short time involving highly transient heat transfer process. Two separate liquidizer-nozzle assemblies are arranged in the extrusion head, one for the model material and the second for the support material. During this solidification process, the filaments establish cross-bonding. The 'road width', defined as the mean distance between two adjacent filaments, is so maintained in the path planning of the extrusion head that the filaments develop a bridge between them, called as 'neck' by the process of viscous sintering. The bonding responsible for these necks to grow within a layer may be termed as the 'intra-layer bonding. At the same time, as one layer is deposited over the other, since the temperature of the previously solidified layer is still high, excellent propensity exists for similar bonds to be formed between the filaments of the two successive layers and these bonds may be termed as 'inter-layer bonding'.

FDM process has shown potential to be used for both prototyping and final part production through direct or indirect route. In the context of final part production, it is crucial to study the evolution of the strength of FDM processed parts, for which it is essential to link the part strength to the intra-layer and inter-layer bonds and neck size. Several researchers in the past have studied the effect of different processing parameters on the strength of the FDM manufactured parts.

Ahn et al. [2] have characterized the differential values of macroscopic strength of simple tension specimens of Acrylonitrile butadiene styrene (ABS) made by FDM system at different orientations. The anisotropic material properties of FDM processed parts have been investigated. The authors considered the various process parameters namely raster orientation, air gap, bead width, color, and model temperature to evaluate and compare the tensile strengths and compressive strengths of directionally fabricated specimens with that of the injection molded FDM ABS P400 material. DOE approach was used to arrive at the minimum amount of FDM process parameters. It was concluded that the parts made with a 0.003 inch overlap between roads demonstrated that the tensile strength ranged between 65 and 72 % of the strength of injection molded ABS P400. Also the compressive strength ranged from 80 to 90 % of the injection molded FDM ABS.

Sun et al. [97] examined the bond formation mechanism among the extruded ABS filaments in the FDM process. Specimens were produced under different processing conditions and their temperature profiles were carried out. The temperature effects on the mesostructures and mechanical properties were observed. The results of the experiments showed that the parts were fabricated along with the envelope temperature and variations in the convection coefficient strongly effects the mesostructure and hence the overall quality of the bond strength between filaments. Sintering phenomenon was found to have a significant effect on bond formation for a very short duration when the filament's temperature was

above the critical sintering temperature.

Rodríguez et al. [77] investigated that the reduced strength and elastic modulus in FDM processed parts is because of presence of voids and lack of molecular orientation, which underlines the importance of neck size and growth of molecules through the neck to the strength of the part. In this study, the modulus of strength has been expressed in terms of void density and relative bond strength factors.

Rodríguez [76] experimentally determined mechanical properties of ABS mono-filament and the in-plane properties of ABS materials with three mesostructures. It has been observed that there was a reduction of 11 to 37% in modulus and 22 to 57% in strength for FD-ABS materials relative to the ABS mono-filament. The authors have attributed that these reductions were due to the presence of voids and a loss of molecular orientation during extrusion of the filament from the FDM extruder head. Also the loss of load-carrying capacity is due to the presence of voids along with a loss of molecular orientation during the extrusion process contribute to the decrease in stiffness and strength with FDM processing.

Bellini and Güçeri [10] concluded that choosing a proper building direction, and thus the orientation of the model, shall play a vital role in deciding the extent of the neck formation. The effect of neck formation on the improvement of strength and reduction of shrinkage has been studied. It has been investigated that the properties and performance of the finished product strongly depends on the road shape and the road to road interaction, along with the extrusion path. The properties of the part depend on the chosen building direction i.e., the orientation of the part to be manufactured along with the chosen path i.e., the way every layer is filled by roads.

Li and Sun [51] investigated the bond formation which is formed when the semi-molten ABS filament material solidifies with the neighboring filament

material due to diffusion after deposition. Authors performed the heat transfer analysis of the FDM process to explain the process of bond formation. Sintering experiments were carried out to evaluate the dynamics of bond formation between polymer filaments. Predictions of the degree of bonding achieved during the filament deposition process were made based on experimental data used in conjunction with heat transfer and sintering models. The bonding quality among ABS filaments in FDM2000 process determines the integrity and mechanical property of resultant prototypes.

There has been a little work in the literature focused on the nature and cause of inter-filament bonding, both intra-layer and inter-layer, based on the viscous sintering of polymer spherical particles provided by Frenkel [30], who proposed a mathematical model for viscous sintering of spherical crystalline particles by taking into account the surface tension and viscous flow. Later Pokluda et al. [68] presented a modified model of sintering by considering balance of work of surface tension and the viscous dissipation while neglecting gravity and other forces. Roto-molding grade polyethylene resins co-polymers are used for the experiments which showed a less satisfactory agreement with the model.

Bellehumeur et al. [9] utilized this spherical particle sintering model in performing thermal analysis of FDM process to estimate the cooling profiles and bond formation studied the modeling of bond formation in the FDM extrusion process. Polymer sintering experiments were conducted and the dynamics of bond formation was evaluated. The degree of bonding that was achieved during the filament deposition process was predicted using the experimental data along with the results of heat transfer analysis. It was shown that extrusion temperature has a more significant impact on the neck growth of the bonding than envelope temperature. However it has been observed that the extruded filaments cannot be retained to higher temperature for the sake of complete bonding.

2.3 Studies Related to Strength

FDM process is gaining distinct advantage in manufacturing industries because of their ability to manufacture parts with complex shapes without any tooling requirement and human interface. The properties of FDM-built parts exhibit high dependence on process parameters and can be improved by setting parameters at suitable levels.

Ang et al. [4] built porous structures aiming at tissue engineering (TE) application that offers many advantages over conventional scaffold fabrication techniques as patient specific scaffolds with well-defined architectures and controllable pore sizes. The effects of air gap, raster width, build orientation, build layer and build profile, on the porosity and mechanical properties of ABS scaffold structures were investigated. Using the design of experiment (DOE) approach the parameters, which can be interdependent and exhibit varying effects on scaffold properties, were identified and examined. The relationship between scaffold's mechanical properties and porosity was established empirically. It was found that air gap and raster width are the most significant parameters that affect the porosity and mechanical properties of the ABS scaffold structures. The relationship between scaffolds mechanical properties and porosity was determined to be logarithmic, with the best mechanical properties observed in scaffolds of low porosity.

Galantucci et al. [31] in their work have proposed to reduce the density of rapid prototyped parts through alternative building styles. Topologically optimized parts have been created with internal geometry, using a narrow-waisted structure that avoids the need for building supports. Experiments have been conducted to characterize and study the behaviour of the obtained low density parts The influence on compressive mechanical strength, time for manufacturing and costs of the internal angle of the cones, of the raster width and of the shell

width has been studied, demonstrating that the raster width is relevant only for the manufacturing time, while it has no influence on the maximum compressive stress while the internal angle and the shell width are very important for these aspects. The study has demonstrated the validity of the approach to achieve a cost, time and material reduction, contributing to a lower economic and environmental impact.

Wang et al. [105] worked on selection of build orientation with allowed maximum tensile strain. A novel object build orientation selection method was proposed based on the tensile strain of an object to be built. To investigate the relationship between build orientation and allowed maximum tensile strain through tensile test experiments, test specimens were built with different build orientations. Golden section search is employed to determine the build orientation of an object consisting of multi-parts in order to get allowed maximum tensile strain. The proposed method was verified by building a truss for its feasibility and reliability.

Lee et al. [49] used Taguchi method to find the optimal process parameters for FDM prototype. Air gap, raster angle, raster width, layer thickness were the four process parameters considered for the study. Elasticity and flexibility were the two response variables whose optimum performance in terms of the process parameters was investigated. An orthogonal array, the signal-to-noise (S/N) ratio, and analysis of variance (ANOVA) were employed to investigate optimum elastic performance of a compliant ABS prototype. Experiments were carried out to confirm the effectiveness of this approach. From the results, it was concluded that layer thickness, raster angle and air gap significantly affect the elastic performance of ABS prototype considered.

Sood et al. [89] considered the effect of layer thickness, raster angle, raster width, air gap (void spacing) and part orientation on distortion of FDM parts along length, width and thickness directions. The three response variables

having different optimal parameter settings were minimized using Taguchi's grey relational method. It was concluded that increase in number of layers increases the temperature gradient that results in distortion within the layers or between the layers. Also inter-layer cracking and part de-lamination or fabrication failure occurs resulting in decrease in strength as residual stress accumulation increases. Small raster angles are not preferable as they results in weak bonding. However small raster angle also means that rasters are inclined along the direction of loading and will offer more resistance thus strength will improve. Similar studies have been reported by Durgun and Ertan [26] to improve the mechanical properties and also the cost of production through changing the various process parameters in FDM process.

Kulkarni and Dutta [45] studied the deposition strategies for the FDM process. Composite modeling and analysis of the deposition paths was performed in comparison to the existing methods of deposition. Experiments were conducted and it was found that the composite laminate analysis were consistent with experimental ones. And the laminate model can thus be used as a design aide to select a deposition strategy based on the stiffness requirements. It was shown that the two modified deposition strategies were better than the existing ones.

Sood et al. [90] studied the effect of process parameters on resistance to compressive loading. Study of anisotropic and brittle nature of build part is important as it enhances the service life of functional parts. To understand this, the effect of five important parameters namely layer thickness, part build orientation, raster angle, raster width and air gap were considered. The work provided an understanding into the mutual interdependence of the process parameters on compressive stress. The study also evolves a statistically validated predictive equation which can be used to obtain optimal parameter setting based on quantum-behaved particle swarm optimization. The nature of the compressive stress was predicted using artificial neural network (ANN) and was compared with predictive equa-

tion. Based on experimental work and the optimization techniques used in the study, it was found that the maximum compressive stress of 17.4751 MPa can be obtained with the following optimum value of layer thickness, orientation, raster angle, raster width and air gap as 0.254 mm, 0.036°, 59.44°, 0.422 mm and 0.00026 mm respectively.

Masood and Song [54] developed a new metal/polymer composite material for use in FDM process to use in direct rapid tooling technique. The material consists of iron particles in a nylon type matrix. The filaments of this composite have been manufactured and tested for its utility. From the experimentation it has been identified that the composites consisting of large filler particles of uniform size and higher volume fraction exhibit lower tensile modulus, tensile stress and elongation. Also it has been observed that the composite with smaller particle size exhibited significant tensile elongation. It was concluded that test results of injection molding inserts material had proven acceptable quality of injection molded parts.

Reddy et al. [71] attempted to design and develop an extruder deposition system that can improve the strength. An extruder has been designed and developed to study the influence of process parameters on surface roughness and bond strength using Box-Behnken design. For the study, three variables namely, nozzle temperature, chamber temperature and inter-road gap have been considered. It has been observed that road gap has maximum percent contribution on bong strength as well as surface roughness. It has been demonstrated that the strength used by the newly developed extruder has shown better results than that of the commercial FDM systems.

2.4 Studies Related to Dimensional Accuracy

Sood et al. [88] experimentally investigated the influence of FDM process parameters namely layer thickness, part orientation, raster angle, air gap and raster width along with their interactions on the dimensional accuracy of the parts produced by FDM. It was observed that shrinkage is predominant along length and width direction of built part. Taguchi's parameter design has been adopted to estimate the optimum parameter setting to minimize the total percentage change in all the dimensions using a standard test specimen. All the three process parameters were expressed as grey relational grade and grey Taguchi method was adopted to obtain optimum level of process parameters to minimize percentage change in length, width and thickness simultaneously. Maximization of grey relation grade showed that layer thickness of 0.178 mm, part orientation of 0°, raster angle of 0°, road width of 0.4564 mm and air gap of 0.008 mm would produce overall improvement in part dimension. It has been observed and felt that the process parameters influence the responses in a highly non-linear manner. Hence the prediction of overall dimensional accuracy is made based on artificial neural network (ANN).

Es-Said et al. [28] studied the effect of different layer orientations of parts of ABS build with FDM machine solid models on tensile strength, modulus of rupture, and impact resistance. The samples were fabricated with five different layer orientations. It was observed that the 0° orientation, i.e. where layers were deposited along the length of the samples, had displayed superior strength and impact resistance over all the other orientations. It has been found that the ultimate and yield strengths were the highest in the 0° orientation followed by the 45/0°, 45/-45°, 90°($\simeq$ 45°) orientations in descending order. It was observed that the fracture path of the tensile samples was dependent on the layer orientation, where de-lamination occurred along the layer interface. This was caused by weak

inter-layer bonding and/or inter-layer porosity. The modulus of rupture value was found to be the highest in the 0° orientation followed by equivalent values in the 45/-45° ($\simeq$ 45/0° $\simeq$ 45°) orientations, which was followed by the 90° orientation. And the Izod impact test data indicated that the 0° orientation samples had the highest absorbed energy values prior to fracture by an order of magnitude over the 90° orientation.

Rodríguez [75] studied the effect of controllable meso-structural features that are related to fiber layout and the presence of voids in the FDM processed parts. Meso-structural features dictate the mechanical properties like stiffness and strength of unidirectional extruded materials were characterized as a function of the processing variables. Test samples were made using the FDM machine. It was shown that the void geometry/density and the extent of bonding between contiguous fibers depended strongly on the fiber gap and extrusion flow rate. Through the study, various settings for minimum void and maximum fiber-to-fiber bonding were determined. It was found that void and bond length densities in the plane transverse to the fiber extrusion direction varied from 4 to 16 % and 39 to 73 % respectively.

Pérez [66] studied the characterization of the surface roughness and dimensional precision obtainable in layered manufacturing processes. Parts were manufactured using FDM process and an experimental analysis of the resulting roughness average (Ra) and rms roughness (Rq) obtained with these manufacturing processes was carried out. Dimensional parameters were also studied in order to determine the capability of the FDM process for manufacturing parts. An uncertainty analysis was performed taking not only the manufacturing process variability into account but also the measurement variability. It was concluded that a better surface finish could have been obtained by reducing the layer height however this will increase the manufacturing time and costs. Surface roughness parameter uncertainties are more or less the same with different slope variations

of the angle. This behaviour was also observed when considering dimensional parameters in which a similar degree of variability was observed.

Anitha et al. [5] studied the effect of layer thickness, road width and speed of deposition on the surface roughness of the parts produced by FDM process. Taguchi method was used to arrive at the minimum number of experiments that should be conducted to optimize the both the process design and the product design. ANOVA results revealed that the effect of layer thickness is more predominant and affects the surface roughness to a greater extent than the other parameters.

Zhang and Chou [109] simulated the FDM process using FEA with simplified material properties and boundary conditions. These simulations were used to investigate the effects of tool-path on residual stresses and distortion pattern of the part. In order to validate the results obtained through simulation, parts were fabricated and measured. A parametric study was done with three factors varied at three levels to evaluate the effects of the FDM machine process parameters on residual stresses and part distortions. It was established from the simulation results that the scan speed is the most significant factor to part distortions, followed by the layer thickness leaving the road width as insignificant. However, the interaction between the road width and the layer thickness was significant. Residual stresses increase with the layer thickness. Simulation results show that tool-path patterns affect the deflection of the part. It was attributed to the fact that residual stresses which were accumulated during the deposition resulted in distortion. Good correlation was obtained between the results obtained from experiments and simulations Chou and Zhang [18].

Wang et al. [105] analyzed the deformation, the essence of the deformation and the interacting principles in the part manufactured by FDM process. A mathematical model of the prototype warp deformation was constructed, and the influence of number of deposition layers, the length of the stacking section, the

chamber temperature, and the material linear shrinkage rate. It was observed that warp deformation increases with increasing deposition layers number and also similar trend is observed with the increase in length of the stacking section. However, the warp deformation linearly decreases with increasing chamber temperature. Similar studies related to the dimensional changes due to error compensation by correcting slice files have been reported (Tong et al. [98]) and investigations on small sized product fabrication using FDM has been reported (Singh [83]).

2.5 Studies Related to Optimization

Pandey et al. [63] studied the optimal part deposition orientation in FDM by using a multi-criteria genetic algorithm. FDM machine takes larger build time to build a model material with thinner slices. However to decrease the build time, if a large slice thickness is chosen, the surface finish is very poor due to stair-stepping. The authors have chosen to optimize these two contradicting objectives namely average part surface roughness and build time by using adaptive slicing which calculates the slice thickness based on local geometry of the computer-aided design model and rapid prototyping machine specifications. The two objectives are minimized simultaneously using a multi-criteria genetic algorithm. The developed system also provides a set of intermediate solutions in which any solution can be used depending upon the preference of user for the two objectives which can be used for any class of component i.e., a freeform or a regular object (Deb and Pratap [23], Deb and Saxena [24], Srinivas and Deb [92], Deb et al. [25]).

Kanagarajan et al. [39] studied the optimization of electrical discharge machining characteristics of WC/Co composites using non-dominated sorting genetic algorithm (NSGA-II). The influence of operating parameters of EDM such as pulse current, pulse on time, electrode rotation and flushing pressure on material removal rate and surface roughness. Experimental results were used to develop

the statistical models for the different process characteristics. NSGA-II has been used to optimize the processing conditions. A non-dominated solution set has been obtained and reported.

Byun and Lee [13] studied the optimal part orientation that improves the surface roughness generated from the stair stepping effect along with minimizing the build time including the structure of the support in fabricating a completely free-form part. To determine the optimal orientation, genetic algorithm was employed that considered the fuzzy weight for surface roughness and build time. The technique was employed to many examples that used different RP systems. The algorithm could help additive manufacturing users to select the best orientation of the part and that results in efficient process planning.

Singhal et al. [84] attempted to achieve minimum average part surface roughness, minimum build time and support structure for stereolithography (STL) and selective laser sintering (SLS) processed parts by determining optimum part deposition orientation. MATLAB-7 optimization tool box has been used to solve the multi-objective optimization problem. The surface roughness simulation was carried out with optimum part deposition orientation to have an idea of surface roughness variation over the entire part's surface before depositing the part.

Kondayya and Gopala Krishna [42] have optimized the laser beam cutting process parameters to minimize the kerf width (Kw) and material removal rate (MRR). Initially genetic programming approach was used for empirical modeling to identify the important performance measures of the laser beam cutting process. Design of experiments was used to conduct the experiments with four variables such as pulse frequency, pulse width, cutting speed and pulse energy. The developed models are used to study the effect of laser cutting parameters on the chosen process performances. Since the output parameters Kw and MRR were mutually conflicting in nature, they were simultaneously optimized by using NSGA- II. Finally Pareto optimal solutions of parameter settings have been

reported that provide the decision maker an elaborate picture for making the optimal decisions. Similar work on multi-objective optimization was however being attempted by in many other rapid prototyping techniques (Aijun et al. [3], Bagchi [7], Nassif et al. [59], Baraskar et al. [8], Mitra et al. [56], Liao and Shie [52], Cheng et al. [14]).

2.6 Studies Related to Tribological Properties

Polymers and polymer-based composites offer a wide variety of combinations of properties that even metal or metal matrix composite or even ceramic materials fail to provide. This is due to the fact that polymer and polymer based composites provide low friction. Due to this reason a variety of polymers are now-days used in dry sliding conditions i.e., lubrication may not be required. The extensive use of polymers has led to a comprehensive research on the tribological properties of friction and wear mechanisms of polymers. Polymers offer low frictional resistance to sliding and hence many polymers are used in dry sliding conditions. The widespread use of polymer as the end products has led to an intense research on the friction coefficient and wears mechanisms of polymers (Dearn et al. [21], Ramesh and Srinivas [69], Ramesh et al. [70]).

Franklin [29] carried out wear experiments on engineering polymers sliding against a hardened steel mating surface under different conditions of sliding speed, mating surface roughness and roughness orientation. It was investigated that increasing the roughness of the mating surface leads to an increase in the wear rate with varying effect for different polymers. When the roughness height is low (Ra = 0.05m), a roughness oriented parallel to the sliding direction results in a higher wear rate than one oriented perpendicular to the sliding direction. The orientation of the roughness on a ground mating surface with respect to the sliding direction influences the wear rate with unfilled polymers.

Pedro et al. [64] studied epoxy resin composites which are applied in moulds manufactured using rapid tooling technologies that are used for wax and polymer materials. Study was done to estimate thermal conductivity and wear resistance, while metallic fillers permit significant improvement in the resin thermal conductivity. From the present work, it was shown that small amounts of milled fibers enhanced the wear resistance. A tribological study of was performed using the neat resin, the aluminium filled resin and tri-phase composites composed by epoxy, aluminium particles and milled glass or carbon fibers. The study was done to understand the role of the particles and fibers in the friction and wear at room temperature and at a typical plastic injection temperature of 160°C. Mixtures of fibers and aluminium particles can be used to optimize mechanical and thermal properties of composites manufactured for rapid tooling applications. At elevated temperatures, it was observed that the mechanical properties of the composite get affected since the resin gets softened and hence causes reduction of the particle and fiber/matrix adhesion.

Jia et al. [38] studied the friction and wear properties of various polymer namely polyamide 66 (PA66), polyphenylene sulfide (PPS) and polytetrafluoroethylene (PTFE) sliding against themselves under both dry sliding and oil-lubricated conditions using a pin-on-disc tribometer. Two parameters namely applied load and sliding speed on the polymer–polymer sliding combinations under dry sliding and oil-lubricated conditions were investigated. It was observed that friction properties of the three sliding combinations could be greatly improved by oil lubrication, the anti-wear properties of PTFE and PPS were improved by oil lubrication. But it was observed that the anti-wear properties of PA66 were decreased by oil lubrication. It was concluded that frictional heat would alter the physical state of polymer sliding surfaces that significantly affect the tribological behaviours of polymer–polymer sliding combinations under dry sliding condition. On the other side, oil lubrication dissipates the frictional heat. It was also investi-

gated that adhesion wear was dominant wear mechanism for dry sliding condition, while adhesion wear combined with erosion wear was the main wear mechanism for oil-lubricated condition.

Babur et al. [6] in their study optimized the effect of injection parameters namely melt temperature, packing pressure, cooling time and injection pressure on the mechanical properties of ABS moldings. Mold materials having two different thermal conductivities were selected for their study. Taguchi's L9 orthogonal array design was used as the experimental plan and the mechanical properties of ABS specimens such as elasticity module, tensile strength and tensile strain at yield, tensile strain at break, flexural modules and Izod impact strength were measured. Based on the signal to noise ratio for mechanical properties of ABS was calculated using the Taguchi method. Later the effect of the parameters on the response was determined using the analysis of variance. Regression analysis was used to create linear mechanical models. It was found that the most important parameter affecting the elasticity module, tensile strength and tensile strain at yield, tensile strain at break was melt temperature when compared to other parameters.

ABS is one of the most industrially useful polymers and can be used in the manufacture of part by FDM. Given the fact that ABS parts made by FDM can have widespread use under several critical relative sliding conditions, tribological study of FDM parts is very important. The current challenge for any industrial application of FDM process is the quality of the parts manufactured by this process. Much of work so far on characterization of quality of FDM parts has been on the bulk properties such as tensile strength, dimensional accuracy etc. in terms of the FDM process parameters (Ahn et al. [1]).

Sood et al. [87] studied the effect of the following FDM process parameters namely, layer thickness, part build orientation, raster angle, raster width and air gap. Parts were manufactured by FDM machine using various combinations

of the above process parameters using the face centred central composite design and sliding tests were performed to understand the sliding wear. The study provided an insight of the mutual inter dependency of wear on process parameters. Different wear mechanisms were explained making the use of scanning electron micro-graphs of the sliding pins. The equation as obtained through the ANOVA results has been used to obtain the optimal parameter setting through quantum-behaved particle swarm optimization (QPSO). Because of the complexity and the non-linearity in their manner of the interaction of the process parameters an artificial neural network (ANN) is employed to validate the results of present study (Equbal et al. [27]).

From the current literature, it suggests that the AM technologies have a number of synergies among them towards the product/prototype properties improvement. However, with the utility of these AM technologies in various fields of science and technology ranging from tooling, automobile, medical implants, food processing, tissue engineering and many more, a greater effort has been spent by many researchers in understanding and tailoring these technologies accordingly. Many researchers have investigated the properties that get affected due to the process parameters and their operating conditions. Among the existing AM technologies, FDM is one such technology where in the possibility of process improvement has been limited. Added to this, due to the inherit advantages like low material cost, easily available raw material, manufacturing tailor made properties etc., has made the current world to use more of FDM process that any other AM technologies. Based on these observations, the following salient research gaps have been identified.

1. FDM machine parts essentially consist of strongly, yet partially, bonded cylindrical filaments, rather than spherical particles, of the build material. The bonding quality among filaments in FDM made parts is an important factor in determining mechanical properties of the parts. It is also evident

from literature survey that the relationship between macroscopic strength of an FDM part and microscopic neck-sizes between the filaments has not been studied. The present work is thus aimed at bridging these gaps by studying the relationship between the neck size formed between cylindrical filaments and macroscopic strength of the FDM processed parts. This helps in complete understanding of evolution of strength from the very basics of neck growth of any part produced by the FDM machine. A mathematical model is developed to arrive at the neck growth between the cylindrical filaments. Strength is derived from the necks formed out of bonding between the filaments and are compared with the experimental values.

2. Finite element simulation has been attempted to understand the neck formation during FDM process. This also helps in validating the results obtained during the mathematical model.

3. From the foregoing literature review it is evident that mechanical properties and final geometry of the part are sensitive to the process parameters. Apart from that, the literature study primarily considers solving a single objective optimization of FDM process parameters by either RSM or Taguchi method. FDM machine manufactured parts in fact needs a multi-objective optimization as there are several quality objectives namely strength and volumetric shrinkage, which are conflicting and are affected by different process parameters. And this type of multi-objective problem has not been investigated thoroughly in the recent past. Filling this gap is very important since a designer will now be in a impressive positioning in obtaining a customer or a designer driven desired solution from a set of optimum solutions for the chosen multiple objectives.

4. From the literature study, it has been observed that polymers are widely used in industry either as end products or as prototypes for various applications

like rapid tooling, bio implants etc. Parts produced by FDM process are of ABS polymer, which have good properties towards wear resistance, strength and dimensional stability. There is a need to investigate into the various FDM process settings that affect the tribological properties of ABS made parts of FDM process and very little research has been done towards the understanding of tribological properties of the parts manufactured by FDM. Filling this gap helps the designer in considering both the manufacturing settings through FDM along with the real time testing conditions through tribological experimental set-up namely the pin on disc machine.

2.7 Summary

In the present chapter a detailed literature study has been carried on various aspects related to FDM process. To start with, a detailed study has been done on studies related to mathematical modeling. From this literature study, it is evident that there is a need to establish a relation between the macroscopic strength to that of the strength evolved due to neck formation. Mathematical studies have to be undertaken to arrive at the strength contributed by the filaments in the FDM process. There has been a much need of finite element simulation for the FDM process, so as to mimic the neck growth during the bond formation. The third section of the literature survey has been devoted to the understanding of the strength that has been contributed due to neck formation. From the study, it has been observed that the strength is dependent on various process parameters, out of which orientation is the most important. However, the understanding of strength contributed due to inter and intra-layer bonding has not been investigated in detail. The fourth section of the chapter has been devoted to dimensional inaccuracies during the manufacturing of parts using FDM process. Very little work has been done in understanding the volumetric shrinkage that occurs during the

solidification process of FDM build parts. The fifth section of the literature study details about the optimization procedures used in AM technologies. Very little or not much work has been attempted in performing multi-objective optimization which is much required for the current needs. And the final section talks about the parametric dependency of FDM process on tribological properties like wear and coefficient friction, where the need has been realized that finished products should have better tribological properties for which the designer should be aware of before manufacturing them. From the current literature study, the gaps in the research have been identified. With this fundamental study, from the next chapter on-wards, a detailed analysis has been attempted to fill these gaps. To start with, the next chapter elaborates about the various measurements carried out in the present thesis.

Chapter 3

Modeling and Measurement of FDM Prototypes

3.1 Introduction

One of the few significant advantages of using the AM technologies and in particular FDM process is that the complex shapes can be produced with complete elimination of tooling, which is quite expensive. Manufacturing of parts/prototypes that undergo frequent design changes, involving complex shapes and intricate geometries makes the process more versatile. Besides these, the manufacturing time is very low in comparison to the traditional manufacturing (Krause et al. [43], Too et al. [99], Wiedemann and Jantzen [106]). As already highlighted in the previous chapter, producing better quality parts still is a challenge (Ippolito et al. [36]). In trying to attempt this challenge, a complete understanding of the FDM process parameters is required so as to make the parts/prototypes more reliable. Before understanding this complete phenomenon of FDM system, which will be done in subsequent chapters, an attempt is made to detail about the fundamentals required for complete understanding of FDM system. In the present chapter, a detailed understanding of the material used in FDM process has been discussed.

Key mechanical properties like strength, volumetric shrinkage, and tribological properties like wear and friction coefficient of the parts produced by the FDM process have been considered. This chapter discusses about the design methodologies that will be used in the subsequent chapters of the thesis emphasizing the different measurement techniques to estimate the above mentioned quality characteristics.

3.2 Material Used

The material used to manufacture test specimens using FDM process is ABS P400, a variant of ABS (Acrylonitrile Butadiene Styrene). ABS is a terpolymer, composed of three monomers polymerized. The chemical formula of ABS is $(C_8H_8.C_4H_6.C_3H_3N)$n. Figure 3.1 shows the chemical formula of ABS in its pure state. ABS P400 is a patented material used in FDM machine and it has certain additives mixed to enhance the mechanical properties and thermal stability. Acrylonitrile, one of the monomer of ABS is a synthetic polymer obtained from propylene and ammonia. Acrylonitrile monomer contributes heat and chemical resistance the ABS polymer while butadiene is a simple conjugated diene with the formula C_4H_6. It is produced as a by-product of the steam cracking process which is used to produce ethylene and other olefins. ABS is made by polymerizing styrene and acrylonitrile in the presence of poly-butadiene. Butadiene provides impact strength and low-property retention to ABS polymer. While styrene is produced from ethyl benzene, (prepared on a large scale by alkylation of benzene with ethylene). Styrene provides surface gloss, rigidity and ease of processing. ABS can be considered as a blend of a glassy copolymer (styrene-acrylonitrile) and rubbery domains (butadiene). ABS forms a graft copolymer which yields best mechanical properties like strength. For the present study, a variant of ABS i.e., ABS P400 is used which is supplied by the FDM machine manufacturer (Robert [73],James

[37],Smith et al. [85], Kirk-Othmer [41]).

3.3 Manufacturing of Test Specimens

3.3.1 FDM machine details

uPrint machine is one among the variants that uses FDM process. In the current thesis, test specimens are manufactured using uPrint, Stratasys™, Minnesota, USA (Stratasys [94]). The uPrint machine builds three-dimensional parts by extruding ABS filament through a computer-controlled extrusion head, producing high quality and ready to use parts. The uPrint builds a maximum part size volume of 203 x 152 x 152 mm^3. Figure 3.2 shows the uPrint machine that has been used for the current work. Along with build material, yet another material carrier is also present namely the support material. It is used only to support the model during the build process. Support material is primarily a water soluble material and has to be removed completely once the part is completed. The raw materials/build material and the support material which are in the form of spools are held in a carrier. Each of these material carriers contain 492 cc of usable material enough to build continuously for about 48 hours. The semi-molten material is deposited in the form of filaments thus forming layers. The available layer resolution is 0.254 mm with a minimum wall thickness 0.914 mm. Parts can be manufactured in uPrint machine through various infill patters, also called as model interior, defined defined as the amount of material that can be used during the manufacturing of the part. Suitable part infill/model interior can be chosen on the need. uPrint offers three types of model interior that can be chosen. They are:

1. *Solid interior* fill is used when a stronger and durable part is desired. For this type of configuration the time taken to build the parts is longer along

with greater consumption of material.

2. *Sparse High Density* is recommended that have shorter build times with optimum material consumption.

3. *Sparse Low Density* is a "honeycombed" or a "hatched" interior pattern that takes the shortest build time and lowest material usage. However there will be substantial decrease in the strength of the parts manufactured since the material consumed is less.

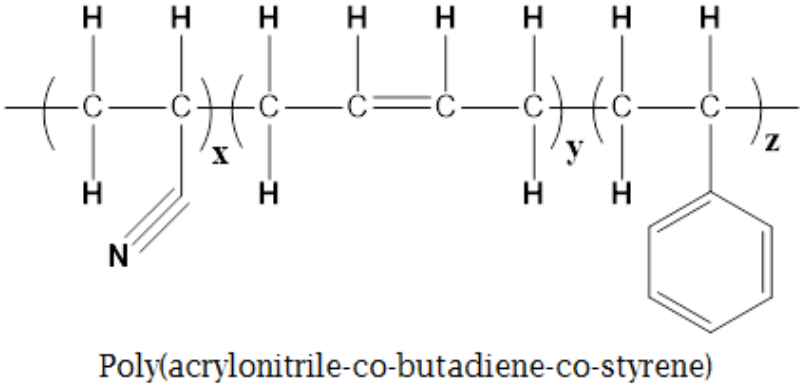

Fig. 3.1 Chemical composition of ABS monomers

To manufacture the specimen in uPrint, the specimens can be modeled in any of the solid modeling software. For the current thesis, Solidworks™ (SolidWorks [86]), has been used. Later the specimens were saved in (*.STL*) format and imported to Dimensional Catalyst, a user interface for the uPrint machine. Once the test specimens were arranged as required with respect to orientation in both horizontal and vertical directions in the model space of the software, they can be manufactured by simply submitting the *.CAB* file to the 3D printer. Once the test specimens are built, they are placed in a solution chamber to remove the support material. The specimens are then dried and readied for the testing.

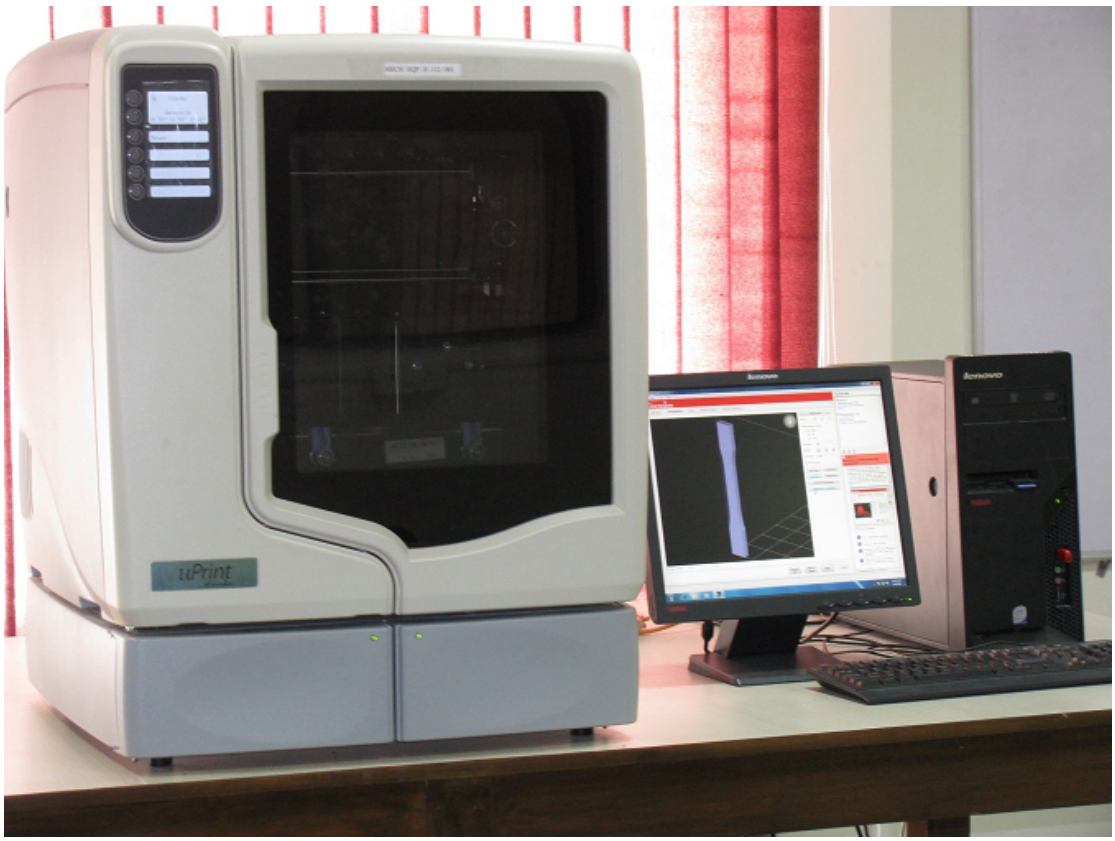

Fig. 3.2 uPrint machine set-up

3.3.2 Fundamentals of part manufacturing using FDM process

As discussed in the previous chapter, in FDM the model material/build material i.e., ABS P400 polymer is heated to near its melting temperature and deposited layer upon layer. Two separate liquefier-nozzle assemblies are arranged in the extrusion head, one for the model material and the second for the support material. During this solidification process, the filaments establish cross-bonding. The 'road width', defined as the mean distance between two adjacent filaments, is so maintained in the path planning of the extrusion head that the filaments develop a bridge between them, called as 'neck', by the process of viscous sintering. The bonding responsible for these necks to grow within a layer may be termed as the 'intra-layer bonding'. At the same time, as one layer is deposited over

the other, since the temperature of the previously solidified layer is still high, excellent propensity exists for similar bonds to be formed between the filaments of the two successive layers and these bonds may be termed as 'inter-layer bonding'. Specimens manufactured by FDM process are composed of cylindrical filaments of ABS polymer. The details of the various stages of part manufacture is shown in Figure 3.3.

The description of the various stages of part manufactured are described as:

Stage 1 Cross section view of strands adjacent to each other forming an intra-layer bonding.

Stage 2 Neck growth and molecular diffusion between the strands in the intra-layer bonding.

Stage 3 Neck growth and molecular diffusion between the strands and also between the intra-layers.

Figure 3.4 demonstrates an idealized schematic concept of intra-layer and inter-layer bonding between strands. Total strength of bonding between two adjacent elements depends on the neck-size between the filaments, formed as a result of a combination of molecular diffusion and cross-linking of polymeric chains and the overall process can be called as viscous sintering. FDM has shown potential to be used for both prototyping and final part production through direct or indirect route. In the context of final part production and as demonstrated, it is crucial to study the evolution of the neck growth which in-turn quantifies the strength of FDM parts. For this, it is essential to link the part strength to the intra-layer and inter-layer bonds and neck size.

3.4 Methodology

In the previous section it has been observed that the properties of the part manufactured depends on various process parameters including the process

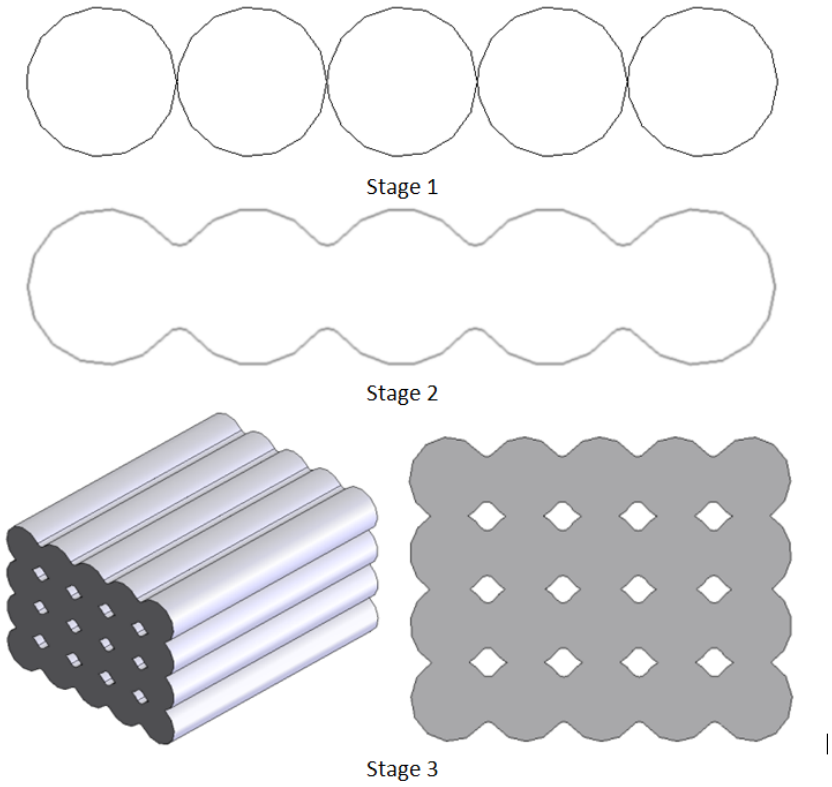

Fig. 3.3 Stages of part manufacturing in FDM process

of manufacturing. Also it is also observed from literature study that the FDM process parameter settings play a dominant role in deciding the properties of the part. From the designer and the manufacturer's view, it is very important to study the effects of these process parameters on the final desired quality of the parts/prototypes that are produced. Among the various techniques, it has been well established fact that the use of experimental design techniques shall provide the best possible results with detailed understanding of the process parameters and their effect on the quality characteristics like strength, volumetric shrinkage, wear properties and dimensional properties.

3.4.1 Design of Experiments (DOE)

Design of experiments (DOE) is a scientific approach referring to the process of planning the experiments so that appropriate data that can be analyzed

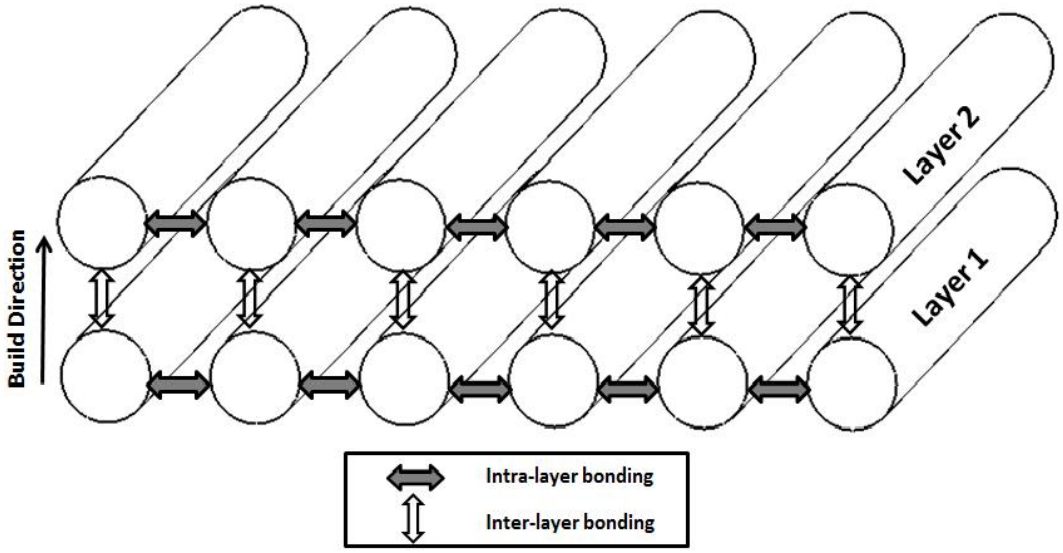

Fig. 3.4 Inter and intra-layer bonding in FDM process

by statistical methods are generated, resulting in valid and objective conclusion (Montgomery [57]). Studying the effect of various process parameters of FDM process on quality of the parts is one among those most eligible problems that needs to be studied with the techniques of DOE. The following are the guidelines for designing the experiments for the FDM process in particular with reference to the current research work.

1. Identification and statement of the problem: Based on the literature study, the identification of the problem is done. It was observed that there has been an increasing trend in the utilization of parts produced by the FDM process as end products. However there are many gaps in understanding the effect of the factors influencing these quality responses.

2. Choice of factors, levels and range: Among the various factors that are assumed to influence the quality variables of FDM parts, the present study specifically focuses on various possible orientations of the part and model interior. For the tribological study, using the pin-on-disc experimental set-up

various settings have been considered along with the FDM process parameter settings. Three levels for each of the factor have been considered while utilizing the full range of each factor's variation.

3. Selection of the response variables: Response variable refers to the quality variables such as strength, shrinkage, wear rate and coefficient of friction which are influenced by the factors considered, their levels and ranges chosen. In the current thesis, quality parameters like strength, volumetric shrinkage and tribological properties like wear and friction coefficient have been considered for the study.

4. Choice of the experimental design: The choice of the experimental design has been chosen based on the number experiments that can be performed to obtain the desired result which enables to understand the influence of the factors individually and in mutual interaction. For the chosen quality parameters, face centred central composite design has been chosen.

5. Performing the experiment: Based on the above step, experiments have been conducted with respect to the chosen factors, their levels and ranges.

6. Statistical analysis of the data: Statistical analysis of the data has been performed using the ANOVA technique and based on the results, various conclusions and recommendations have been generated.

3.4.2 Response surface methodology (RSM)

Response surface methodology (RSM) is a collection of statistical and mathematical techniques that are useful for developing, improving and optimizing the processes. The performance measure or quality characteristic of the process is called the response. The response yield y is a function of the two factors namely

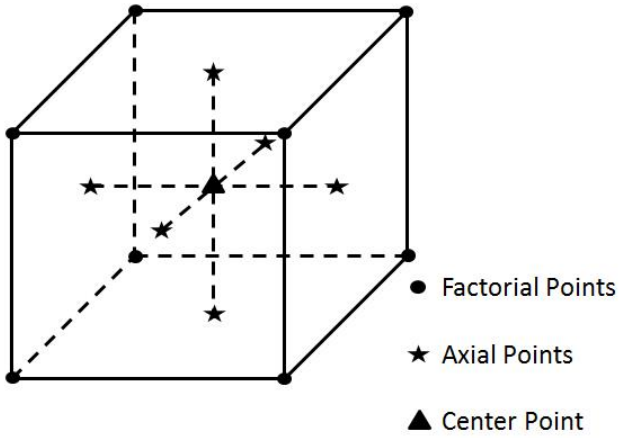

Fig. 3.5 A face central composite design layout for three factors

x_1 and x_2, say

$$y = f(x_1 + x_2) + \epsilon \tag{3.1}$$

where ϵ represents the noise or error observed in the response y. The surface represented by f(x_1, x_2) is called a response surface. The response can be represented graphically, either in the three-dimensional space or as contour plots that help visualize the shape of the response surface. Among the various response surface designs, in the present thesis face centred central composite design (FCCCD) has been chosen. For the FCCCD set up, the experiments to be conducted are can be depicted as positions of a factor mentioned in Figure 3.5.

As per the FCCCD, total number of experiments that needs to be conducted are given given with the relation $2^k + 2 * k + n$, where k is the number of process parameters considered for the experiments to be conducted. A three level setting is chosen i.e. a process parameter will have three levels (low, medium and high) of value. 2^k are the factorial points, $2 * k$ are the axial points and n are the number of center points. The experiments with n center points will be repeated to attain uniform standard deviation of the predicted response over a large design space. In the present thesis, three factors at three levels are being chosen with 6 as the repeated number of experiments at the center point. Hence the total number of

experiments to be conducted are 20 ($2^k + 2 * k + 6$). More details of FCCCD can be found in Montgomery [57].

Table 3.1 provides the details of the various combinations of the 20 experiments to be conducted for the chosen three factors A, B and C. Details of the factors with the level setting chosen will be elaborated in Chapter 5 and 6. In the table, the level settings '-1' represents the lowest value, '0' represents the mid value and '1' represents the highest value of the factor chosen. Based on this DOE scheme, all the 20 the experiments will be conducted to evaluate the responses chosen for the study.

Table 3.1 Experimental Runs of FCCCD

S No.	A	B	C	S No.	A	B	C
1	0	-1	0	11	0	0	0
2	-1	0	0	12	0	0	0
3	0	1	0	13	0	0	0
4	-1	-1	1	14	0	0	1
5	-1	1	-1	15	0	0	-1
6	0	0	0	16	1	0	0
7	0	0	0	17	1	-1	1
8	0	0	0	18	1	1	-1
9	-1	-1	-1	19	1	-1	-1
10	-1	1	1	20	1	1	1

3.5 Measurements

As stated in the previous section about the responses, in the current thesis the following are the measurements taken. Chapter 4 and 5 estimates the affect of three factors on quality responses namely the strength and volumetric shrinkage.

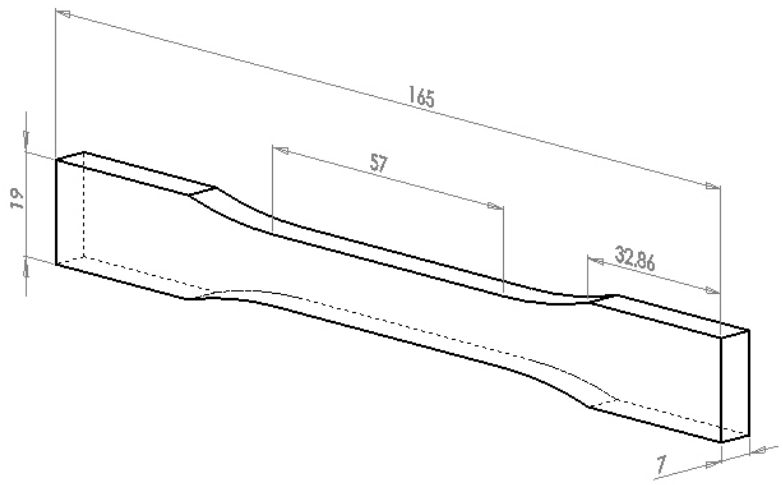

Fig. 3.6 Specimen used for tensile testing (in mm)

And chapter 6 estimates the affect of three factors on quality responses namely wear and friction coefficient. The estimation of the quality responses as required for the study are explained in the following sections.

3.5.1 Estimation of strength

In order to estimate the bulk strength of the FDM processed parts, test specimens are manufactured using the FDM process as per the FCCCD scheme mentioned in Table 3.1. The dimensions of the test specimens are adopted from ASTM D638-10. The dimensional details of the specimen are shown in Figure 3.6. The manufactured specimens are then tested for strength using an electromechanical universal testing machine (UTM) at a constant strain rate of 0.01 per second. The UTM is attached with an electronic and computer controlled accessories to conduct the simple tension test. Figure 3.7 is the UTM set-up used for determining the tensile strength. Since the ABS specimens are relatively weaker compared to metals, a more accurate 100 kN capacity with a load cell 5 kN is used electromechanical universal testing machine (UTM) is used to test the specimens. Since ABS polymer exhibits brittle fracture, the specimens are fixed in roller grippers

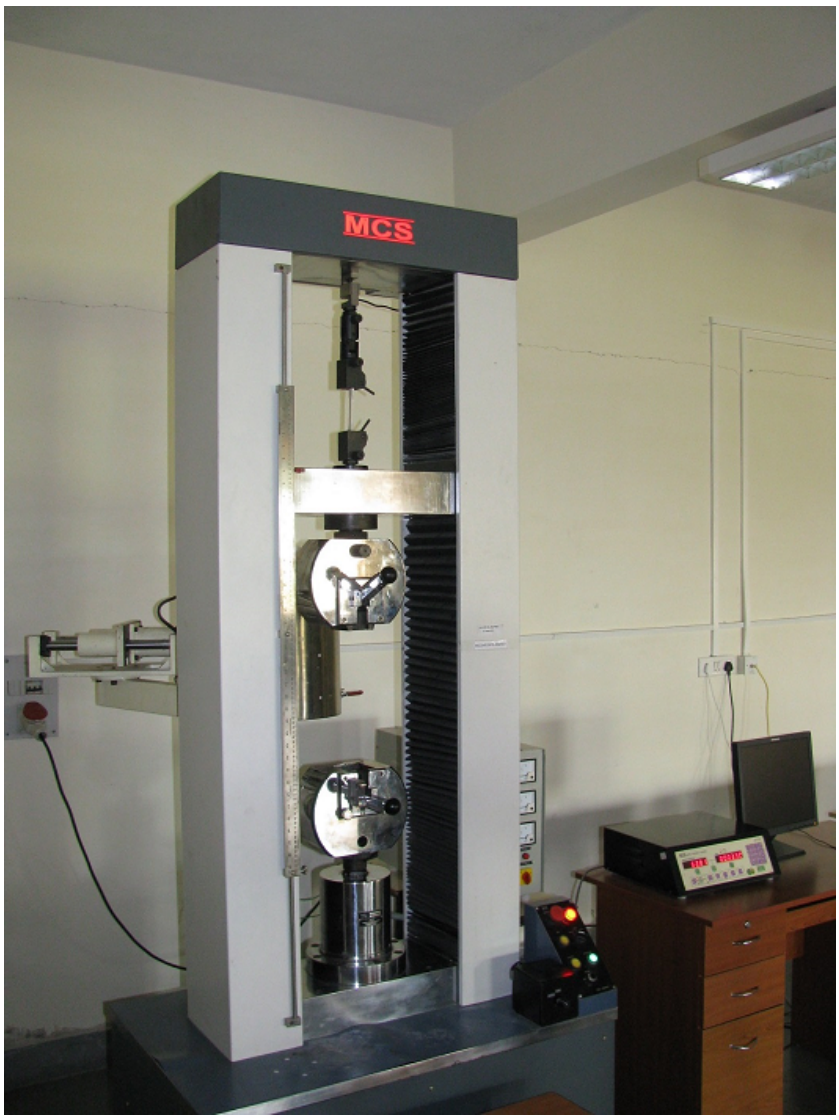

Fig. 3.7 Universal Testing Machine set-up

unlike the usual metal grippers. The details of the specimen mounting in the roller grippers are highlighted in Figure 3.8.

3.5.2 Estimation of volumetric shrinkage

The test specimen used to estimate the volumetric shrinkage is shown in Figure 3.9. The specimens for estimating volumetric shrinkage are manufactured by the same procedure as highlighted for strength. Volumetric shrinkage is obtained by measuring the percentage shrinkage in dimensions of the fabricated

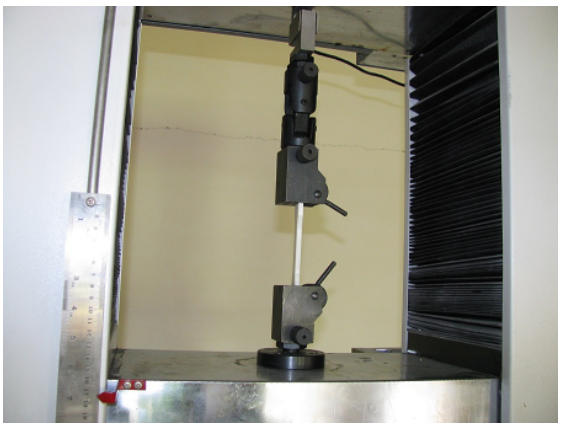

Fig. 3.8 Roller grippers used to grip ABS polymer specimens

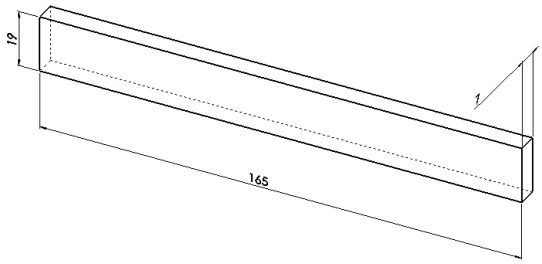

Fig. 3.9 Specimen used for estimating volumetric shrinkage(in mm)

parts versus the actual dimensions of the specimen that were used during solid modeling in Solidworks^{TM} modeling software. The dimensions are measured using Mitutoyo standard laboratory digital vernier calliper having least count of 0.01 mm. Vernier calliper is a precision instrument that can be used to measure internal and external distances accurately.

3.5.3 Estimation of wear and friction coefficient

In order to estimate the surface strength properties, tribological tests are performed using the standard Pin-on-Disc (PoD) experimental set-up (Ducom, TR-20LE-M5). Figure 3.10 shows the PoD experimental set-up that is used to estimate the wear and friction coefficient of ABS polymer parts manufactured by FDM process. PoD experimental set-up constitutes a pin and a disc. For the current study, the set-up consists of the disc rotating at constant speed for a given

Fig. 3.10 Pin-on-Disc experimental set-up

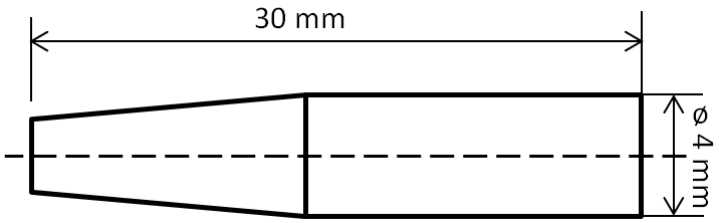

Fig. 3.11 Dimensions of pin used in Pin-on-Disc experimental set-up

amount of time or length of travel. And the pin is held fixed and comes in contact with the disc. A constant force was applied on the pin which in turn exerted on the disc. Computer software enables feeding all the required details of the test run and the actual operation of sliding was closely monitored. The results at the end of sliding test were extracted from the software. In order to estimate wear rate and friction using the sliding wear test on PoD apparatus, pins are manufactured from ABS polymer using the FDM process. The pins are manufactured as per a similar DOE scheme to minimize the number of experiments. Figure 3.11 shows the dimensions of the pin used for the tests. EN 31 steel of hardness RC 62 and roughness (Ra) 0.28-31 μm is used for the disc. The wear rate test parameters and their settings are explained in detailed in Chapter 6.

3.6 Summary

In the present chapter, the material used for specimen and the process used for manufacturing the specimens are explained. The DOE technique and the DOE specific scheme used in the present work, namely FCCCD are explained. A detailed discussion on the manufacturing procedure of the ABS polymer test specimens is presented. Test specimen preparations to estimate each of the quality responses have been discussed. Key measurement techniques involved in estimating the quality characteristics like strength, volumetric shrinkage and the tribological properties like wear rate and friction coefficient have been detailed. The present chapter also discusses about the evolution of parts, through various stages by neck formation both in inter and intra layer configurations.

With this fundamentals of evolution of neck growth, the next chapter discusses as how the neck growth contributes to the strength of the parts produced by the FDM process. The discussion starts with the complete understanding of neck growth that forms a basis for strength, followed by manufacturing of the test specimens (as per the DOE plan), testing, interpretation and the discussion of the results. The next chapter also discusses the modeling of neck growth between the filaments as obtained through mathematical approach. Finite element simulation for the neck growth has been attempted and the obtained neck sizes are interpreted.

Chapter 4

Modeling of Neck Growth between the Filaments

4.1 Introduction

The previous chapter highlighted the various stages of part manufacture. It was established that the neck growth between the inter-layer and intra-layer bonding are important since they decide the key properties of the part manufactured. Also from the review of literature it is quite evident that a clear understanding of the nature and extent of neck growth through the inter-layer and intra-layer bonds are crucial in understanding the properties like strength, dimensional stability, surface roughness etc. FDM parts essentially consist of strongly, yet partially, bonded cylindrical filaments, rather than spherical particles, of the build material. It is also evident from literature survey that the relationship between macroscopic strength of a FDM part and microscopic neck-sizes between the filaments has not been studied considering the filaments to be cylindrical in shape. The present chapter is aimed at bridging these gaps by studying the relationship of neck-sizes between cylindrical filaments and macroscopic strength of the FDM parts. The chapter is discussed in three sections. The first section details about the exper-

imental work in understanding the strength as contributed by the neck growth. Second section details on mathematical evolution of the neck growth and the resulting theoretical strength due to neck formation. The theoretical strength so obtained has been compared with the strength as obtained through experiments, with the purpose of validation of the mathematical model introduced in this thesis. And finally this chapter discusses estimation of the evolution of neck growth using finite element simulation. The outcome of the present chapter is an important step towards understanding the strength and dimensional changes that occur during neck formation in FDM process.

4.2 Experimental Work

In order to estimate the strength contributed by the bonds between the filaments, a clear understanding of formation and growth of the bond is essential and the same has been analysed. The bi-directional process of bond formation by the two filaments as idealized is shown in Figure 4.1. Since the total time and heat available for intra-layer and inter-layer bonding can be different, two specimens with different orientation of layers have been considered to investigate the effect of orientation on the macroscopic strength of the specimen.

4.2.1 Specimen manufacturing

As already discussed Stratasys' Dimension series uPrint FDM machine is used for manufacturing the specimens with a pre-planned orientation, so that one specimen has its layers perpendicular to the loading direction whereas the other specimen has its layers deposited parallel to the loading direction. In order to evaluate the macroscopic strength of the FDM manufactured parts, two types of specimens are manufactured as per the ASTM D638-10 standard, which has been discussed in the earlier chapter. The test specimens are manufactured using the

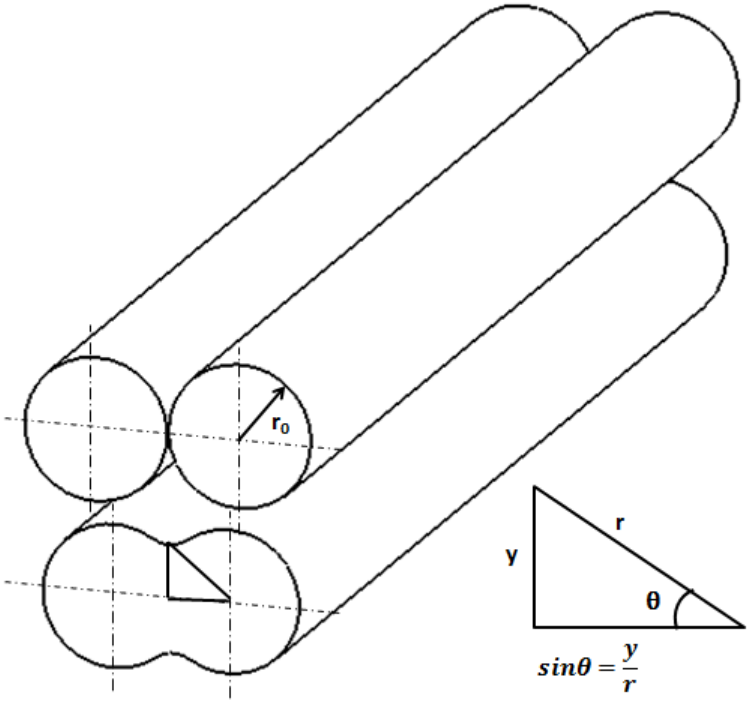

Fig. 4.1 Stages of bond formation in FDM process

configuration mentioned in two orientations to facilitate the prediction of contribution of the intra-layer and inter-layer bond to the strength. The details of the same are shown in Figures 4.2a and 4.2b. In order to minimize the effect of noise in experiments, four repetitions of tensile test on each configuration of specimens are conducted. The test specimens have been fabricated with solid fill option so that they are manufactured with maximum material density.

4.2.2 Tensile testing of the specimens

All the test specimens as manufactured by the FDM machine are then tested for ultimate tensile load. The testing has been conducted as per the recommendations of ASTM D638-10. Tests are conducted at 25 ± 5^0C and the RH as $50 \pm 5\%$. Load versus displacement graphs have been obtained for all the test specimens. The details of the specimen dimensions, UTM machine and its accessories have already been discussed in the earlier chapter.

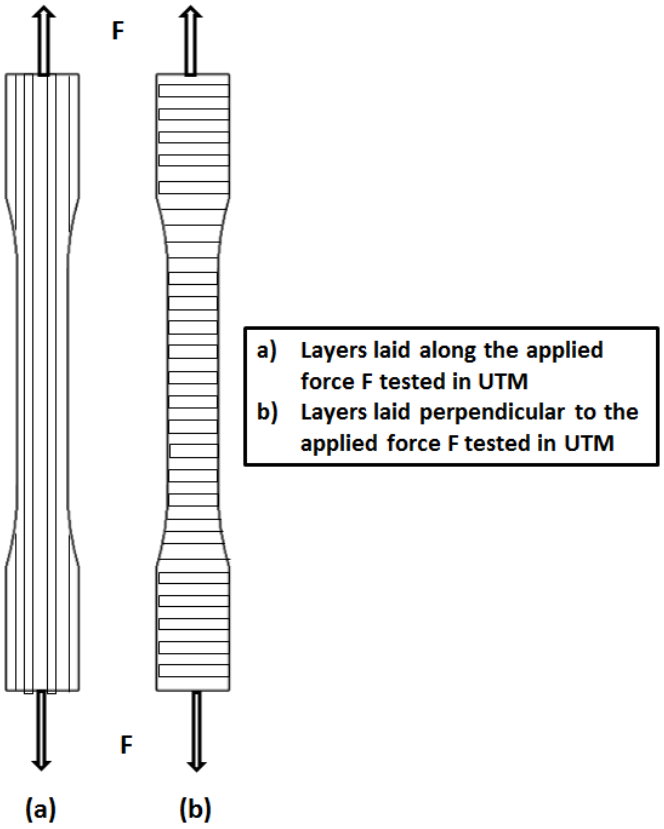

Fig. 4.2 Layers deposited in two orientations

4.3 Mathematical Model of Neck Growth between Filaments

4.3.1 Background of the mathematical modeling

Mathematical model for neck growth between two adjacent cylindrical filaments is derived based on viscous sintering phenomenon. In this work, the models of Frenkel [30] and Pokluda et al. [68] for spherical particles have been re-derived for cylindrical filaments to establish the relationship for the time dependence of neck-size between any two adjacent filaments in the part, treating it as average neck-size for all the filaments in the part.

FDM is a complicated process and hence it is difficult to mathematically model the process without any assumptions. One of the causes for complexity is that the

material is continuously deposited resulting in a transient heat and mass transfer system. Moreover, the flow of molten ABS is non-Newtonian flow. Since the primary interest in the present work is to predict the neck growth between the filaments, it is assumed for mathematical modeling purposes that the full-length filaments are already in place adjacent to each other and that the neck growth evolves as the heat is dissipated from maximum temperature value of filaments to the chamber temperature. For the sake of simplicity and to avoid non linear terms, the material flow is assumed to be Newtonian fluid. A two-dimensional model of two adjacent cylindrical filaments are considered for analysis. Several mechanisms are found to be responsible for the neck growth between the filaments, including, viscous sintering and diffusion. The sintering of the adjacent filaments is mainly driven by physical need of minimizing the free energy of both of the filaments resulting in reduction of surface area. Viscous sintering is reported to be the most predominant mechanism in the neck growth for most polymers and hence the same has been assumed to hold good in the present work also. The energy gained by surface reduction is dissipated by viscous flow, which sets the time scale for sintering. Frenkel [30] mentioned that, provided heat is available for sufficiently long time, two spherical particles may ultimately coalesce into a single spherical particle of larger radius. The balance of the work of surface tension and work of viscous dissipation was considered while neglecting the effect of gravity and various other external forces. Based on this methodology, Pokluda et al. [68] derived the model for the time rate of change of neck growth for spherical particles which Bellehumeur et al. [9] applied to rota-moulding process and obtained acceptable results.

4.3.2 Mathematical modeling

To mathematically model, the evolution of neck growth is derived by first considering the neck formed between two cylindrical filaments. It is assumed that the neck formed between any two filaments either in inter-layer or intra-layer is considered to be same. Once the effective growth of neck in the filaments is derived, the net effective neck growth in the specimen shall be the sum of the neck growths across the specimen. Consider an initial radius and length of a filament as r_0 and l_0, respectively assuming that the change in length to be negligible. As the viscous sintering process proceeds from the time of deposition to the time of solidification, the instantaneous radius of the filament at any given time t is r and any two adjacent filaments establish bonds and grow a bridge called as 'neck' with an instantaneous half-angle of θ and half-neck-size y equal to

$$y = r * sin\theta \tag{4.1}$$

Once the sintering has started, and after some time t, the two filaments might have coalesced. For volume constancy, equating the sum of the volumes of the two adjacent cylindrical filaments at $t = 0$ (before coalescing) and at time t (after coalescing), the relation between the radius of the filaments after time $t(r)$ and the initial radius of the filaments (r_0) is obtained as

$$r = \frac{r_0 * \sqrt{\pi}}{\pi - \theta + \sin\theta * \cos\theta} \tag{4.2}$$

Once the filaments are in contact with each other, the instantaneous net surface area (S) at time t is expressed as the total neck size ($2 * y$) times the length of the filament (l). It can be written as

$$S = 2 * l * r * \sin\theta \tag{4.3}$$

Frenkel's model of sintering has been derived by assuming that the work of surface tension (W_s) is equal to that of the viscous dissipation (W_v) keeping all other forces like gravity as negligible Frenkel [30]. The work of surface tension of the particles coming in contact with each other under the influence of surface tension is given as

$$W_S = -\Gamma * \frac{\mathrm{d}S}{\mathrm{d}t} \tag{4.4}$$

where Γ is the coefficient of surface tension. Work of surface tension (W_S) is obtained by substituting equation 4.3 in equation 4.4. Expressing the total surface area (S) in terms of only (r_0) and evaluating the differentiation with respect to time t, the work of surface tension is obtained as

$$W_S = 2 * \Gamma * \sqrt{\pi} * r_0 * \left[\frac{(\pi - \theta)\cos\theta + \sin\theta}{(\pi - \theta) + \sin\theta * \cos\theta}\right] * \dot{\theta} \tag{4.5}$$

where

$$\dot{\theta} = \frac{\mathrm{d}\theta}{\mathrm{d}t} \tag{4.6}$$

Assuming the flow of the material between the filaments to be a Newtonian flow, the work of viscous forces can be expressed as

$$W_V = \oint 3 * \eta * \dot{\varepsilon}^2 * dV \tag{4.7}$$

where η is the viscosity of the material, V being the volume of the sintering system i.e., the combined volume of the two cylindrical filaments and ε as the strain rate. Relating the Frenkel's model of obtaining the strain can be derived as

$$\dot{\varepsilon} = \frac{(\pi - \theta)\sin\theta}{[\pi - \theta + \sin\theta\cos\theta]} \tag{4.8}$$

Now, substituting the strain rate values in the work of viscous forces equation (Equation 4.7) and performing the volume integral, the work of viscous forces can

be deduced as

$$W_V = 6 * \pi * r_0^2 * l * \eta * \left[\frac{(\pi - \theta)^2 \sin^2 \theta}{[\pi - \theta + \sin\theta \cos\theta]^2} \right] * \dot{\varepsilon}^2 \tag{4.9}$$

As mentioned earlier and by the assumption of equating the work of surface tension (as mentioned in Equation 4.5) to the work of the viscous forces of the sintering system (mentioned in Equation 4.9), the value of the rate of change of the neck formed is obtained as

$$\dot{\theta} = \frac{d\theta}{dt} = \frac{\Gamma}{3 * \sqrt{\pi} * r_0 * \eta} \left[\frac{[(\pi - \theta)\cos\theta + \sin\theta]\sqrt{[\pi - \theta + \sin\theta * \cos\theta]}}{(\pi - \theta)^2 * sin^2\theta} \right] \tag{4.10}$$

Rearranging and integrating both sides,

$$\int \frac{\Gamma}{3 * \sqrt{\pi} * r_0 * \eta} dt = \int \frac{(\pi - \theta)^2 * sin^2\theta}{[(\pi - \theta)\cos\theta + \sin\theta]\sqrt{[\pi - \theta + \sin\theta * \cos\theta]}} d\theta \tag{4.11}$$

Assuming that Γ and η as constants in the left hand side of the above equation and integrating the right side of the expression by substitution of equivalent polynomial, the relation between time and half-angle of neck can be obtained as

$$\int \frac{\Gamma}{3 * \sqrt{\pi} * r_0 * \eta} = 0.0034\theta^4 - 0.036\theta^3 + 2.745\theta^2 + 0.3413\theta \tag{4.12}$$

Since obtaining values of the neck size with respect to the time is complex, the neck size can be plotted with respect to the time. Since the values of θ ranges between zero and $\pi/2$, Equations (4.1) and (4.12) are used to observe the variation of neck growth with respect to time. Figure 4.3 shows the plot between the dimensionless time versus dimensionless neck radius. It can be observed that the neck radius grows sharply during the initial stages and then later stabilizes.

4.3.3 Prediction of theoretical ultimate load

The theoretical ultimate tensile load was determined from the information between layer thickness which is a machine specification and the average final neck size between filaments predicted by the mathematical model developed in the previous section. Effective neck area is arrived at by estimating the number of necks formed in the specimen. Finally strength of the part has been estimated by the load taken by the effective neck area. The neck size so obtained is a relation between half-angle of neck θ and time t. This relation now enables us to estimate the simulated ultimate tensile load by evaluating the effective area of the specimen under consideration with an ultimate tensile strength of 33 MPa (as obtained from build material vendor). The neck formed is expressed in terms of the initial radius of the filament and the ultimate tensile load is calculated from the total effect neck area of the specimen. A detailed flow chart as how to obtain the simulation based ultimate tensile load from the half neck angle θ is demonstrated in Figure 4.4. The building resolution i.e., the layer thickness is purely dependent on the size of the filament that is deposited during the model building. Hence the procedure to obtain the ultimate tensile load is very well applicable for any FDM machine irrespective of any building resolution. For the current work, the building resolution is taken as 0.254 mm.

The values obtained from the experiments are plotted along with the simulation based ultimate tensile load as derived from the evolving neck size with respect to the dimensionless time are mentioned in the Table as mentioned in Appendix A. Figure 4.5 provides the details of the experimental and simulated load values as obtained through the procedure mentioned in Figure 4.4.

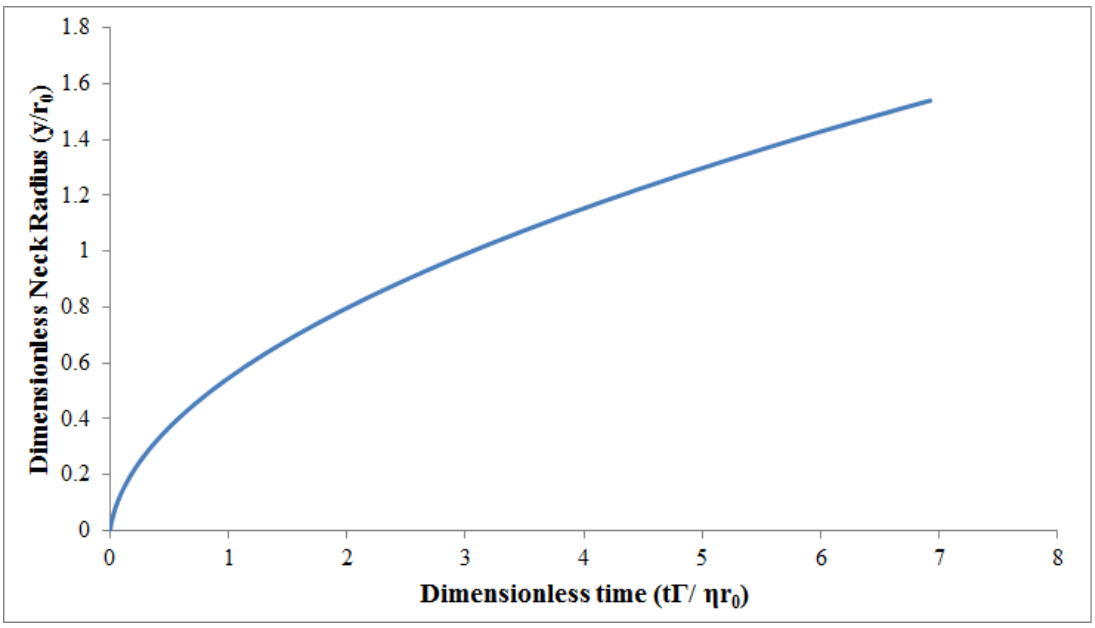

Fig. 4.3 Dimensionless neck radius vs dimensionless time

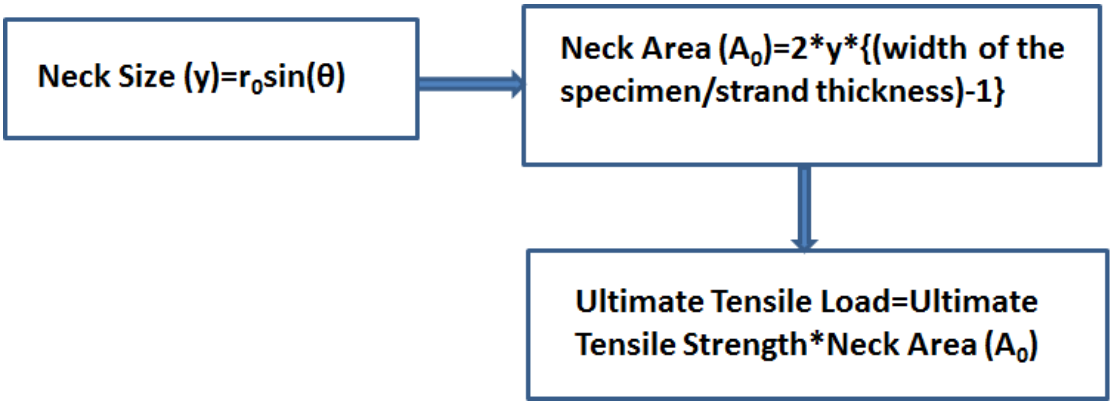

Fig. 4.4 A procedure to evaluate the ultimate tensile load using theoretical neck size

4.4 Finite Element Simulation of Neck Growth in FDM process

Although the mathematical model and simplified numerical solutions of it are able to predict the neck growth accurately, they nevertheless involve some simplifying assumptions. A finite element method based analysis is believed to more accurately predict the neck growth do its well known potential to include geometric non-linearities associated with transient contact between the filaments.

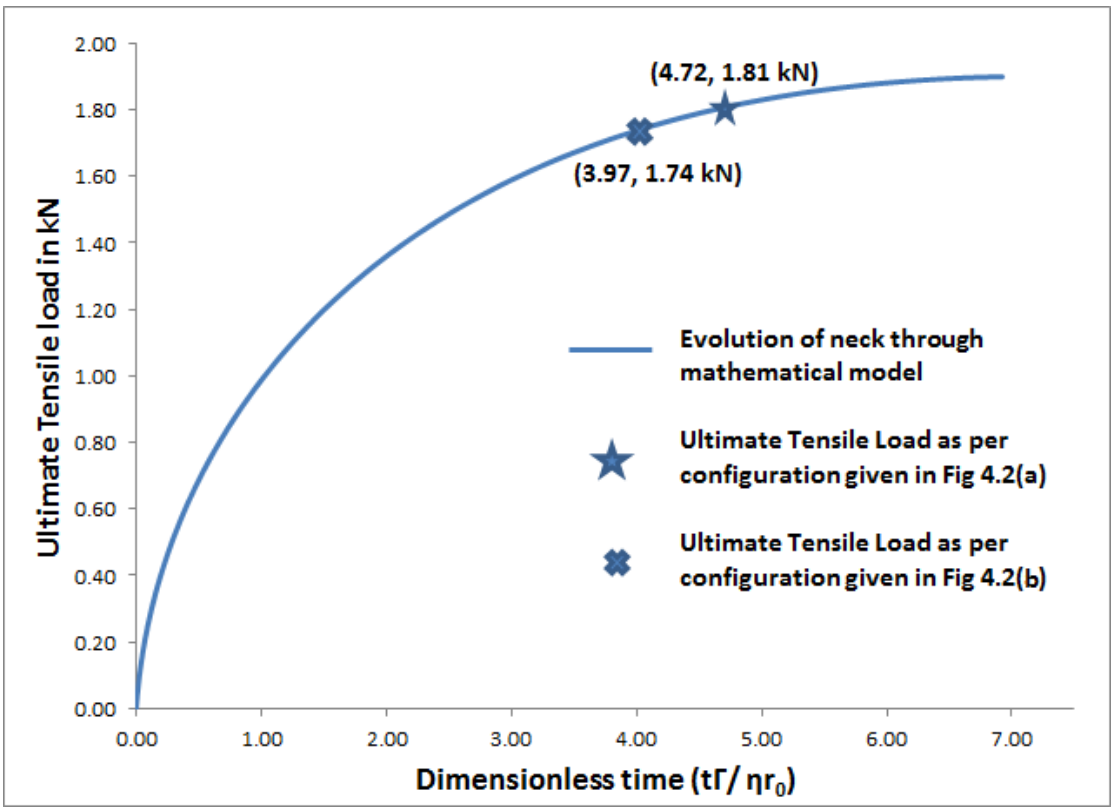

Fig. 4.5 Ultimate tensile load vs dimensionless time ($t\Gamma/\eta r_0$)

4.4.1 Problem definition

The evolution of the neck growth is the resultant of the coalescence of the two filaments into one filament. It has been learned from the literature study that the two filaments come in contact to each other due to sintering operation. ABS plastic consists of many polymer chains which are orientated randomly with in the given structure. In FDM process, the molten ABS is made through the nozzle and is being deposited on the bed layer by layer. As the molten ABS cools rapidly from its melting temperature to the FDM machine chamber temperature, depending on the availability of the energy, the filaments which are being deposited one besides other or one over the other, come in contact with each other. This results in coalescence. Necks result during this coalescence and acts as a fundamental unit towards the quality characteristics of the parts produced. The present thesis aims at predicting this neck growth due to the multi-physics involved during sintering

operation using the finite element technique. ABS is a thermoplastic material and behaves like viscous fluid at temperatures near to melting temperature.

4.4.2 Assumptions

The following are the assumptions made in the current finite element analysis (FEA) of neck growth.

1. The filaments are considered to be cylindrical in shape. A two-dimensional plane strain model for prediction of intra-layer bonding and neck growth is assumed. It is assumed that the extent of neck growth in the inter-layer bonding is exactly similar to that in the intra-layer bonding.

2. The filaments are considered to have already been deposited one beside the other.

3. The material properties of general ABS available in (Robert [73],James [37], Wang et al. [103]) have been used in the model because the properties of the actual FDM material namely ABS P400 are not available as it is proprietary material of Stratasys.

4. In the present thesis finite element simulation is being attempted using the viscoelastic constitutive modeling and the viscoplasticity modeling. The complexity in the multi-physics involved has made to understand the necking through these two techniques.

4.4.3 Boundary conditions

The two filaments were considered to be just deposited and the necking between the adjacent filaments have been idealized. The two filaments are deposited on a flat insulator material. The number of degrees of freedom for the insulator has been fixed to zero. Both the quadrants of the filament are free to

deform under the action of deformation due to high temperatures. Initially the filaments were made to touch each other forming a contact pair.

4.4.4 Geometry

For the current finite element simulation, COMSOL Multiphysics® software has been used (Comsol [20]). To minimize the computation time, quarter of the total geometry has been used to leverage the advantage of symmetry. Figure 4.6 shows the model that has been considered. For the current work, the radius of the filament is considered to be $12.7\times10^{-5}m$, which is half of the layer thickness.

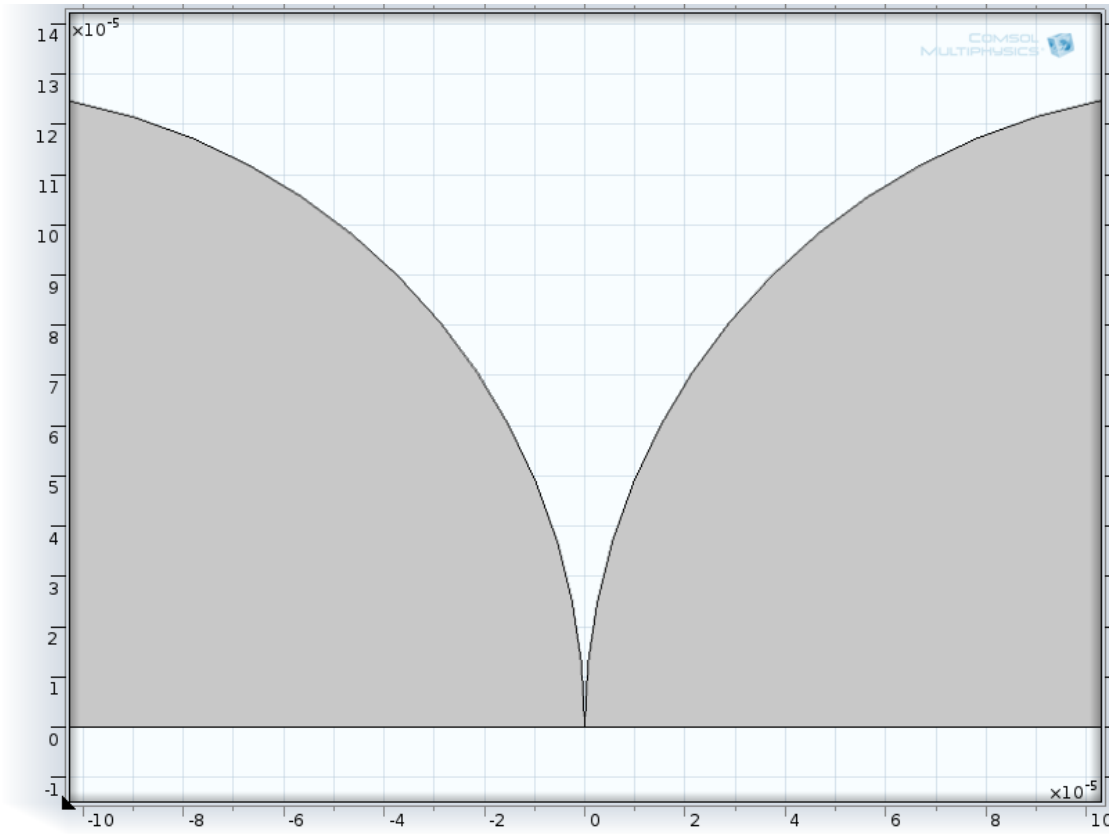

Fig. 4.6 Model under consideration for FEM (all dimensions in m)

4.4.5 Meshing

Filaments were meshed with tetragonal elements. Since the area coming under contact and the coalescence is of interest, fine meshing has been performed along the circular edges. Figure 4.7 details the meshing under consideration.

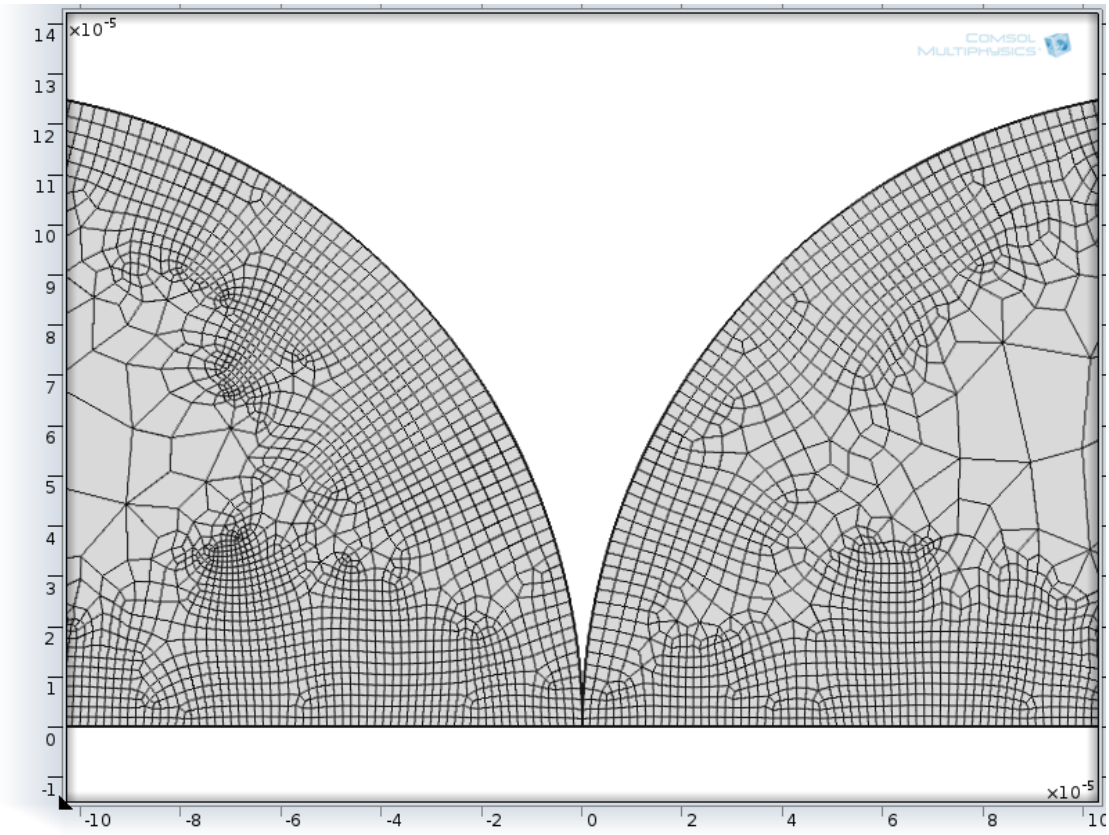

Fig. 4.7 Mesh of the quadrants of the filaments

4.4.6 Material properties

The material properties that were used for the FEM study is listed in Table 4.1. Average melting temperature (T_m) and average glass transition temperature (T_g) are considered as 280^0C and 108^0C are considered for ABS material. 70^0C is maintained for the filaments to cool down inside the uPrint machine chamber.

Table 4.1 Material properties of ABS filament

Name	Value	Unit
Heat capacity at constant pressure	1970	J/(kgK)
Density	1040	kg/m^3
Thermal conductivity	0.15	W/(mK)
Young's modulus	2.28	GPa
Poisson's ratio	0.35	1

4.4.7 Physics considered for the study

Since the neck growth is the resultant of sintering operation, the study involves multiple physics. In order to solve this thermo-mechanical problem, the application of the boundary conditions are divided into two stages.

Stage 1: First the filaments are subjected to heat transfer conditions. The filaments are made to cool from its melting temperature to the chamber temperature in successive intervals of time.

Stage 2: Once the filaments under thermal conditions are being solved, the resultant solution of the heat transfer is coupled with the structural mechanics physics. And during the structural mechanics interface, structural load, that is the load due to gravity has been added to the filaments as a body load. The evolution of the neck growth hence is the resultant of the thermal gradients along with the structural loads due to self-weight. In the present thesis, the present problem has been solved using two approaches namely the viscoelastic problem and viscoplasticity problem. An attempt has been made to solve this viscoelasticity problem using a generalized Maxwell's model of viscoelasticity.

Generalized Maxwell's model of viscoelasticity

In this model, the temperature effects on the viscoelastic stress relaxation is studied with a generalized Maxwell material with four branches. It is assume that the viscous part of the deformation is in-compressible, so that the volume change is elastic. The relaxation shear modulus function is approximated in a Prony series as mentioned in Equation 4.13.

$$\tau(t) = G_0 \left[\mu_0 + \sum_{m=1}^{N} \mu_m exp\left(\frac{-t}{\tau_m}\right) \right] \tag{4.13}$$

where G represents the stiffness of the spring in the respective Maxwell branch, and τ_m is the relaxation time constant of the spring-dash-pot pair in the same branch and the constant μ_m are such that

$$\sum_{m=0}^{N} \mu_m = 1 \tag{4.14}$$

ABS being a thermoplastic polymer, it is highly sensitive to variations in temperatures. With a common assumption is that the material is thermo-rheologically simple, a change in the temperature can be transformed directly into a change in the time scale. Thus, the relaxation time for a ABS material is taken by the shift functions which are taken care by Williams-Landel-Ferry constants. The two Williams-Landel-Ferry constants for ABS material are 17.44 and 51.6 respectively. The ambient temperature of the FDM process is taken 343 K with a surface emissivity of 0.95. Table 4.2 provides the details of the shear modulus constants used for the current study. The finite element simulation is run for the thermomechanical model and the neck growth has been observed (Comsol [20]).

Table 4.2 Generalized Maxwell's model of viscoelasticity

Branch No.	Shear Modulus (Pa)	Relaxation Time(sec)
1	$1e^9$	30
2	$2.19e^9$	300
3	$2.46e^9$	3000
4	$6.85e^9$	12000

Anand's model of viscoplasticity

Anand's model is suitable for isotropic and viscoplastic deformations with a combination of small elastic deformations. The following flow equation takes strain rate dependence on the stress into account(Stuart et al. [95])

$$\dot{\epsilon}_p = Aexp\left(-\frac{Q}{RT}\right)\left[\sinh\left(\xi\frac{\sigma}{s}\right)\right]^{1/m} \tag{4.15}$$

where $\dot{\epsilon}_p$ is the inelastic strain rate, A is the pre-exponential factor, Q is the activation energy, m is the strain rate sensitivity, ξ is the multiplier of stress, R is the Boltzman constant, and T is the absolute temperature. The internal variable s is called deformation resistance, and it obeys the evolution equation

$$\dot{s} = \left\{h_0|1-\frac{s}{s^*}|^a sign\left(1-\frac{s}{s^*}\right)\right\}\dot{\epsilon}_p \tag{4.16}$$

where

$$s^* = \hat{s}\left[\frac{\dot{\epsilon}_p}{A}exp\left(\frac{Q}{RT}\right)\right]^n \tag{4.17}$$

is the saturation value of s, h_0 is the hardening constant, a is the strain rate sensitivity of hardening, s is the coefficient for deformation resistance saturation, and a is the strain rate sensitivity of deformation resistance. The following Table 4.3 shows the model data considered for the viscoplastic behaviour of ABS samples

as per Anand's model.

Table 4.3 Model data for the viscoplastic ABS samples

Property	Value	Description
A	1.49×10^7	Pre-exponential Factor
Q/R	10,830 K	Activation Energy/Boltzmann Constant
m	0.303	Strain rate sensitivity of stress
n	0.0231	Sensitivity for deformation resistance
a	1.34	Strain rate sensitivity of hardening
s	80.42 MPa	Coefficient for deformation resistance saturation
s_0	56.33 MPa	Initial value of deformation resistance
ξ	11	Multiplier of stress
h_0	2640.75MPa	Hardening constant
T_0	550K	Initial Temperature

4.4.8 Post-processing of the results

Figure 4.8 shows the result of the total displacement of the two filaments after performing the finite element analysis using Generalized Maxwell's model of viscoelasticity. The neck growth estimated using this model is $5.13x10^{-5}m$. Arrived neck growth is for a quarter model of the original filaments. Assuming symmetry, the total neck growth of the two filaments is $10.26x10^{-5}m$. Similarly, neck growth estimated using the Anand's viscoplasticity model is $3.65x10^{-5}m$. Again considering the symmetry, the effective neck growth between the two filaments is $7.30x10^{-5}m$. Figure 4.9 shows the deformed filaments with the formation of neck between the two filaments. The values of the neck growth as obtained through the FEM models will be correlated with that as obtained from necks formed due to sintering process as mentioned in the SEM micrographs explained in subsection

5.4.2 of Chapter 5.

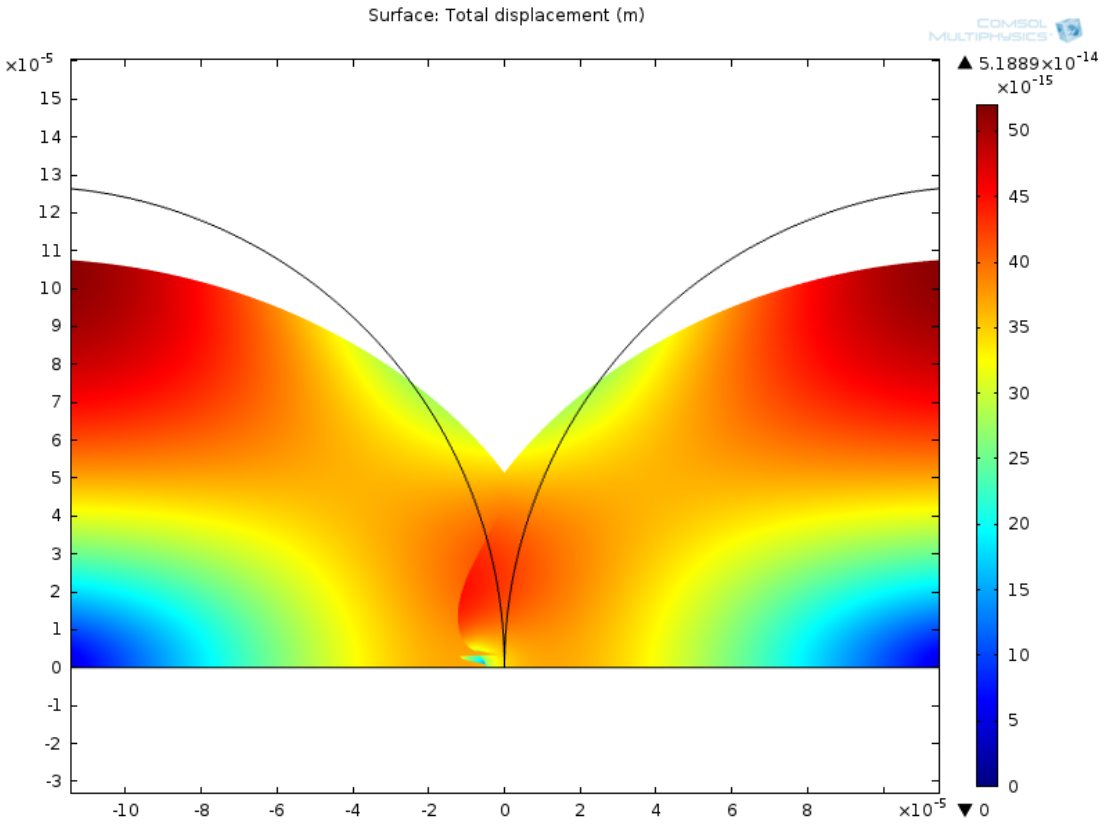

Fig. 4.8 Evolution of neck growth using Maxwell's model

4.5 Results and Discussion

The averages of the ultimate tensile load values for the two configurations as shown in Figures 4.2a and 4.2b are estimated as 1.81 kN and 1.74 kN, respectively. Table 4.4 shows the values of the ultimate tensile load of four samples. The average values are close to the ultimate tensile load of 1.92 kN for ABS reported by Rodríguez [76].

It is clear from this data that the commonly held notion that the strength of the parts manufactured through FDM process in the build direction is lower than that in the transverse direction is supportable because the average strength in

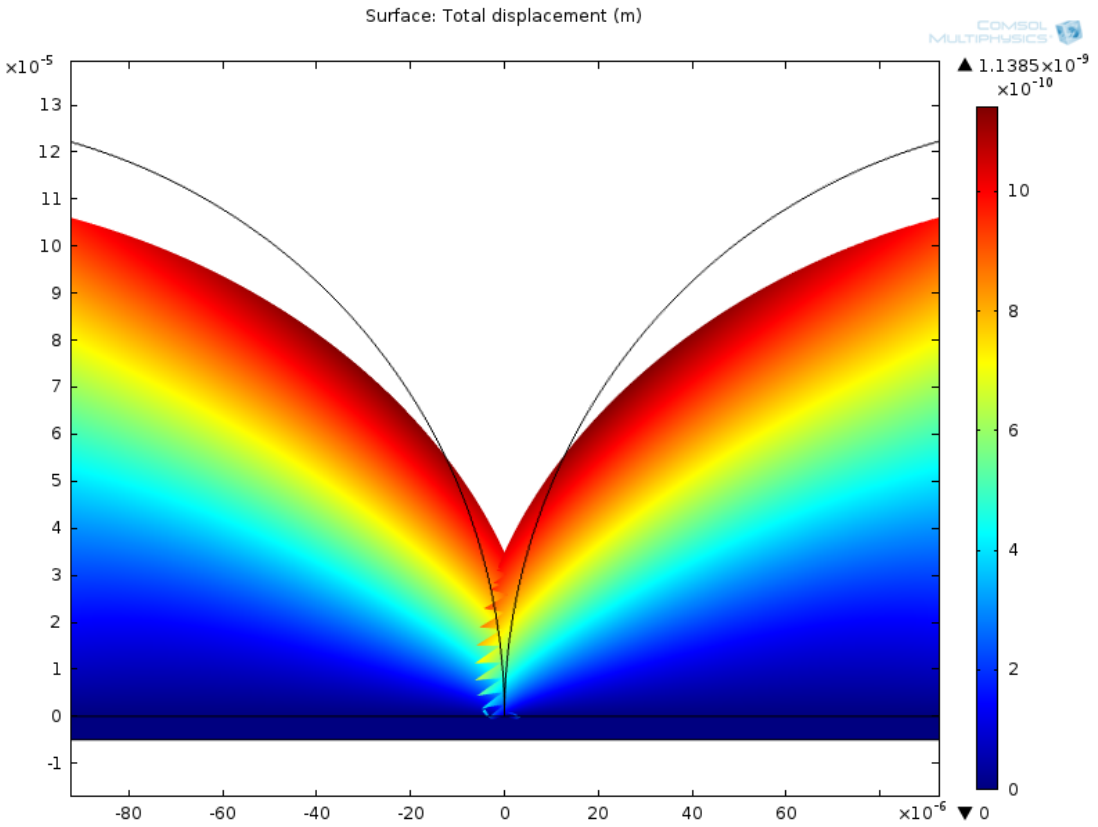

Fig. 4.9 Evolution of neck growth using Anand's model

intra-layer testing configuration is higher than that in the inter-layer testing configuration. What is more important to observe though is that the difference of tensile strength in the two configurations is only marginal which is clear from the average values and the standard deviation for each configuration as given in the Table 4.4. Owing to this reason, the mathematical model, the results of which are presented and discussed later in this section, can be applied to any of the two configurations.

Figure 4.3 shows the variation of the dimensionless neck radius as a function of the dimensionless time. The minimum and maximum values of the dimensionless time considered here are indicative of the actual time period for which active neck growth is possible before the filaments fully solidify. This is evident from the asymptotic nature of this curve to a value of dimensionless neck radius of about 1.5, which is almost same as the theoretical value of 1.414, obtained from volume

Table 4.4 Ultimate Tensile Load (kN)

Specimen No	Intra-layer (Figure 4.2(a))	Inter-layer (Figure 4.2(b))
Specimen 1	1.82	1.78
Specimen 2	1.81	1.68
Specimen 3	1.82	1.72
Specimen 4	1.81	1.77
Average Tensile Load	1.8165	1.74
Standard Deviation	0.007	0.042

constancy.

$$2 * \pi * r_0^2 * l = \pi * r_f^2 * l \tag{4.18}$$

Rearranging the above equation, we get

$$\frac{r_f}{r_0} = \sqrt{2} = 1.414 \tag{4.19}$$

However, it needs to be noted that the actual time period for which the sintering takes place in an FDM process depends on the actual heat transfer boundary conditions and the geometry of the part. Therefore, as it will be evident from the discussion that follows, in the present FDM process there was not enough time for complete coalescence though some previous work on rotational molding reported that such coalescence of spherical ABS powder particles is possible. Figure 4.3 demonstrates the fact that the initial neck growth rate is substantial due to presence of heat until a suitable time has been elapsed. Beyond this time range, the growth rate of the necking decreases to finally become asymptotic to the final value. Once a relation between the dimensionless neck radius and dimensionless time has been obtained, the ultimate tensile load can be estimated from the neck size. Figure 4.5 shows the results of the experimental work carried out to obtain

macroscopic part strength and it supports the above fact. It is important to observe that the time required for the two cylindrical filaments for finally coalescing completely into one single filament is not available before complete solidification and cooling to the chamber temperature occurs. As it can be seen in this figure plotted for ultimate tensile load as a function of dimensionless time, the average neck size grows to such level that the sum-mated neck areas times the solid tensile strength of ABS (obtained from build material vendor) approaches a limiting value before the filaments fully solidify, and it is almost equal to the experimentally measured macroscopic strength of the part. This provides an indirect validation to the limiting time of the neck growth. The rate of growth of the neck with respect to the dimensionless time gets stabilized at approximately ($t\Gamma/\eta r_0 = 7.5$). The results also showed that the ultimate tensile load is higher in configuration Figure 4.2a compared to that of configuration Figure 4.2b. Since the extrusion head of the FDM machine deposits the molten ABS material layer-by-layer, the time available at elevated temperature required for the necks to grow is more in configuration of Figure 4.2a because of the broader slices when compared to that in Figure 4.2b.

From the Figure 4.5, the neck radius of the filaments can be estimated through the dimensional-less quantity ($t\Gamma/\eta r_0$) for both the configurations using the Figure 4.3. For the dimensional-less quantities of 3.97 and 4.72, the estimated neck size is approximately 0.116 mm and 0.12 mm respectively. It can now be established with the fact that the approximate neck that grows during these configurations is around 0.116 and 0.12 mm respectively. A rough estimate of the time required for the neck to grow can also be approximated assuming the value of $\Gamma = 0.029 N/m$ and $\eta = 5100 Pa - s$ measured at $240^0 C$ with an assumption of initial radius of the filament when it deposited as 0.127 mm, the neck growth between the filaments can be arrived for both the configurations mentioned in Figure 4.2 (Bellehumeur et al. [9]). Substituting the values of dimensional-less quantity along with the

constants and the radius of the filaments, the approximate time required for neck formation is 90.23 and 107.27 sec respectively for the configurations Figure 4.2a and Figure 4.2b. However, the ultimate tensile load predicted by the simulation model is found to overshoot the experimental value in the stabilization zone. Several causes may be responsible for this deviation and the most important are discussed in the following.

1. The first reason may be that the sintering takes place more among the layers deposited in the bottom portion of part because more heat for longer time is available for these layers but the same decreases in the upper layers. Hence there may be more cross-linking of chains of ABS in the bottom layers than in the upper layers whereas uniform levels of sintering have been assumed in the mathematical model.

2. Secondly, when the semi molten ABS filament leaves the extruding nozzle it has circular cross-section. After it is deposited, the circular cross-section is deformed into an oval, of which the actual shape and dimensions depend on the level of interaction with the adjacent filaments. This oval shape has not been taken into account in the mathematical model.

3. Finally, it is predictable as well as evident from the Scanning Electron Microscope (SEM) micro-graph (Figure 4.10) that not every pair of adjacent filaments builds the same size of the neck. In fact, some of the pairs of filaments may not build any necks at all as evident from Figure 4.10. These differences in neck sizes among different pairs of filaments may be primarily due to local variations in temperature as well as differences in localized cooling rate. In the mathematical model, however, uniform size of necks has been assumed.

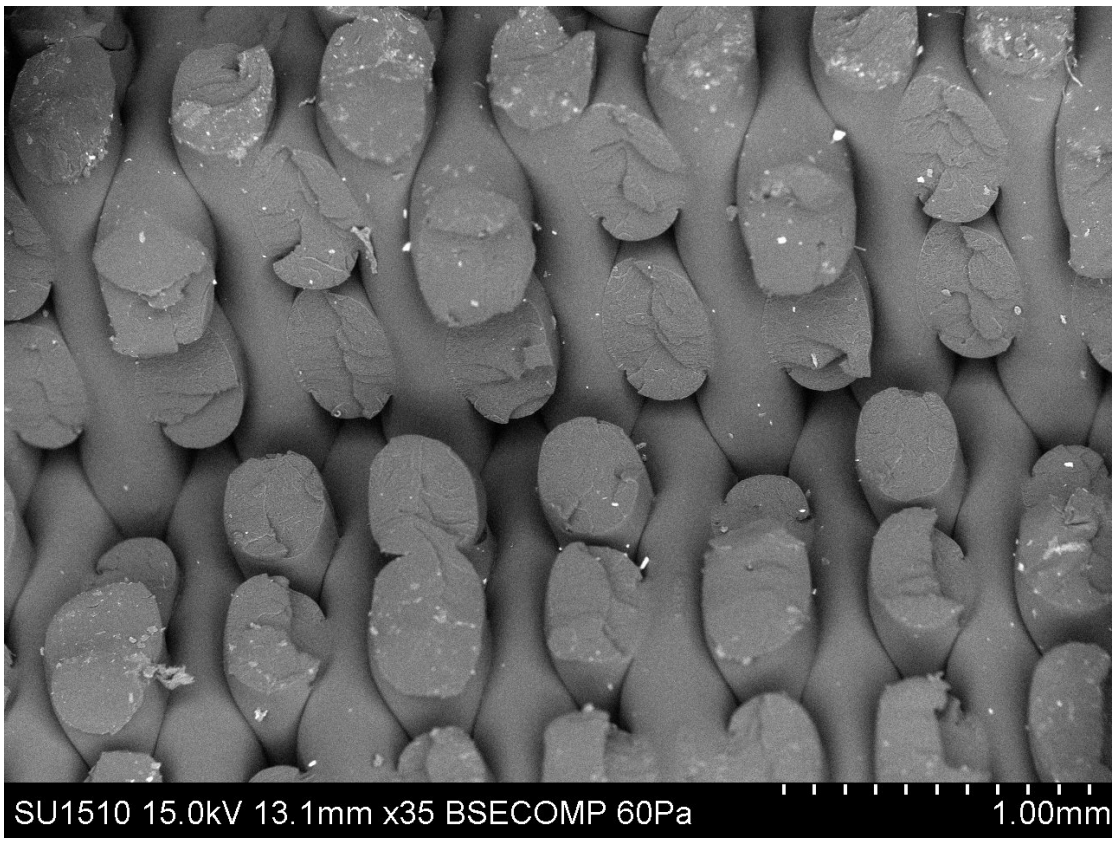

Fig. 4.10 SEM micro-graph showing the necks among some of pairs of strands

The tensile test showed that the failure of the specimen with configuration shown in Figure 4.2a occurs due to inter-layer bonding. Further, the failure of the configuration shown in Figure 4.2b occurred across the layers at roughly 45^0 to the loading direction, involving failure of both intra-layer and inter-layer bonds, though majority the former. The failure of the specimen loaded in the building direction occurred similar to brittle fracture in metals which is due to the separation of the two successive layers. While the failure of the specimen loaded in the transverse direction i.e., the filaments are parallel to the loading direction of the tensile test, the failure occurred at an angle which may be due to reason that the crack might have propagated across the filaments. These two phenomenon of failure can be clearly observed in Figure 4.11.

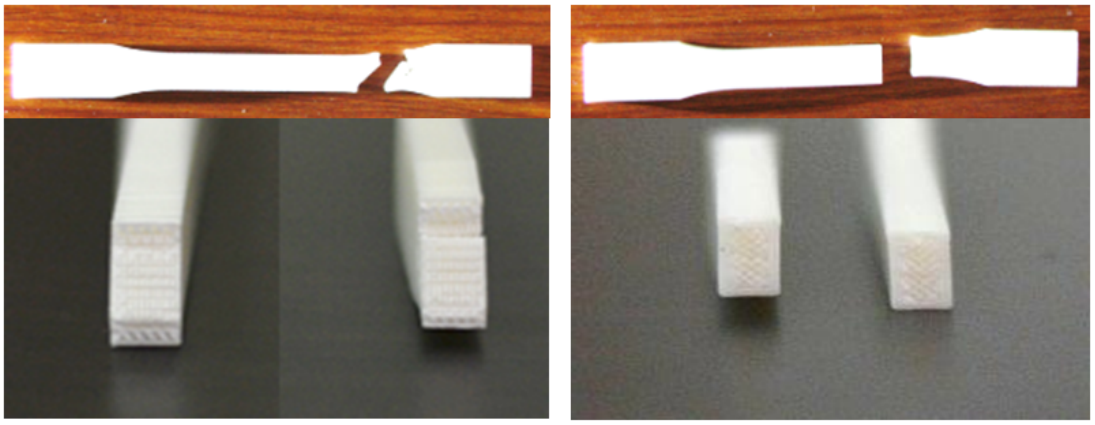

(a) Intra-Layer Bonding (b) Inter-Layer Bonding

Fig. 4.11 Variation of mode of fracture due to inter and intra-layer bonding

4.6 Summary

In the present chapter, modeling of neck growth between filaments has been attempted, derived mathematically through the principles of sintering. In order to establish the relation between the neck growth and strength, simple tension test on specimens of standard size and with two different build directions made by FDM machine are conducted. Ultimate tensile load is obtained experimentally. Theoretical ultimate tensile load as obtained from the mathematical model is then verified by comparing with that of the experimental ultimate tensile load of the specimen. Agreement between theoretical and experimental ultimate tensile load indicates that the strength of the FDM part is primarily a consequence of intra-layer bonding and inter-layer bonding of filaments. SEM generated micro-graphs of the fracture surface of the specimen indicate that the part strength can be attributed to the necks between filaments. Further, it seems to lend credence to the hypothesis that from the time of deposition to the time of solidification the total time and heat available to the filaments are just sufficient to grow necks of size smaller than radius of the filaments but are not enough to fully coalesce.

It can also be observed that the neck formation results in increase in strength as well as change in dimensions. It is evident from the SEM micro-graphs that the

so called circular cross-section filaments are no more circular rather distorted elliptical. Hence it is observed that a change in dimensions of the part has occurred which is due to necking.

In order to understand fully the dependency of the part evolution i.e., the process parameters/machine settings of the FDM process namely the uPrint machine, the next chapter discusses the effect of process parameters and their interdependency on strength and change in dimensions i.e., volumetric shrinkage due to neck formation. Also the next chapter discusses the multi-objective optimization of two of these prominent quality characteristics using genetic algorithm technique namely NSGA –II.

Chapter 5

Multi-Objective Optimization of Strength and Volumetric Shrinkage

5.1 Introduction

From the previous chapters, it has been established that the neck growth affects not only the strength but also the dimensional stability of the part manufactured. In addition to this, FDM manufactured parts are being increasingly used as final functional parts. Despite their wide popularity and ease of use, AM technologies still stand large opportunity of their parts being improved in various characteristics, particularly the strength and geometric accuracy. As investigated, FDM process produces parts fairly rapidly yet the mechanical properties depend on the various system settings and process parameters and their combinations posing challenging in obtaining optimal values of desired attributes for the part. In FDM process, few of the most important quality related response variables are roughness, stiffness, strength, dimensional accuracy etc., and few of those important process parameters are air gap, raster width, build orientation, build layer

and build profile. Besides understanding how process parameters affect strength and volumetric shrinkage, it is also important to investigate and evolve an optimal solution set i.e., the best possible machine settings parameters that can satisfy both the strength and volumetric shrinkage simultaneously. As per the earlier chapter on literature study on strength, dimensional accuracy and optimization, it was evident that mechanical properties and final geometry of the part are sensitive to the process parameters. Though most of the research work has been done investigating the affect of these parametric dependence, still there is a lot of scope for understanding the fundamentals. Also it has been found that, optimization studies have been limited mostly towards the single objective optimization of FDM process parameters. However, FDM process is a complex system with several process parameters affecting quality characteristics, a multi-objective optimization was found needed for thorough inspection.

With the objectives set to understand the parametric dependence on the response variables and perform multi-objective optimization, the present chapter is devoted to studies related to the experimental design techniques used in arriving at the minimum number of experiments to be conducted to understand the responses. Based on these responses, the ANOVA is conducted to help in identifying the most significant factors that affect the chosen responses. ANOVA also helps in understanding as how the process parameters along with their interactions affect the responses. Once the objectives have been arrived, a genetic algorithm based multi-objective optimization has been performed. The solution set arrived from the multi-objective optimization problem yields the process parameter settings that would determine their effect on optimum values, called the 'Pareto optimal curve', of the chosen quality characteristics. For the current study, the multi-objective optimization problem is solved by a non-dominated sorting genetic algorithm (NSGA-II), a very popular technique using genetic algorithms for solving conflicting objectives. The out-put of the multi-objective problem is a so-

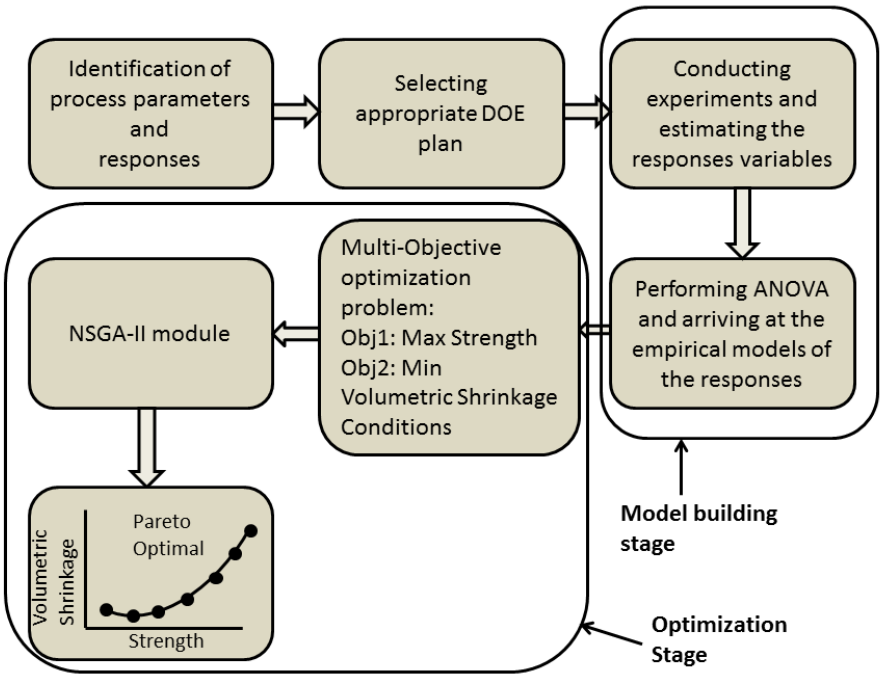

Fig. 5.1 Proposed methodology to arrive at Pareto's optimal curve

lution set that comprises is an optimal parameters solution that relates both the responses namely the strength and volumetric shrinkage. The current chapter is divided into three sections where in the first section describes the methodology adopted to carry out experiments followed by usage of statistical techniques like DOE and ANOVA to arrive at the two objectives. The second section describes the multi-objective problem formulation and implementation of NSGA-II tool. And the chapter closure is done in the third section discussing the results obtained from the current study followed by summary of the entire chapter. The proposed methodology adopted for obtaining the optimal solution set is mentioned in Figure 5.1.

5.2 Methodology

The first step towards the formulating the multi-objective optimization is to design the experiments based on the type of experimental design technique chosen. As already mentioned in Chapter 3 that FCCCD experimental design technique is used in designing the experiments.

5.2.1 Experimental plan and procedure

Based on the literature survey it has been well established that the properties of the part produced using any of the RP technologies typically depend on various process parameters. In FDM, the strength and volumetric shrinkage of the parts produced depend on various key parameters. The three process parameters namely model interior, horizontal direction and vertical direction have been selected. They are defined as follows (Stratasys [94]):

I. Model interior (A, in coded form) defined as the type of fill used for interior of the parts namely solid, full density, sparse density. It defines the quantity of material that will be deposited during the manufacturing of the component.

II. Horizontal direction (B, in coded form): Inclination of the filaments in the X-Y plane of the machine.

III. Vertical Direction (C, in coded form): Inclination of the filaments in the X-Z plane of the machine.

Factors B and C refer to the inclination of the part in the build platform with respect to X, Y and Z axis where X and Y- axis are parallel to the platform and Z- axis is perpendicular to the platform. The above three parameters have been set at the three levels as specified in the Table 5.1.

Test specimens (as mentioned in Figures 3.6 and 3.9 of Chapter 3) are modeled

Table 5.1 Factors and their levels

S.No	Factor	Name	Level Settings		
			-1	0	+1
1	A	Model Interior (Cubic cm)	14.43	17.53	22.72
2	B	Horizontal Direction (Degrees)	0	22.5	45
3	C	Vertical Direction (Degrees)	0	45	90

using the Solidworks™ modeling software. The details of the various level settings for each of the respective experimental run have been mentioned in Table 5.2.

5.2.2 Effect of curl on volumetric shrinkage

As already highlighted in the previous chapters that in FDM process, the parts are manufactured by the combination of both sintering and diffusion operation. Strands are laid at around 270^0C and are exposed to 70^0C because of which the strands may not have sufficient time to diffuse and bond well with the adjacent strands. Due to this phenomenon, there will be a marked difference in the dimensional inaccuracy that may evolve during the part manufacture. From the literature that has been discussed in Chapter 2, and the theory of sintering and diffusion that occurs in FDM process, it is important to understand as how various process parameters may affect the dimensional inaccuracy that may creep in once the models have been fabricated by varying different process parameters. This effect has been studied by highlighting the concept of curl on the dimensional inaccuracy. Curl is defined using the schematic as mentioned in Figure 5.2.

5.2.3 Experimental set-up and measuring instruments

All the 20 models were fabricated with the various level settings as shown in Table 5.2 using Stratasys uPrint™ Stratasys [94]. The manufactured specimens

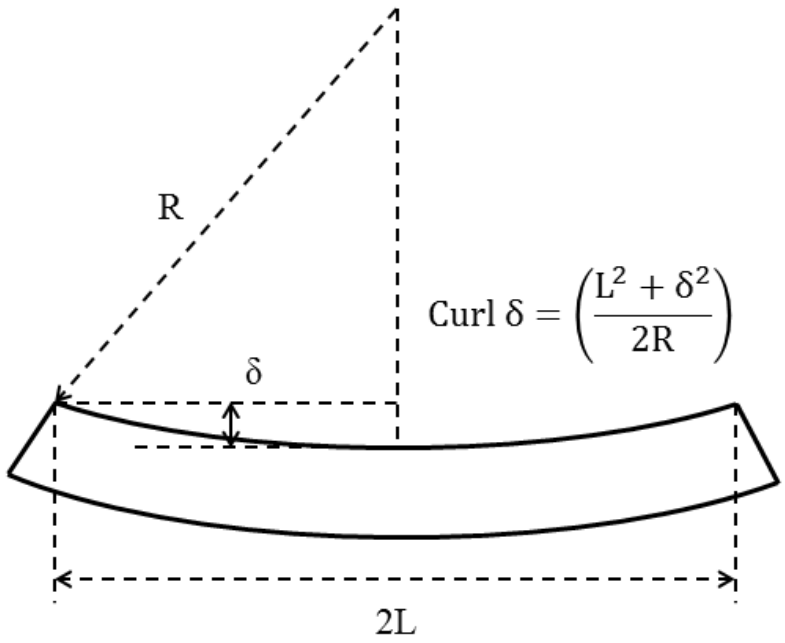

Fig. 5.2 Definition of curl

were then tested for strength using an electromechanical Universal Testing machine. Volumetric shrinkage has been obtained by measuring the dimensions of the fabricated parts using standard laboratory level digital vernier callipers. The following procedure is adopted to evaluate the corrected volumetric change.

Step 1: Measure the length, breadth and thickness of the specimen as mentioned in Figure 3.9 of Chapter 3.

Step 2: The effect of curl has been reported in the measurement of the thickness direction. A Metzer-M binocular stereo zoom microscope (Model METZ - 218/VISION PLUS 7000 BZM) has been used to obtain the microscopic images.

Step 3: The obtained images have been measured for this extra dimension called as 'curl' using Material Plus software. Figure 5.2 provides the microscopic picture of one of the specimens and the evaluation of curl as observed.

Step 4: In order to correct the effect of curl resulting in the measurement of thick-

ness by vernier, the curl as obtained from the software has been subtracted from the thickness. Now the thickness has been adjusted to the original thickness excluding the effect of curl.

Step 5: The new corrected volume change has been evaluated and it is reported in Table 5.2.

The strength and the corrected volumetric change as obtained for various level settings have also been listed in Table 5.2. It has been observed that the volumetric change reported has shown a decrease in volume and hence the volumetric change has been redefined as volumetric shrinkage.

Table 5.2 Experimental Runs of FCCCD

Exp No	A	B	C	Strength (MPa)	Change in Volume (%)	Corrected Change in Volume (%)
1	1	1	1	31.53	7.3	6.88
2	0	0	0	17.15	3.79	3.24
3	0	0	0	18.35	3.99	3.85
4	-1	-1	1	13.28	2.96	2.86
5	-1	1	-1	15.07	3.58	3.48
6	1	1	-1	28.87	6.12	5.90
7	0	1	0	12.86	3.82	2.95
8	0	0	0	18.11	4.45	4.26
9	0	0	-1	27.42	7.02	6.79
10	0	-1	0	10.02	2.48	2.41
11	0	0	1	24.27	6.94	6.48
12	-1	-1	-1	17.25	6.91	6.71
13	0	0	0	16.83	3.73	3.55
14	1	-1	1	28.2	1.2	1.07
15	1	0	0	28.06	4.02	3.77
16	-1	0	0	11.52	4.08	3.98
17	0	0	0	18.29	4.28	4.05

continued ...

... continued

Exp. No	A	B	C	Strength (MPa)	Change in Volume (%)	Corrected Change in Volume (%)
18	0	0	0	17.18	4.97	4.89
19	-1	1	1	17.79	7.76	7.49
20	1	-1	-1	30.13	7.41	7.05

5.2.4 Statistical modeling of experimental data

Statistical models based on second order polynomial equations are developed for the different process parameters using the experimental results. The generated model of strength and volumetric shrinkage helps in interpretation of the process parameters that affect both the response variables. The final equations 5.1 and 5.2 of the models in coded form are thus obtained through ANOVA in terms of coded factors using Design Expert® software (Stat-Ease [93]).

$$Strength = 17.51 + 7.19 * A + 0.73 * B + 1.41 * B * C + 2.50 * A * A - 5.86 * B * B + 8.56 * C * C \quad (5.1)$$

$$Volumetric\ Shrinkage = 3.98 + 0.66 * B - 0.52 * C + 0.41 * A * B - 0.65 * A * C + 1.85 * B * C - 1.32 * B * B + 2.64 * C * C \quad (5.2)$$

Here the factor symbols stand for Model Material (A), Horizontal Direction (B), and Vertical Direction (C). The fit summary recommended that the quadratic model is statistically significant for the analysis of the responses and are subsequently used for the multi-objective optimization. The model equations have been validated and the average relative error between the predicted value from

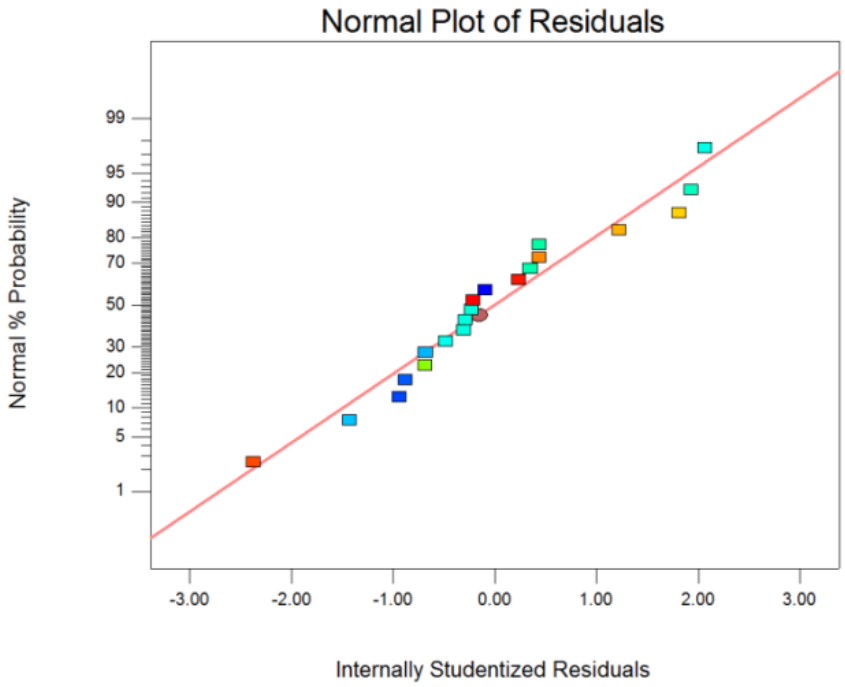

Fig. 5.3 Normal plot residuals for Strength

the model and the values as obtained during experimentation was found to be less than 4.5% and less than 1.5 % for strength and volumetric shrinkage, respectively. The R^2 values for the models have been reported as 0.9662 and 0.9558 for strength and volumetric shrinkage respectively. The normal probability plot of the response variables has been plotted as shown in Figures 5.3 and 5.4. It is quite evident that the errors are normally distributed and the regression model is fairly well fitted to the observed values since the residuals are located on a straight line. The empirical statistical models highlighted in equations (5.1) and (5.2) have been validated and the average relative error between the predicted value from the model and the values as obtained during experimentation was found to be less than 4% and less than 1.5% for strength and volumetric shrinkage respectively. The results indicate that the model is significant and the lack of fit is insignificant. The results of ANOVA for strength and volumetric shrinkage are given in Tables 5.3 and 5.4 respectively.

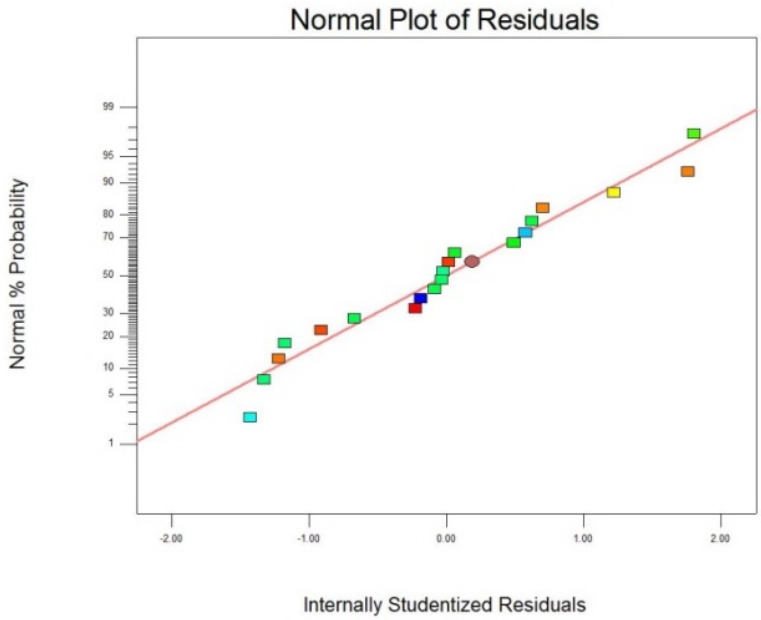

Fig. 5.4 Normal plot residuals for Volumetric Shrinkage

Table 5.3 ANOVA table for Strength response variable

Source	Sum of Squares	df	Mean Square	f Value	p-value Prob > F
Model	848.58	9	94.29	85.26	0.0001
A-Model Interior	516.67	1	516.67	467.2	0.0001
B-Horizontal Direction	5.27	1	5.27	4.77	0.049
C-Vertical Direction	1.35	1	1.35	1.22	0.2956
AB	8.45E-03	1	8.45E-03	7.64E-03	0.9321
AC	0.49	1	0.49	0.44	0.5207
BC	15.9	1	15.9	14.38	0.0035
A^2	17.23	1	17.23	15.58	0.0027
B^2	94.33	1	94.33	85.3	0.0001
C^2	201.42	1	201.42	182.13	0.0001
Residual	11.06	10	1.11		
Lack of Fit	8.8	5	1.76	3.91	0.0806
Pure Error	2.25	5	0.45		
Cor Total	859.64	19			

Table 5.4 ANOVA table for Volumetric Shrinkage response variable

Source	Sum of Squares	df	Mean Square	f Value	p-value Prob > F
Model	64.27	9	7.14	40.24	0.0001
A-Model Interior	0.058	1	0.058	0.33	0.5809
B-Horizontal Direction	5.81	1	5.81	32.72	0.0002
C-Vertical Direction	2.38	1	2.38	13.42	0.0044
AB	1.39	1	1.39	7.86	0.0187
AC	3.46	1	3.46	19.49	0.0013
BC	30.11	1	30.11	169.66	0.0001
A^2	0.23	1	0.23	1.27	0.2852
B^2	3.87	1	3.87	21.83	0.0009
C^2	19.21	1	19.21	108.26	0.0001
Residual	1.77	10	0.18		
Lack of Fit	0.68	5	0.14	0.62	0.6932
Pure Error	1.09	5	0.22		
Cor Total	66.04	19			

5.3 Multi-Objective Optimization Using Genetic Algorithms (GA)

In day-to-day industries, manufacturing processes are dominated with the growing needs for quality, minimal production cost, frequent design changes, complex geometries and most importantly, with short manufacturing times. In order to meet these demands, the manufacturing process setting parameters have to be chosen such that the demands are met in the best possible way. With the increasing capital and manufacturing costs, an economical way to operate these machines as effectively as possible is the order of the day. The selection of the man-

ufacturing process depends upon the selection of appropriate process parameters. Hence the selection of optimum process parameters plays a very important role to ensure that the quality of the product is achieved without compromising with the manufacturing cost along with increased productivity. In this context, optimization of the process parameters is a challenging task. Traditional optimization algorithms are deterministic algorithms. The solutions are obtained using specific rules of moving from one solution to the other. Few of them are namely, nonlinear programming, geometric programming, quadratic programming, dynamic programming, etc. Problems related to manufacturing problems are complex in nature. These are characterized by discrete variables with discontinuous and nonconvex design spaces. In such cases, the traditional optimization techniques fail to perform to provide an optimal global solution since they get trapped in local optimum solution set. Problems like convergence are quite common in traditional optimization techniques. To overcome these problems, non-traditional methods for optimization have been evolved. Non-traditional optimization algorithms are in general stochastic in nature, with probabilistic transition rules. Most of these non-traditional optimization techniques are based on biological, molecular, or neurological phenomenon that imitates natural biological evolution of the species. Few of those non-traditional optimization techniques include genetic algorithm (GA), particle swarm optimization (PSO), artificial bee colony (ABC), shuffled frog leaping (SFL) etc. Out of these GA techniques have gained wide popularity in most of the engineering applications and in specific manufacturing process (Subashini and Bhuvaneswari [96], Venkata Rao [102]). As the name suggests, GA derive their working principle from the natural genetics and natural selection. GAs are used in finding solutions to linear and nonlinear problems by exploring multiple regions of the solution space and exponentially exploiting potential areas through different operators like selection or reproduction operator, crossover operator and the mutation operator. The working principle and algorithm can be found in many popular

books on (Deb [22], Goldberg [34]) and shall be presented briefly. Among many of the GA techniques, NSGA-II has secured wide popularity due to its effective use in most of the additive manufacturing applications (Kanagarajan et al. [39], Chockalingam et al. [16]). The flow chart of the NSGA-II program is shown in Figure 5.5. The first step is a random initial generation. The parents and offspring are combined to form a string. When the objective functions of all strings in a generation are calculated, the solutions are classified into various non-dominated fronts. The crowded tournament selection operator is used to compare two solutions and returns the winner of the tournament according to two attributes: (1) a non-dominated front in the population: This attribute makes sure that the chosen solution lies on a better non-dominated front, and (2) a local large crowding distance. And this attribute ensures a better spread among the solutions. The simulated binary crossover is used to create two offspring from two-parent solutions. The random simplest mutation operator is applied randomly to create a solution from the entire search space. Multi-objective optimization problems give rise to a set of Pareto optimal solutions. Pareto optimal solutions are the solution where no solution said to be better than any other solution when all the objectives are considered. This in turn forms a goal in a multi-objective optimization to find as many such Pareto optimal solutions as possible. Unlike most classical search and optimization problems, GAs work with a population of solutions and thus are likely candidates for finding multiple Pareto optimal solutions simultaneously.

In the present chapter a dual goal multi-objective optimization is being solved. The algorithm helps in finding a set of solutions which are supposed to be as close as possible to the Pareto optimal front. However the diversity of the solutions presented shall be preserved. The two-objective GA optimization method used in the present work is an elitist NSGA-II, using the elite-preserving operator (Deb [22]). The operator favours the best of a population set by providing a chance to be directly taken over to the next generation. The fittest individuals of the

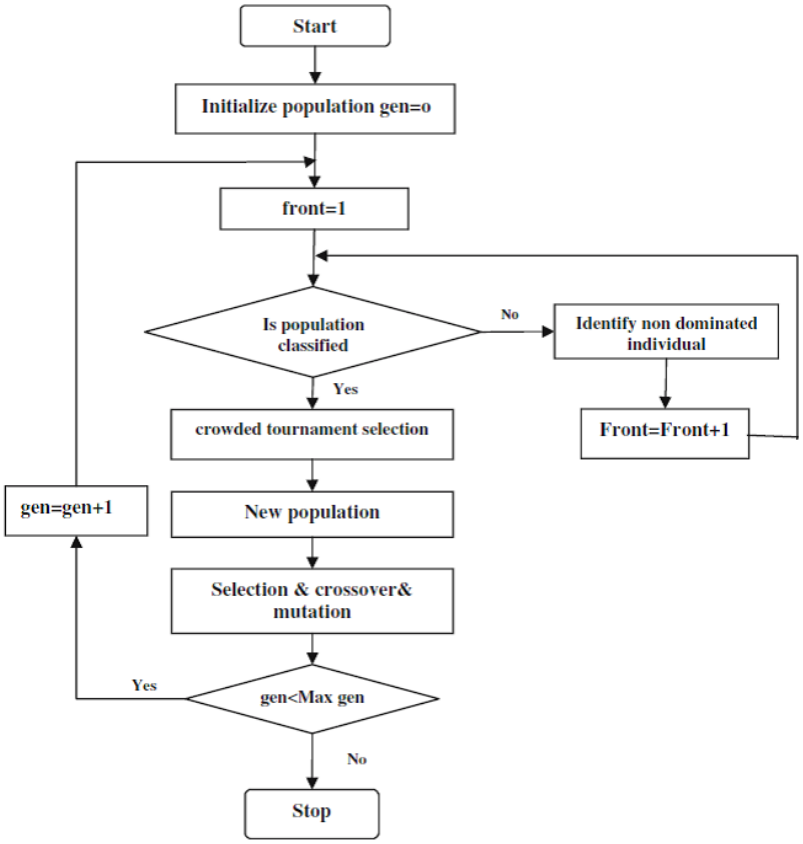

Fig. 5.5 NSGA-II flow chart

population are the solution sets which survive and participate in the reproduction thus improving the successive generations where the good solutions are duplicated and the bad solutions are eliminated in that population. The crossover operator and the mutation operators are applied to create new set of solutions from the good solutions as obtained previously during the selection operator implementation. Indirectly the objective of these two operators is mainly responsible for the search aspect of GAs. In the present thesis, the multi-objective problem has been set-up so as to simultaneously maximize the strength and minimize the volumetric shrinkage. The equations mentioned in equation 5.3 and 5.4 (in coded form) are the objective functions derived from the response variables expressed in equation

5.1 and 5.2 respectively, along with the limiting conditions in equation 5.5.

$$Objective1 : Maximize(Strength) = 17.51 + 7.19 * A + 0.73 * B + 1.41 * B * C + 2.50 * A * A - 5.86 * B * B + 8.56 * C * C \quad (5.3)$$

$$Objective2 : Minimize(Volumetric\ Shrinkage) = 3.98 + 0.66 * B - 0.52 * C + 0.41 * A * B - 0.65 * A * C + 1.85 * B * C - 1.32 * B * B + 2.64 * C * C \quad (5.4)$$

$$Subject \quad to = -1 \leq A \leq 1, -1 \leq B \leq 1, -1 \leq C \leq 1 \quad (5.5)$$

The multi-objective optimization of the objectives given in equations 5.3 and 5.4 has to be optimized simultaneously within the limits as specified in equation 5.5. As mentioned earlier, among the various methods of multi-objective optimization, NSGA-II has been proven to be an efficient technique in multi-objective optimization. As the results of the Pareto's front are heuristic, repeated simulations have been performed to obtain commensurate values for the parameters. Finally, a population size of 100, size of generation as 100, crossover probability of 0.90 and mutation probability of 0.10 have been arrived for the existing problem.

Table 5.5 lists the 100 non-dominated optimal solutions as obtained from NSGA-II program. This table provides information about the various combinations of the process parameters namely Model Interior (A), Horizontal direction (B) and Vertical direction (C) and the possible optimum values of strength and volumetric shrinkage. This solution set is called Pareto optimal solution set. The Pareto optimum set is obtained by simultaneously optimizing both the objective functions for the given process parameters.

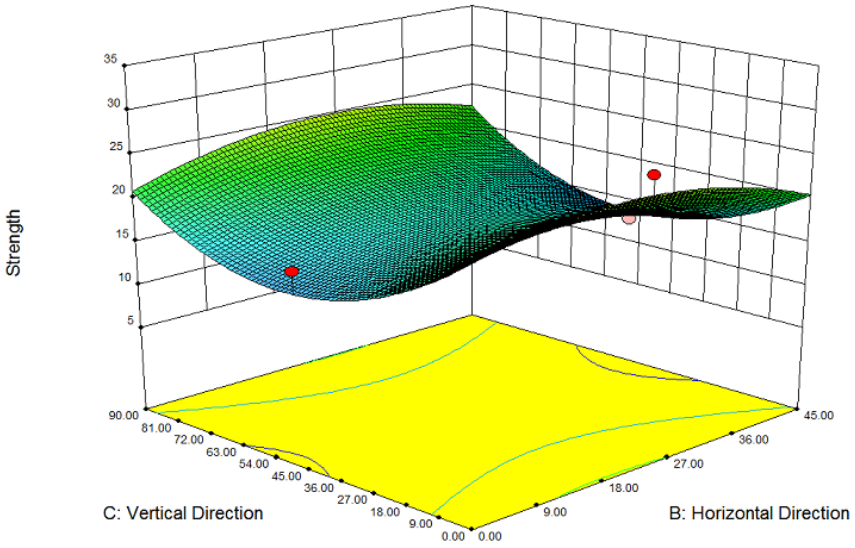

Fig. 5.6 Surface plot of Strength with B, C at A=0

5.4 Results and Discussion

Figure 5.6 depicts the response surface plot of strength, Figures 5.7-5.9 response surface plots of volumetric shrinkage and Figures 5.10-5.14 show the SEM micrographs of the specimens.

5.4.1 Discussion on strength

Figure 5.6 shows the response surface plot of strength as affected by the interaction of parameters B and C with the parameter A held at mid position i.e., 0 (in coded form). Both the process parameters, B (horizontal direction) and C (vertical direction) do not result in any considerable change in strength individually, but their interaction with the model interior shows a clear affect on strength. With the implementation of the multi-objective optimization a better understanding can be evolved. It is observed that the value of A is always equal to 1(in coded form) in Table 5.5 that yielded a maximum strength value with various combinations of the other two process parameters, B and C. This correlates with Figure 5.6 which depicts the minmax situation with the saddle point

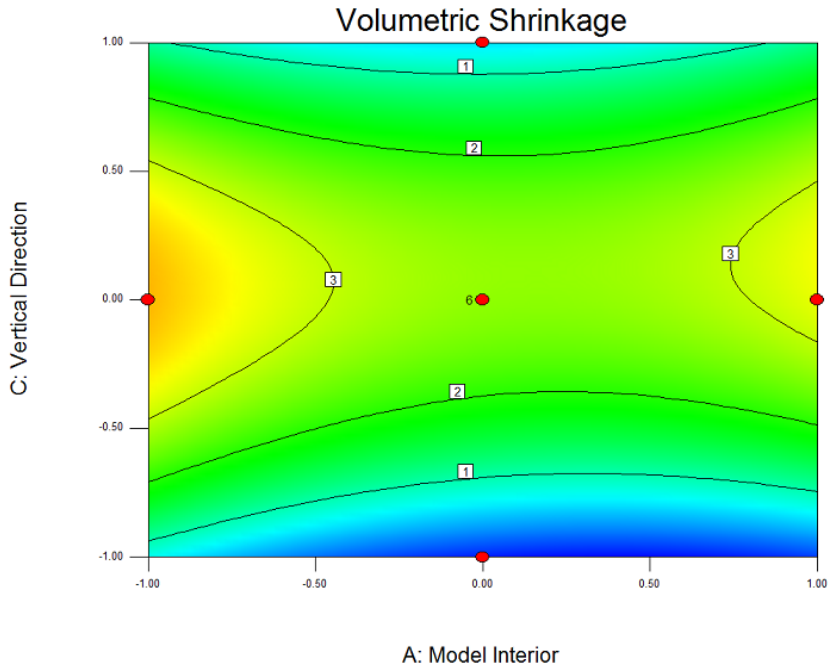

Fig. 5.7 Contour plot of Volumetric Shrinkage with A, C at B=0

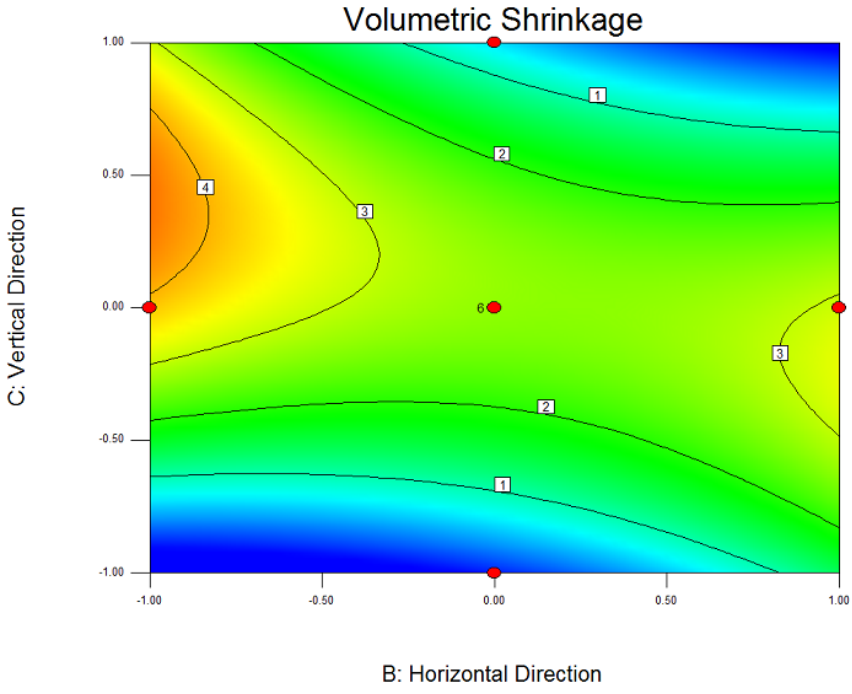

Fig. 5.8 Contour plot of Volumetric Shrinkage with B, C at A=0

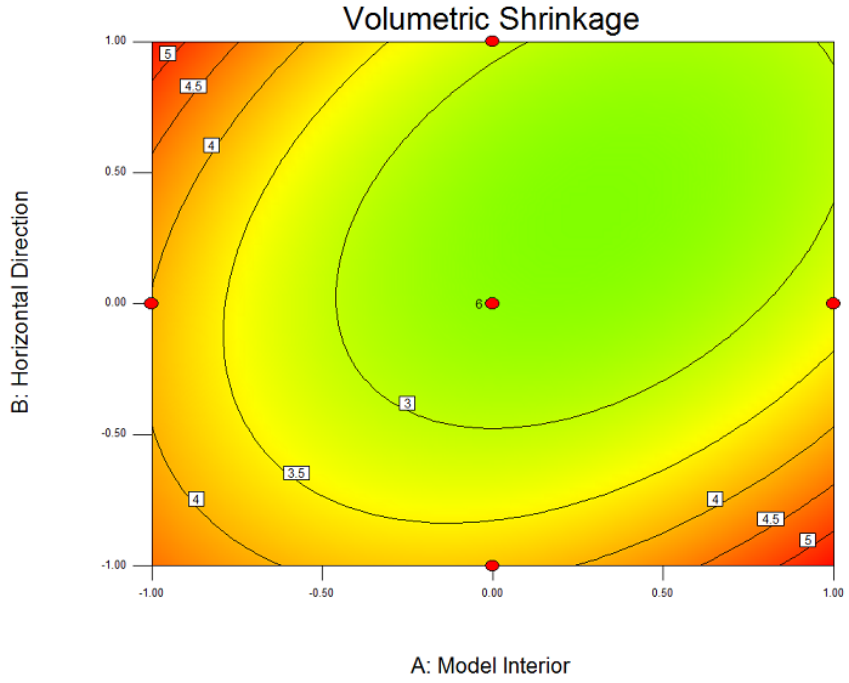

Fig. 5.9 Contour plot of Volumetric Shrinkage with A, B at C=0

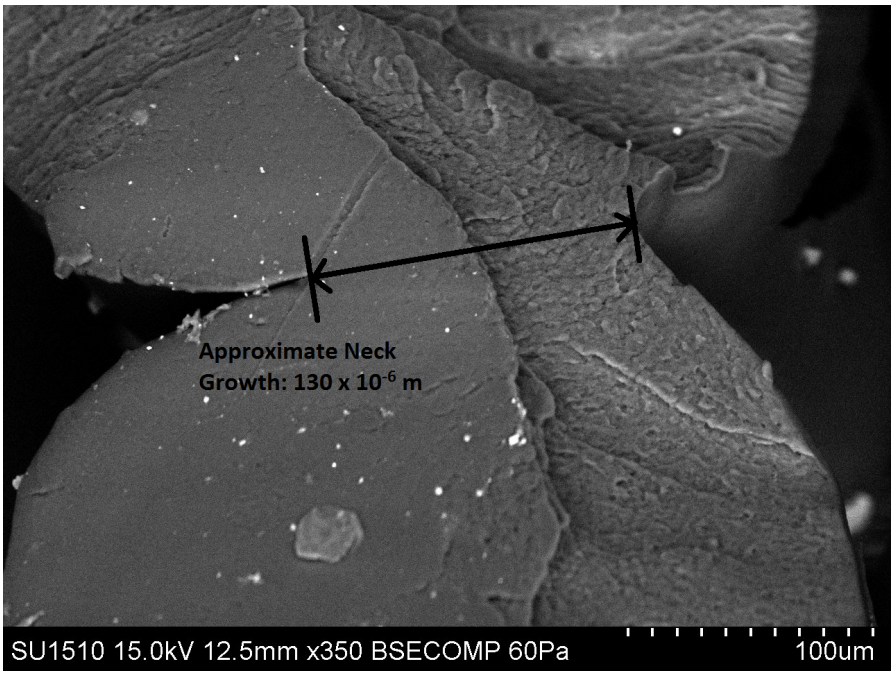

Fig. 5.10 The interaction of two filaments during horizontal built

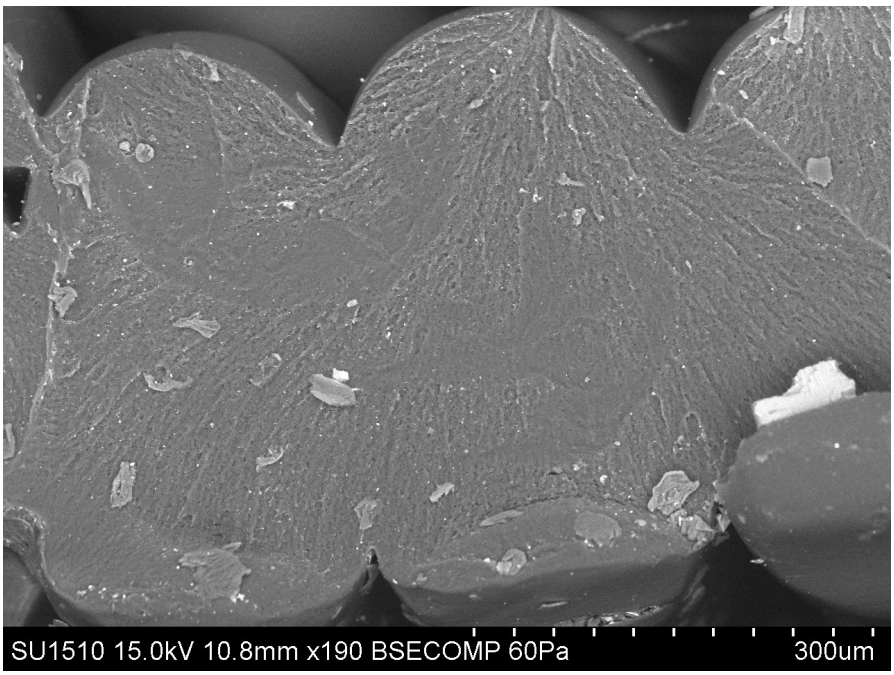

Fig. 5.11 The interaction of filaments during horizontal built

in the mid values of both the factors B and C. Also observing the p-value, it can be interpreted that the effect of interaction of B and C on strength is found to be significant. In addition to that, the affect of B^2, C^2 is significant on both the objectives. From Table 5.5, as C is varied from -1 to 1 (in coded form) the strength increases. When C is set to 1 (in coded form) along with the increase in B, the layers are deposited perpendicular to the direction of loading. This interaction effect of both the Horizontal and Vertical directions will increase the specimens load bearing capacity.

Figure 5.14 depicts the vertical lay where the filaments of one layer get bonded with the next layer due to which the resulting inter-layer bond strength increases significantly. In Table 5.5, B ranges from -1 to 0.18 (in coded form). It indicates that as the angle of the deposition of material along the part contour increases there is a remarkable increase in strength. This may be attributed to the fact that the filaments are more aligned towards the loading condition during testing in universal testing machine. This enables the filaments to take more load when

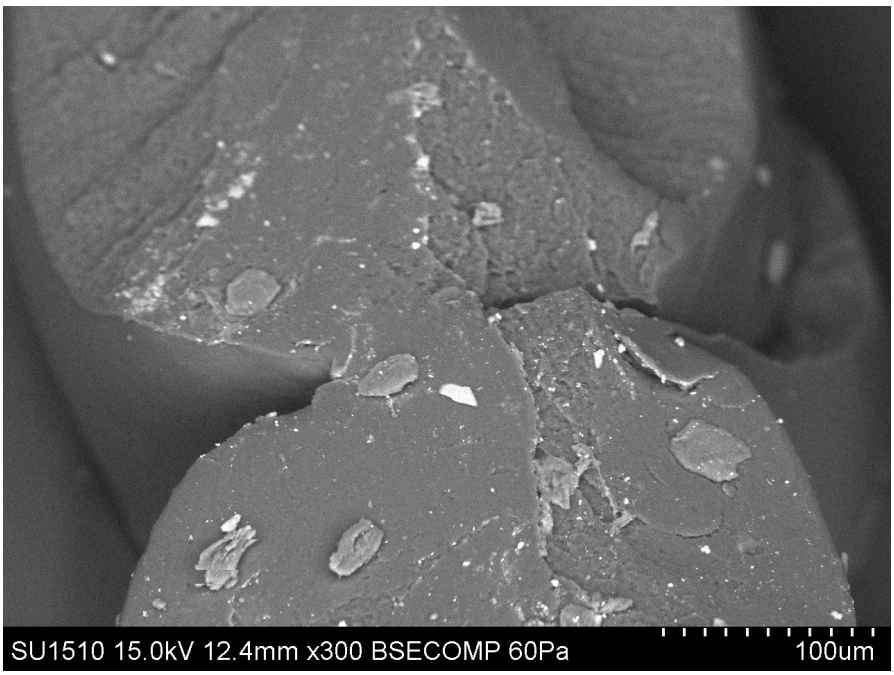

Fig. 5.12 The interaction of two filaments during horizontal built and the approximate neck growth

compared with other two extremities of the filament direction. Strength in bonding between the filaments in a layer is attributed to the load bearing capacity by the effective cross-sectional area of the specimen. As the material volume is increased, the effective area in contact will increase resulting in greater strength. In FDM process, the strength is ideally carried by the circular filaments deposited in the specimen. But it has been observed from the SEM micro-graphs of Figures 5.10-5.12 that the effective area is contributed by not only the circular cross sectioned specimens but also by the oval like cross-section resulting from the overlapping between the adjacent filaments. Due to this phenomenon the effective area in contact increases resulting in increase in strength. Finally, from the ANOVA results and the SEM micro-graphs, it is also established that the interaction between process parameters, i.e., horizontal and vertical build directions affect the layers there by bind themselves resulting in effective area of contact.

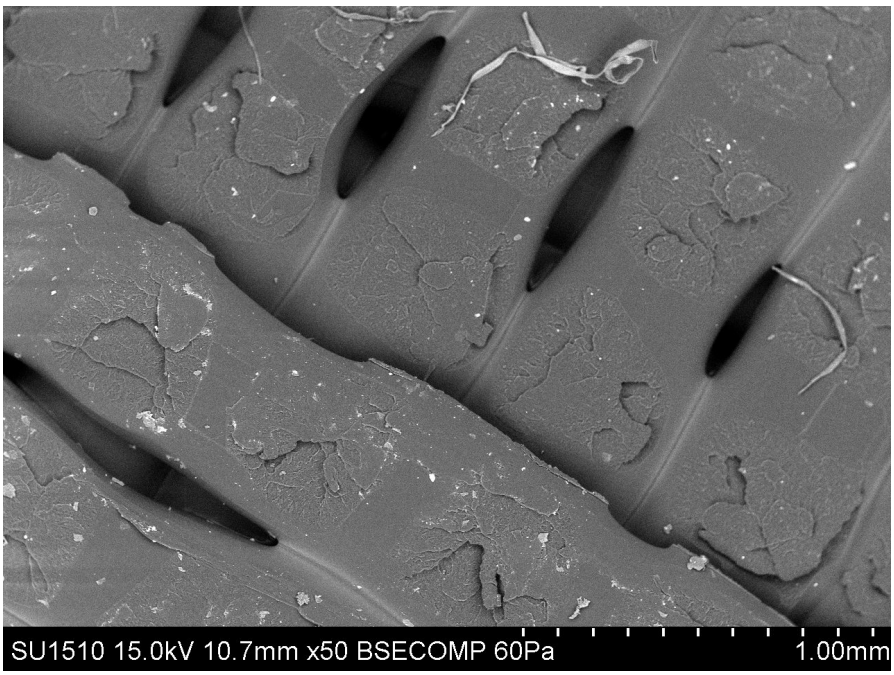

Fig. 5.13 SEM micrograph of fractured surface during vertical built

5.4.2 Discussion on volumetric shrinkage

The interaction effect of all the process parameters was found to be profound on volumetric shrinkage, unlike in the case of strength, yet the volumetric shrinkage does not depend on the model material (A) alone. The contour plots of the interacting parameters i.e., B and C have a minmax situation as shown in Figures 5.7-5.8. The saddle point for volumetric shrinkage is approximately at values slightly greater than the mid value (in coded form) for both the factors A vs C and B vs C at B equals to 0 and A equals to 0 (in coded form), respectively. In Figure 5.9 the situation of minimum value of shrinkage is obtained with the factors A and B being held at C equals to 0. It can be observed that the value of volumetric shrinkage varies at A equal to 1. Volumetric shrinkage, unlike strength, is not affected by Model Interior term A^2 or the interaction effect with either Horizontal direction or Vertical direction. However, unlike strength, amount of material deposited within the interior of the part affects the volumetric change only slightly. In Table 5.5, B ranges from -1 to 0.18 (in coded form) and it is evident from this

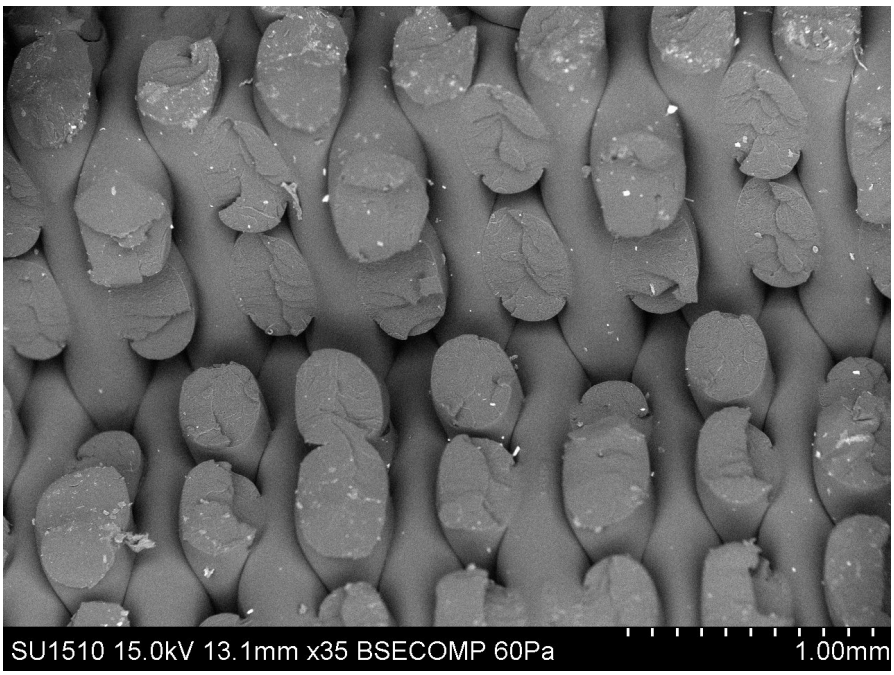

Fig. 5.14 SEM micrograph of fractured surface during horizontal built

figure that as angle of the deposition of material along the part contour increases there is a remarkable increase in strength at the expense of volumetric shrinkage which is not desirable as the component shrinks more. Also as C is varied from -1 to 1 (in coded form) the strength increases at the expense of volumetric shrinkage. This is attributed to the fact that as the value of C is increasing, the filaments at the bottom most layers will be subjected to distortion at the expense of the layers deposited above them. This effect can be observed from the SEM micro-graphs of Figures 5.12-5.14. The filaments are round in shape as they are extruded from the nozzle head. But due to the plasticity and diffusion process, the filaments tend to obtain the shape of oval like structure and will no more be circular. In either of the cases of build direction, the filaments are no more circular in cross-section. The oval like cross-section filaments interact with each other resulting in further dimensional inaccuracy. Because of these reasons the dimensional stability decreases and thus results in part distortion causing volumetric shrinkage. From the ANOVA results and from the SEM micro-graphs, it is evident that the hori-

zontal and vertical direction laying pattern has predominant change in volumetric dimensions. The same phenomenon has been reported from Table 5.5, where the volumetric shrinkage value increases with the increase in B and C values.

From both the results of strength and volumetric shrinkage, one can observe that the effect of necking, which results due to the pattern in which the deposition of semi-molten ABS, does affect the properties like strength and volumetric shrinkage effectively. It can be closely observed that necking is desirable in case strength is of high priority and necking should be minimized, if the volumetric shrinkage is of high priority. Clearly it stands out to be a case of multi-objective optimization, where a desired level of solution has to be obtained that satisfies and correlates both the objectives.

From the SEM micrograph as shown in Figure 5.12, the approximate neck growth can be estimated. Adopting the scale of the microgrpah, the approximate neck growth that has resulted during the sintering process is estimated as $130x10^{-6}m$. It can be recollected from the earlier chapter that the neck growth as estimated in through FEM mentioned in the subsection 4.4.8 of Chapter 4 is in the order of the same magnitude. The approximate neck size as obtained through the visco-elastic and viscoplastic models is respectively $102.6x10^{-6}m$ and $7.3x10^{-6}m$ which can be correlated to that of as obtained from the SEM micro-graphs.

5.4.3 Discussion on Pareto optimal

Observing the values in Table 5.5 one can relate the effect of each of the combinations over the strength and volumetric shrinkage. From Table 5.5, B ranges from -1 to 0.18 (in coded form). It indicates that as angle of the deposition of material along the part contour increases there is a remarkable increase in strength at the expense of volumetric shrinkage. Also, as C is varied from -1 to 1 (in coded form) the strength increases at the expense of volumetric shrinkage.

This clearly explains the concept of mutually conflicting objectives. In addition to the details provided in Table 5.5, the values of strength and volumetric shrinkage are plotted Figure 5.15. This plot of multi-objective optimization is termed as Pareto optimal front. The two ends of the Pareto's front are extending with an asymptotic behaviour. Any change in parameter level settings other than as highlighted in Table 5.5 may not yield a better strength than 35.83 MPa, however at the expense of shrinkage.

Conflicting objectives explains the phenomenon that increase in strength increases

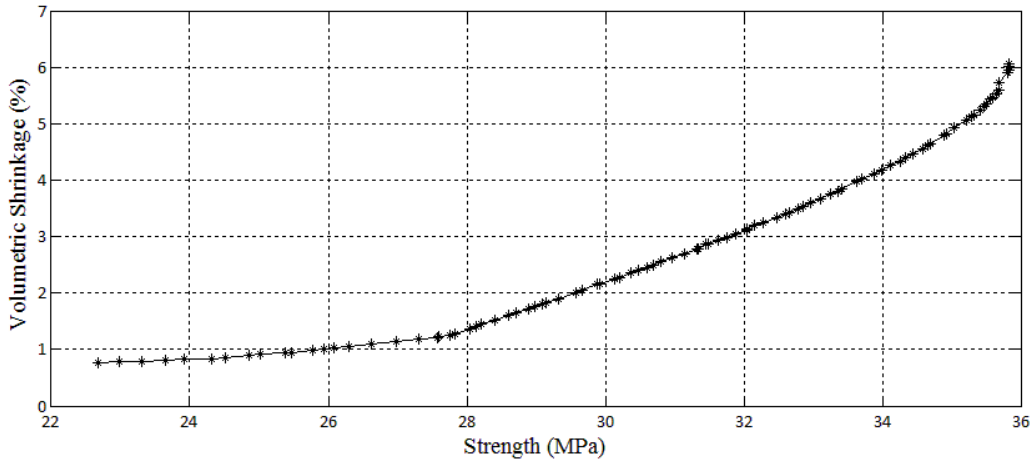

Fig. 5.15 Pareto optimal front

the volumetric shrinkage, which is undesirable. Similarly, any improvement in the shrinkage beyond 0.77 % cannot be obtained. Pareto's optimal front has a wide range of optimal values. This Pareto front now enables the decision maker to take decisions that are required as per the requirement. To validate the existence of these optimal parameters, other than the values tabulated in Table 5.2, a random of three optimal solutions from the Pareto's curve have been taken and the models have been fabricated with the level settings as obtained from the optimal set of solutions as shown in Table 5.5.

5.4.4 Validation tests

In order gain the confidence on the solutions as obtained from the NSGA-II and the Pareto's plot, validation tests have been performed. Table 5.6 provides the model level settings and the comparison of the strength and volumetric shrinkage between the optimal setting parameters as reported by NSGA-II and the experiments. Experiments have been conducted with these model settings. From Table 5.6 it is quite evident from the values of the strength as reported from NSGA-II and that of the experiments are almost matching. It can hence be concluded that the results obtained from the NSGA-II are accurate based on the above investigation. The results and their comparison have been reported in Table 5.6.

5.5 Summary

This chapter highlights the effect of necking on both the conflicting objectives namely strength and volumetric shrinkage. This has been detailed by discussing the multi-objective optimization of part strength and volumetric shrinkage of parts produce by FDM system as affected by three process parameters. The investigation was carried out by first conducting experiments based on DOE with FCCCD based experimentation. DOE study highlights a well-established normal distribution curve that indicates the best possible fit for the selected three process parameters in terms of the two response variables. The study also highlights the use of ANOVA in arriving at the critical parameters expressed as objective functions that are required to maximize the strength and minimize the volumetric shrinkage, simultaneously. Due to the inherent nature of mutually conflicting objectives, NSGA-II technique was used to arrive at the Pareto optimal solution set. It is clear from the Pareto's front that the best possible strength and volumetric shrinkage can be interpreted which helps for better selection of limits for the process parameters. Validation of the results from the Pareto optimal front provides

accurate results for the above investigation. It is also evident from the present work that FDM process needs a multi-objective optimization because there are several quality variables which often are conflicting and each of these response variables are affected by different process parameters.

With the understanding of evolution of neck, the present chapter considered the affect of the FDM process deposition strategies like deposition along vertical and horizontal direction. Having understood the importance of orientation of deposition of semi-molten material on bulk mechanical properties like tensile strength also the volumetric shrinkage, an attempt has been made on how this parameter along with the PoD machine parameters affect the surface strength characteristics, namely the tribological properties of the parts manufactured by FDM has been investigated. In the next chapter, the FDM process parameter namely orientation and the Pin-on-Disc (PoD) apparatus process parameters will be investigated on the tribological properties of the parts that are produced by FDM system.

Table 5.5 Optimal values of the parameter settings in coded form as obtained from NSGA-II

S. No	Model Interior (A)	Horizontal Direction (B)	Vertical Direction (C)	Strength (MPa)	Volumetric Shrinkage
1	1	-1	0.59	22.68	0.77
2	1	-1	0.62	22.98	0.78
3	1	-1	0.65	23.31	0.79
4	1	-1	0.65	23.31	0.79
5	1	-1	0.69	23.65	0.8
6	1	-1	0.71	23.92	0.82
7	1	-1	0.75	24.31	0.84
8	1	-1	0.77	24.52	0.86
9	1	-1	0.8	24.86	0.89
10	1	-1	0.81	25.02	0.91

continued ...

. . . continued

S. No	Model Interior (A)	Horizontal Direction (B)	Vertical Direction (C)	Strength (MPa)	Volumetric Shrinkage
11	1	-1	0.84	25.38	0.94
12	1	-1	0.84	25.46	0.95
13	1	-1	0.87	25.78	0.99
14	1	-1	0.88	25.94	1
15	1	-1	0.89	26.09	1.03
16	1	-1	0.91	26.29	1.05
17	1	-1	0.93	26.62	1.09
18	1	-1	0.95	26.98	1.14
19	1	-1	0.97	27.3	1.18
20	1	-1	0.99	27.57	1.21
21	1	-1	1	27.6	1.22
22	1	-0.99	1	27.76	1.26
23	1	-0.99	1	27.82	1.28
24	1	-0.97	1	28.04	1.37
25	1	-0.97	1	28.14	1.41
26	1	-0.96	1	28.2	1.44
27	1	-0.95	1	28.41	1.52
28	1	-0.93	1	28.61	1.61
29	1	-0.92	1	28.71	1.65
30	1	-0.91	1	28.9	1.72
31	1	-0.9	1	28.99	1.76
32	1	-0.89	1	29.09	1.8
33	1	-0.89	1	29.14	1.82
34	1	-0.87	1	29.32	1.9
35	1	-0.87	1	29.32	1.9
36	1	-0.85	1	29.57	2.01
37	1	-0.85	1	29.67	2.05
38	1	-0.83	1	29.89	2.15
39	1	-0.83	1	29.91	2.15

continued . . .

... continued

S. No	Model Interior (A)	Horizontal Direction (B)	Vertical Direction (C)	Strength (MPa)	Volumetric Shrinkage
40	1	-0.81	1	30.14	2.25
41	1	-0.8	1	30.2	2.28
42	1	-0.78	1	30.37	2.36
43	1	-0.78	1	30.47	2.4
44	1	-0.76	1	30.6	2.45
45	1	-0.75	1	30.7	2.5
46	1	-0.75	1	30.81	2.55
47	1	-0.73	1	30.96	2.62
48	1	-0.71	1	31.15	2.7
49	1	-0.7	1	31.32	2.78
50	1	-0.69	1	31.34	2.79
51	1	-0.68	1	31.45	2.86
52	1	-0.68	1	31.49	2.86
53	1	-0.67	1	31.63	2.93
54	1	-0.65	1	31.76	2.99
55	1	-0.64	1	31.89	3.05
56	1	-0.62	1	32.04	3.12
57	1	-0.62	1	32.04	3.13
58	1	-0.6	1	32.15	3.2
59	1	-0.6	1	32.28	3.24
60	1	-0.58	1	32.47	3.34
61	1	-0.56	1	32.61	3.41
62	1	-0.56	1	32.66	3.43
63	1	-0.54	1	32.79	3.5
64	1	-0.53	1	32.86	3.54
65	1	-0.52	1	32.97	3.6
66	1	-0.5	1	33.11	3.67
67	1	-0.48	1	33.25	3.75
68	1	-0.47	1	33.36	3.81

continued ...

. . . continued

S. No	Model Interior (A)	Horizontal Direction (B)	Vertical Direction (C)	Strength (MPa)	Volumetric Shrinkage
69	1	-0.46	1	33.42	3.84
70	1	-0.43	1	33.63	3.97
71	1	-0.43	1	33.63	3.97
72	1	-0.42	1	33.71	4.03
73	1	-0.4	1	33.88	4.11
74	1	-0.38	1	33.99	4.18
75	1	-0.36	1	34.12	4.27
76	1	-0.34	1	34.26	4.34
77	1	-0.32	1	34.34	4.4
78	1	-0.31	1	34.45	4.47
79	1	-0.28	1	34.58	4.56
80	1	-0.27	1	34.65	4.62
81	1	-0.26	1	34.69	4.64
82	1	-0.22	1	34.9	4.8
83	1	-0.21	1	34.92	4.82
84	1	-0.18	1	35.04	4.92
85	1	-0.18	1	35.04	4.92
86	1	-0.14	1	35.22	5.07
87	1	-0.13	1	35.28	5.13
88	1	-0.12	1	35.32	5.16
89	1	-0.09	1	35.41	5.25
90	1	-0.07	1	35.46	5.31
91	1	-0.05	1	35.5	5.36
92	1	-0.04	1	35.56	5.43
93	1	-0.02	1	35.59	5.47
94	1	0	1	35.64	5.53
95	1	0.02	1	35.68	5.6
96	1	0.07	1	35.69	5.72
97	1	0.12	1	35.81	5.9

continued . . .

. . . continued

S. No	Model Interior (A)	Horizontal Direction (B)	Vertical Direction (C)	Strength (MPa)	Volumetric Shrinkage
98	1	0.14	1	35.82	5.95
99	1	0.17	1	35.83	6.02
100	1	0.18	1	35.83	6.06

Table 5.6 Validation of results obtained from NSGA-II

Parameter Settings				Results from from NSGA-II		Results from Experiment	
S No.	(A)	(B)	(C)	Strength (MPa)	Volumetric Shrinkage %	Strength (MPa)	Volumetric Shrinkage %
1	1.00	-1.00	0.8	24.86	0.89	30.8	0.02
2	1.00	-1.00	1.00	27.6	1.22	29.23	2.13
3	1.00	-0.5	1.00	33.11	3.67	31.22	4.15

Chapter 6

Friction and Wear Rate Characteristics of FDM processed parts

6.1 Introduction

In the previous chapter, the effect of different orientations on mechanical properties like strength and volumetric shrinkage has been studied. It was established that the neck growth affects the properties and the selection of process parameters have to be chosen as per the requirement. As already highlighted, the FDM processed parts are widely used not only as prototypes but also as end products out which most of them are made of polymers. Polymers are widely used as AM materials. Polymers offer low frictional resistance to wear and because of which most of the engineering polymers find its increased usage in day today industrial as well as domestic needs. Additionally polymers show remarkable results in dry sliding conditions. ABS, the material used in the FDM machine, is one of the most widely polymer. Given the fact that ABS parts made by FDM can have widespread use under several critical relative sliding conditions, tribological

study of FDM parts is very important. As any other design of material and its manufacturing are considered, the challenge for any application of FDM process is the quality of the parts manufactured by this process. From the literature review as it can be observed that much of work so far has been done on characterization of quality of FDM parts that includes the bulk properties such as tensile strength, dimensional accuracy etc. in terms of the FDM process parameters has been performed. A very little work that includes the surface quality and tribological performance of FDM parts has been done using conventional as well as artificial neural networks. Most of the study has been either limited to the consideration of only FDM machine process parameters or only the tribological estimation techniques and machines.

The current chapter is dedicated to the study of tribological properties like wear rate and friction coefficient of FDM processed parts. The process parameters of both the FDM system and the Pin-on-Disc (PoD) experimental set-up are used to understand their effect of the parts manufactured by FDM process to understand wear rate and friction coefficient. The details of the PoD machine have already been mentioned in Chapter 3. The present work is envisaged to help the designer in considering both the manufacturing settings through FDM along with the real time testing conditions through PoD machine.

6.2 Methodology

6.2.1 Process parameters and machine settings

Based on the literature survey, the following parameters have been considered to estimate the tribological properties.

a. Normal Load (A): It is defined as the load that shall be applied while conducting the PoD experiment.

b. Sliding Speed (B): It is the speed with which the disc rotates.

c. Orientation (C): It is the build direction along which the pin has been manufactured in FDM.

All the above three parameters are set as per the three levels specified in the Table 6.1 with all other factors as fixed. The levels are selected based on the permissible minimum and maximum settings recommended by the manufacturer, previous work, experiences and real industrial applications.

To build the model for friction coefficient and wear rate, PoD experimental set-up

Table 6.1 Factors and their level settings

S.No	Factor	Name	Level Settings		
			-1	0	+1
1	A	Normal Load (N)	5	10	15
2	B	Sliding Speed (m/s)	0.5	1	1.5
3	C	Orientation(Degrees)	0	45	90

is used. In order to reduce the number of levels, a cubical CCD known as face centered central composite design (FCCCD) in which axial distance (α) equals to unity is considered for the present work. As discussed earlier in Chapter 3, a total of 20 experiments are to be conducted to obtain a model equation in terms of the process parameters. The levels are designated as low level (-1), center level (0) and high level (+1) as shown in Table 6.1. To obtain a reasonable estimate of experimental error, six center runs are chosen. In order to estimate the friction coefficient and wear properties of ABS, pins are manufactured using Dimensional Series of uPrint™, a variant of FDM machine. Figure 6.1 shows the details of the pin used in PoD experimental set-up. In order to observe the effect of orientation along with the two response variables, parts have been manufactured as per the orientation highlighted in Table 6.1. For the present work, the loads that are applied loads are 5, 10 and 15 N, the rotation speeds of the disc used are 0.5,

1 and 1.5 m/s. In order to maintain constancy, the sliding distance is assumed to be 2000 m. EN 31 hardened steel of RC 62 hardness and roughness of (Ra) 0.25–0.35 μ is used as the disc material. Friction and wear rate testing is done using PoD apparatus. The details of the PoD experimental set-up have been discussed in detail in section 3.5.3 of Chapter 3. Based on the configuration set-up highlighted in Table 6.1, the friction coefficient and wear tests are performed at room temperature with a relative humidity of 50 $\pm$ 10 %.

6.2.2 Estimation of wear rate and friction coefficient

The friction coefficient is obtained through the calculation of friction torque measured with a loaded cell sensor of the PoD machine. The wear volume W_v is measured by the loss of volume of pin which is equal to the volume of the frustum of the cone, as provided in equation 6.1. The wear rate K (mm^3/Nm) reported in this study is calculated according to the equation 6.2.

$$W_v = \frac{1}{3} * \pi * h * (r_1^2 + r_2^2 + r_1 * r_2) \tag{6.1}$$

$$K = \frac{W_v}{L * F} \tag{6.2}$$

In the above equations, r_1, r_2 are radius of the pin before and after the wear test and h is the difference in heights before and after the test as shown in Figure 6.1. L is the distance travelled by the disc with pin sliding over it. For the current study, L is set to 2000 m. F is the load applied during the test. To avoid the buckling of the pins, the load chosen is very less when compared to that of metal specimens. Based on the configuration settings as obtained from DOE study, pins for the PoD test are manufactured using the FDM process and tests are conducted on PoD machine for all the 20 experimental runs.

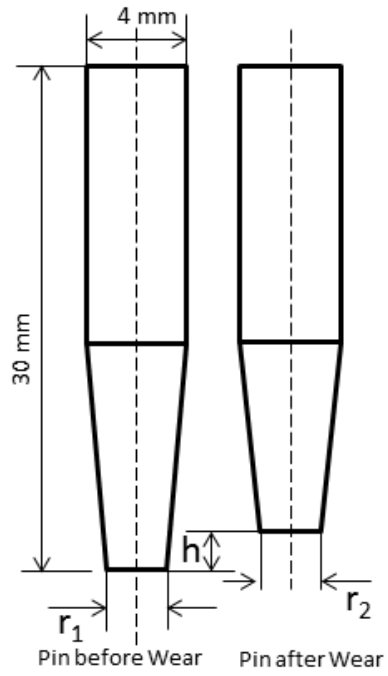

Fig. 6.1 Pin used in the Pin-on-Disc experimental set-up

Friction coefficient and wear rate are evaluated and are tabulate in Table 6.2. Based on the experimental data in Table 6.2 of the ABS pins on EN 31 disc, ANOVA has been carried out on MINITAB R14® software (Minitab [55]) resulting in full quadratic response surface models for the two response variables, namely, friction and wear rate. These models are helpful in drawing conclusions on the effect of the process parameters on these response variables. In order to understand the interaction effect of the process parameters over the two objective functions response surface plots are obtained. The statistical models thus obtained through ANOVA may also be subsequently used for the multi-objective optimization of both these responses variables against the three process parameters.

Table 6.2 Experimental Runs of FCCCD

Exp. No	A	B	C	Friction Coefficient	Wear Rate (mm^3/Nm) x 10^{-5}
1	0	0	0	0.43543	33.33759

continued ...

Table 6.2 Experimental Runs of FCCCD

... continued

Exp. No	A	B	C	Friction Coefficient	Wear Rate (mm^3/Nm) x 10^{-5}
2	0	0	-1	0.378	37.80654
3	0	1	0	0.3926	6.379667
4	-1	-1	1	0.1806	8.763836
5	-1	1	-1	0.27707	32.29713
6	0	0	1	0.4004	44.62958
7	1	1	1	0.3298	30.10002
8	0	0	0	0.4118	29.83024
9	0	0	0	0.425	17.96209
10	0	0	0	0.454	20.26451
11	1	0	0	0.4304	13.02975
12	1	1	-1	0.3785	10.03334
13	-1	0	0	0.3521	7.895669
14	1	-1	1	0.2047	5.749431
15	-1	1	1	0.3178	22.50694
16	0	-1	0	0.2505	8.09688
17	0	0	0	0.4982	28.02762
18	0	0	0	0.45763	43.19964
19	-1	-1	-1	0.2466	72.16183
20	1	-1	-1	0.3874	24.79421

6.3 Results and Discussion

6.3.1 ANOVA results

ANOVA results for friction coefficient and wear rate are highlighted in Table 6.3 and 6.4 respectively. F-value given in ANOVA tables is used to check

the significance of the values so obtained. Probability of F value greater than calculated F value due to noise is indicated by p value. Significance of the corresponding term is established if the p value is less than 0.05. Similarly for lack of fit, p-value must be greater than 0.05. An insignificant lack of fit is desirable as it indicates that any term left out of the model is not significant and that the developed model fits well. Figure 6.2 and 6.3 show the normal probability plots for residual at 95% of confidence. The normal probability plot p-value for both the responses is greater than 0.05 which shows that the model is a good fit. As p-value of the normality plots is found to be above 0.05, it indicates that residuals follow normal distribution and the predictions made by the mathematical model are in good agreement with the experimental values. Tables 6.3 and 6.4 provide the estimated regression coefficients of model terms of friction coefficient and wear rate respectively. The individual significance of each term is calculated at 95 % percent of confidence and terms having p value less than 0.05 are considered as insignificant. The final response surface equations for friction coefficient and wear

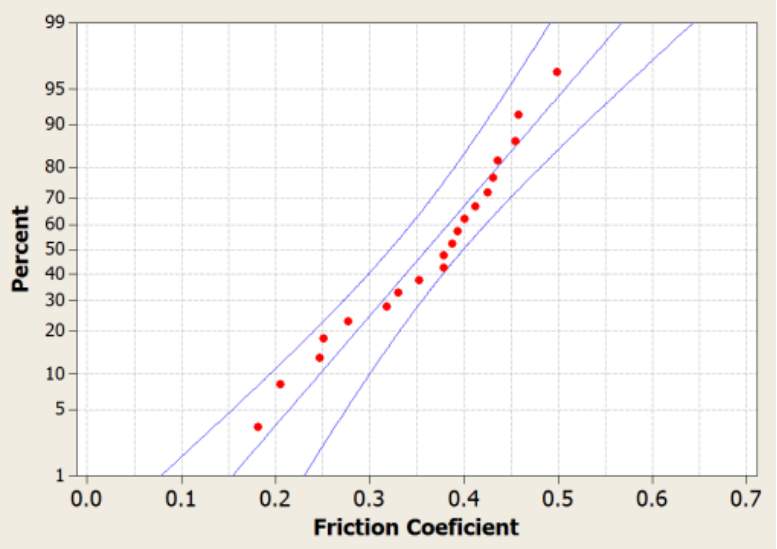

Fig. 6.2 Residual probability plot at 95 % confidence for Friction Coefficient

rate in coded units are given in equations (6.3) and (6.4) respectively.

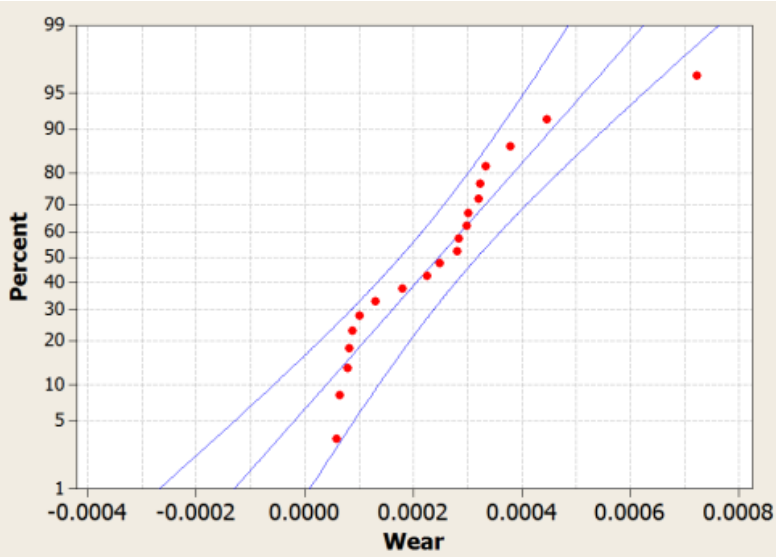

Fig. 6.3 Residual probability plot at 95 % confidence for Wear rate

$$Friction\ Coefficient\ (\mu) = 0.435 + A * 0.0357 + B * 0.0426 - B^2 * 0.095 - A * C * 0.0258 + B * C * 0.0301 \quad (6.3)$$

$$Wear\ Rate\ (K) = 0.00025 - A * 0.00006 - C * 0.000065 - B^2 * 0.000125 + C^2 * 0.000215 - A * C * 0.000093 + B * C * 0.000116 \quad (6.4)$$

The equations are expressed in terms of the machine setting parameters that predominantly affect the response variables. These expressions are helpful in defining the nature of the response surface for the selected parameters.

6.3.2 Factors affecting friction coefficient

In FDM, the raw material in the form of solid filament is allowed to pass through the extrusion head where it is heated to a semi-liquid state and deposited with a nozzle on the build platform one layer at a time resulting in staircase effect. Due to this phenomenon, in general, the parts manufactured by FDM do not have good surface finish. In order to establish good contact surface of the pins with the

Table 6.3 ANOVA table for Friction Coefficient

Term	Coefficient	t	F	p
Constant	0.435035	35.45	11.96	0
A	0.035663	3.159	9.98	0.01
B	0.042597	3.774	14.24	0.004
C	-0.023427	-2.075	4.31	0.065
A x A	-0.025822	-1.2	1.44	0.258
B x B	-0.095522	-4.437	19.69	0.001
C x C	-0.027872	-1.295	1.68	0.224
A x B	-0.006434	-0.51	0.26	0.621
A x C	-0.025766	-2.042	4.17	0.049
B x C	0.030091	2.384	5.68	0.038

disc, the pins are polished on a double disc polisher. It is ensured that the roughness of the pins is within the limits so as to maintain a better surface contact with the disc. During the test, as the duration of the test increases, due to the inherent frictional behaviour, the friction remains constant for some time. But due to the consistent wear, the ABS specimen which is in the solid state turns into powder. Because of this phenomenon, the friction coefficient decreases consistently before it reaches a stable value. This is also due to the fact that after sufficient time, once the asperities are smoothed, the friction coefficient decreases and becomes stable. This eroding action of surface is very well depicted in Figure 6.4 that shows the variation of friction with the total duration of the test. It can be observed from the ANOVA table for friction coefficient in Table 6.3 that the factors that predominantly effect friction coefficient are the interaction of disc sliding speed (B) with orientation (C) of the filaments of the FDM machine. Similarly the effect of interaction of normal load (A) with orientation (C) on friction coefficient can be observed whose p-value is nearly less than or slightly greater than 0.05. Figure

Table 6.4 ANOVA table for Wear rate

Term	Coefficient	t	F	p
Constant	0.000248	7.859	5.45	0
A	-0.00006	-2.061	4.25	0.050
B	-0.000018	-0.628	0.39	0.544
C	-0.000065	-2.247	5.05	0.048
A x A	-0.000093	-1.674	2.8	0.125
B x B	-0.000125	-2.256	5.09	0.048
C x C	0.000215	3.873	15	0.003
A x B	0.000045	1.373	1.89	0.2
A x C	0.000093	2.854	8.14	0.017
B x C	0.000116	3.565	12.71	0.005

6.5 shows the effect of the individual process parameters A, B and C on friction coefficient. With the increase in either load(A) or sliding speed(B) the friction coefficient first increases, due to asperities, which is explained earlier and then decreases gradually. This phenomenon is usually found in most of the polymers (Jia et al. [38], Rymuza et al. [79], Equbal et al. [27]). As orientation(C) of the filaments increase from lowest value (-1) to the middle value (0), the friction increase but decreases with the increase in C. The reason for this decrease may be due to fact that the layers will now be flat to the surface of the disc. There is a consistent wear along the cross section of the layer due to which the friction coefficient is decreasing. The coefficient of friction during the further duration of the decrease due to flattening of these roughness asperities but does not become altogether negligible. Rather it reaches a value of 0.3 after 2000 seconds. Figures 6.6 and 6.7 respectively show the response surfaces of this interaction on friction coefficient. By observing the response surface in Figure 6.6, friction is lowest under the consideration that the filaments are deposited such that the orientation is

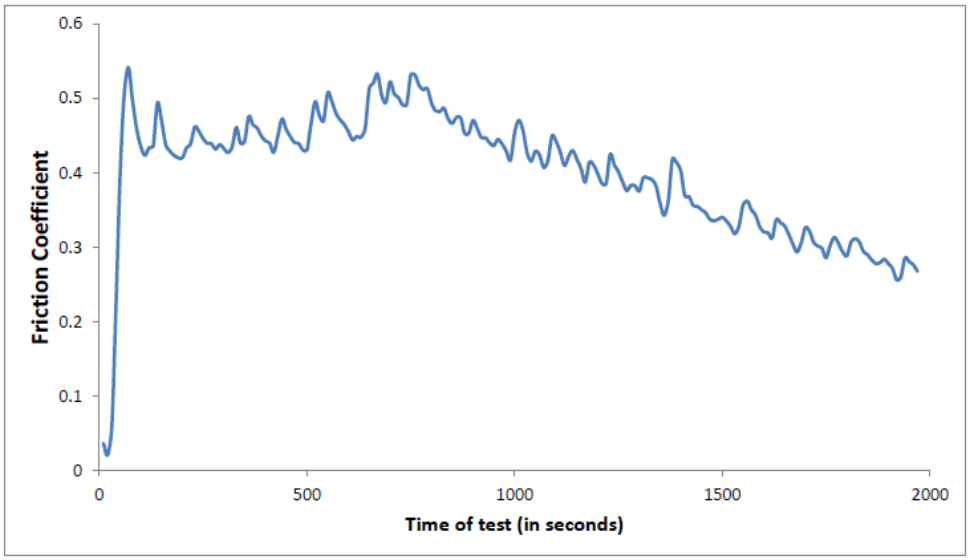

Fig. 6.4 Variation of Friction Coefficient with the duration of test

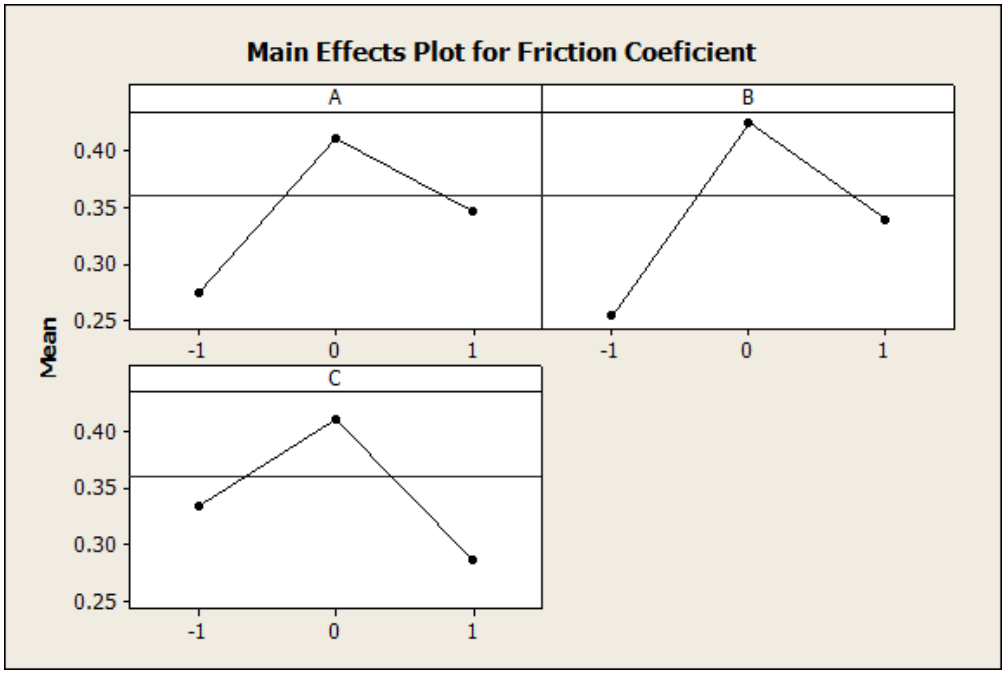

Fig. 6.5 Affect of individual parameters on Friction Coefficient

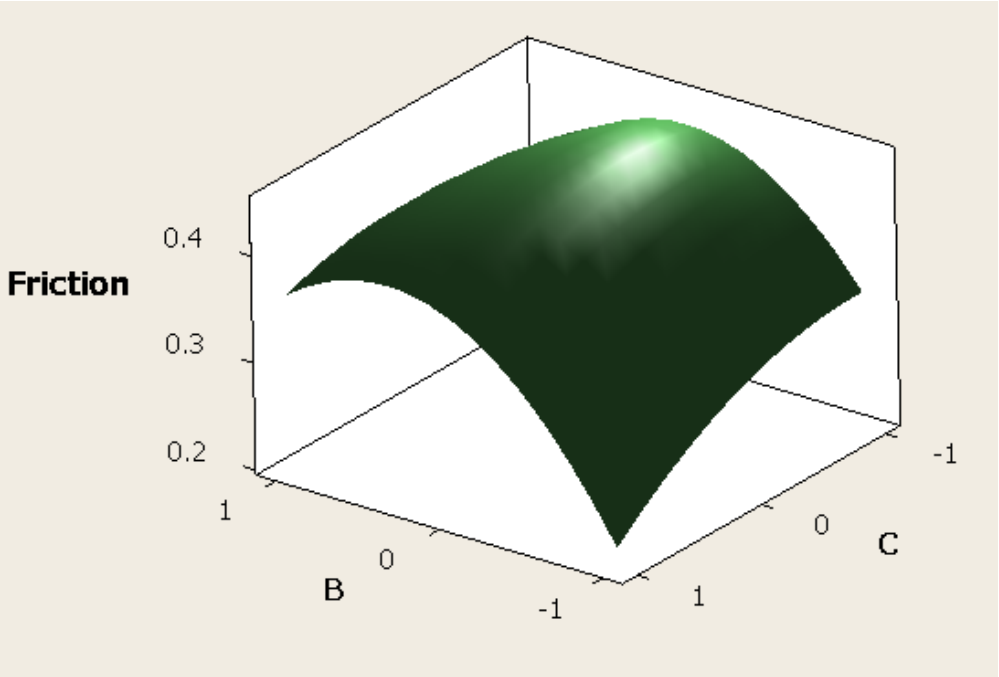

Fig. 6.6 Response surface of Friction Coefficient at A=0

maximum. Hence the sliding speed of the disc will move past the smooth contours of the single layer of the pin resulting is low friction between the pin and the disc. However, it can be observed that as the orientation decreases, that is the filaments are deposited parallel to the build plane, the load and the sliding speed of the disc moves past a section of filaments, causing more friction. Also with the increase in load, one can observe the cracks formed between the filaments which will be explained in the coming sections. Similar observations are found Figure 6.7 where in friction is the least at the lowest load value either at low or high orientation. This is because the filaments in the intra-layer and inter-layer can just take the load that is being applied on the pin. But as the load increases, the filaments when deposited in vertical direction, the intra-layer will take the whole load, but fails when the same load when applied on the filaments which are deposited along the build plane, the filaments in the inter-layer fail to take the load resulting in separation of the filaments and hence cause more friction.

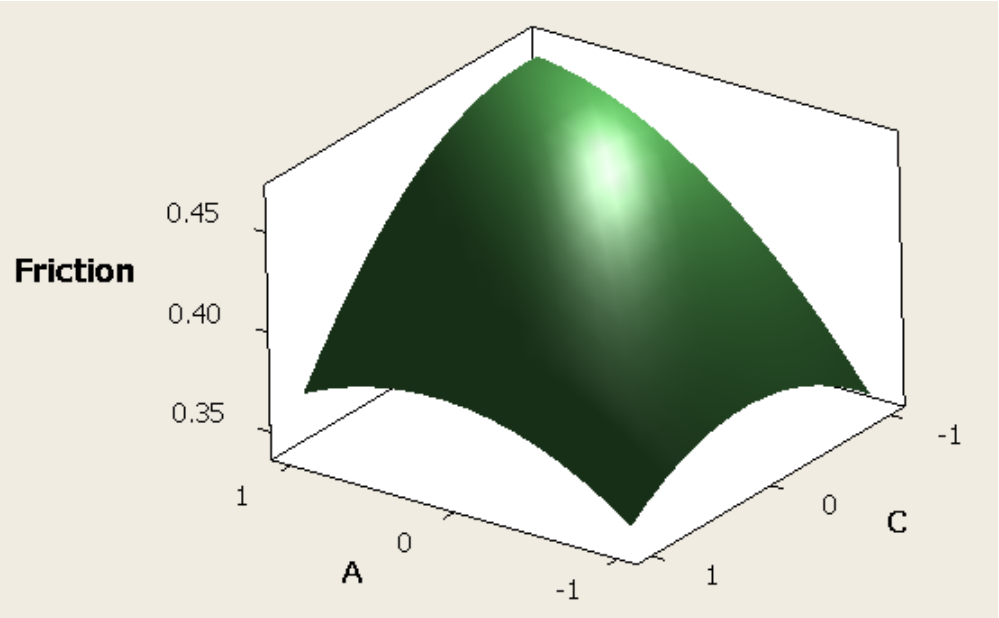

Fig. 6.7 Response surface of Friction Coefficient at B=0

6.3.3 Factors affecting wear rate

Figure 6.8 shows the experimental plot of wear with respect to time of test. Wear initially jumps from minimum to a value and beyond which the rate stabilizes and follows a linear plot. This phenomenon is just like the one explained during friction coefficient. At initial phase, the presence of asperities makes the wear to jump from zero position to a value from where it follows a linear path. After certain duration of test, the wear rate is found to be constant. Figure 6.9 shows the effect of the individual process parameters A, B and C on wear. With the increase in the load (A) the wear decreases which is observed phenomenon in most of the polymers. With the increase in orientation (C), the wear decreases gradually and stabilizes. This may be because the wear is more predominant at lower values of orientation since voids are found more at the terminal cross sections of the adjacent filaments. Observing the p-values in the ANOVA table of wear rate in Table 6.4, normal load (A) and orientation (C) have predominant effect on wear when they are taken individually with not much of contribution from sliding speed (B). While observing the p-values of the interaction of factors A with C and factors

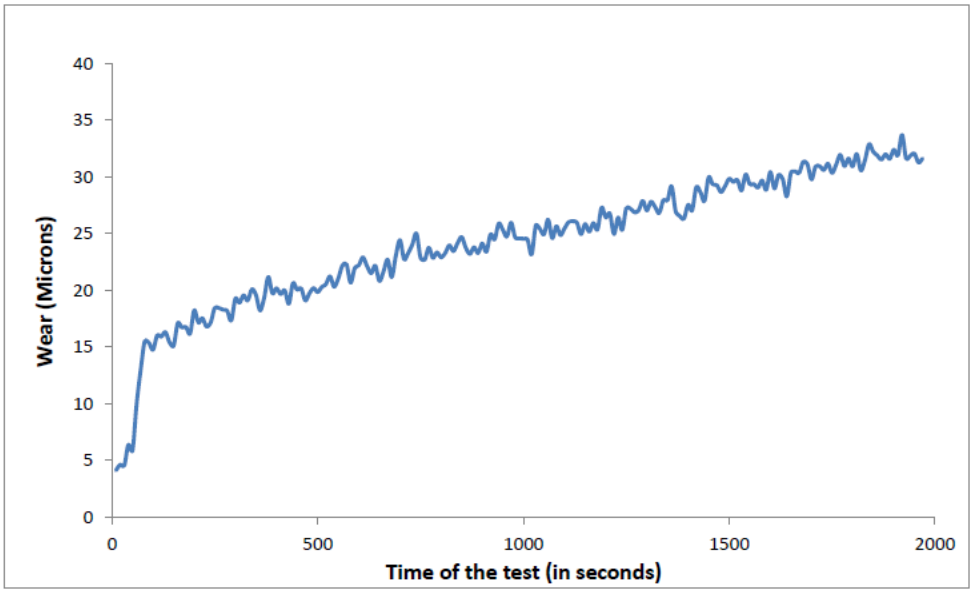

Fig. 6.8 Variation of Wear rate of pin with the duration of test

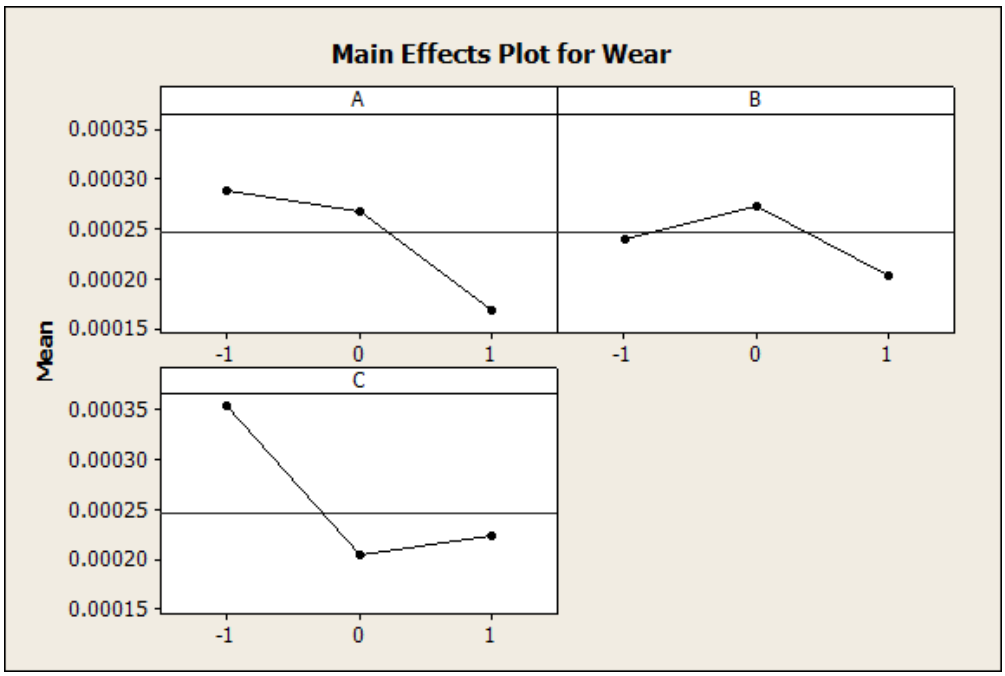

Fig. 6.9 Affect of individual parameters on Wear rate

B with C is predominant. The response surfaces of the interaction of these factors are shown in Figures 6.10 and 6.11 respectively. Observing Figure 6.10, wear is lowest when C is optimum at higher and lower values of sliding speed i.e, for minimum wear condition, the desired orientation is at middle values, irrespective of the sliding speed of the disc. But at lower orientations, i.e, when the part is manufactured with the material deposited along the build plane, the wear is observed to be more. Similar trend is observed in Figure 6.11, where at lower or higher loads, the wear rate is more when the orientation of the filaments is along the build direction. Orientation of filaments along vertical direction also has some appreciable wear rate, but the best conditions are obtained when the orientation is at the middle value. This may be due to the fact that load might have partially be taken by the inclined filaments which tend to wear out uniformly when compared to either of the directions. For the wear condition, the desirable conditions are optimum orientation followed by filaments deposited in vertical direction followed by horizontal direction, provided all the measurements are carried at lower loads. In general, wear initially will be high due to high roughness value of the FDM manufactured part. One reason for this persistently high coefficient of friction could be the third body wear, where the third body particles are the initially dislodged surface asperities. Close observation of worn surfaces showed these third body particles to be prevalent at the interface as shown in Figures 6.12a (Figures are captured through Zeta-20 Optical Profiler, Zeta Instruments©). The excessive amount of third body particles may be attributed to the ploughing action of EN 31 asperities through the wear tracks of the pin surface.

The ploughing action continues during the rest of the sliding movement of the disc where the wear rate is constant during the entire span the test. The ploughed particles of the ABS material might have got crushed and resulted into powder. It can also be observed from the figure that powder is the resultant of this ploughing action which gets embedded to both the pin as well as the disc. Figure 6.12b

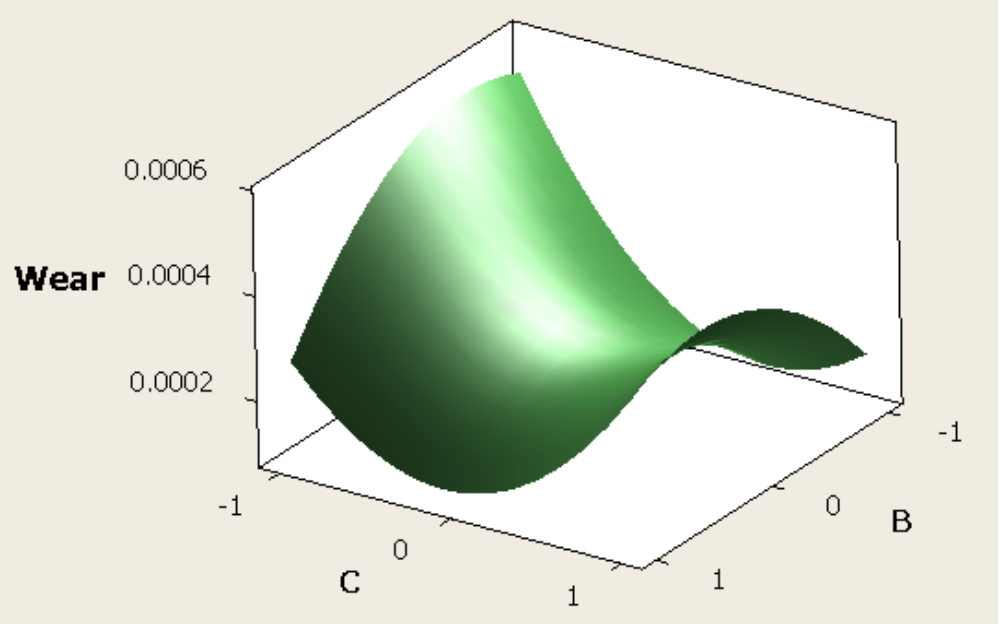

Fig. 6.10 Response surface of Wear rate(mm^3/Nm) with A=0

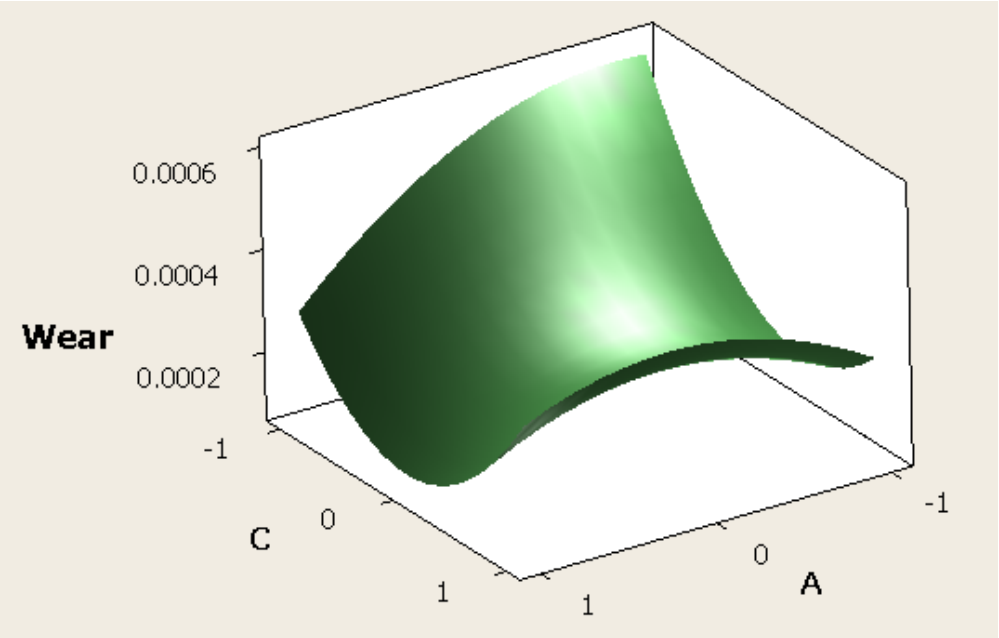

Fig. 6.11 Response surface of Wear rate (mm^3/Nm) with B=0

shows the wear analysis of the pin measured at various sections as highlighted in Figure 6.12a. Wherever the ploughing action is predominant (as shown in Figure 6.12a) the respective line demonstrates the wear rate along that section. Sudden drop in the curves of Figure 6.12b indicates the ploughing action that might have occurred.

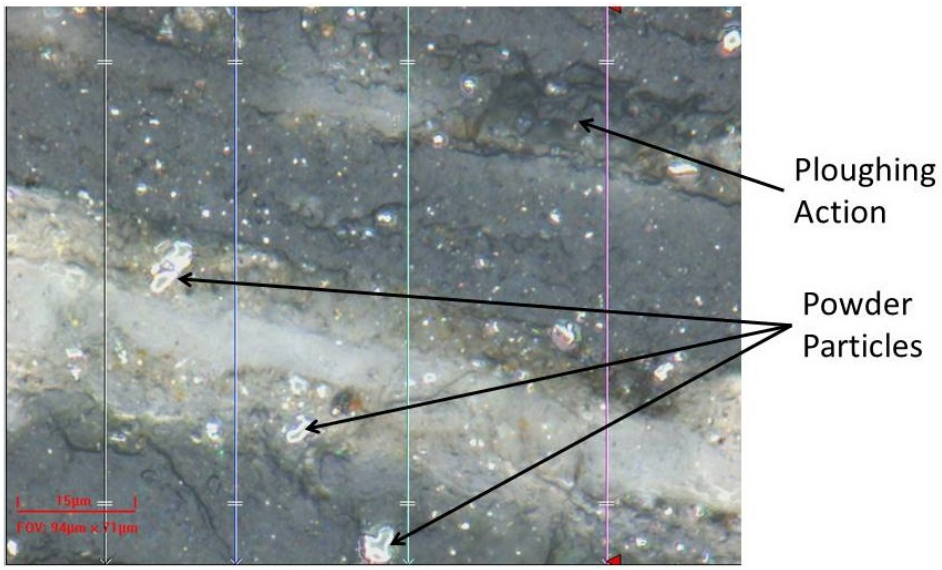

(a) A profiler image of the ploughing action

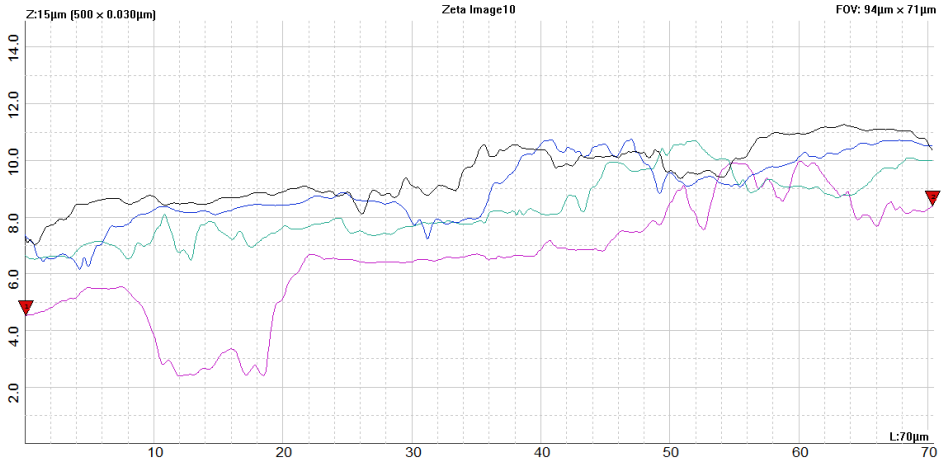

(b) Wear rate analysis of the pin at various sections

Fig. 6.12 Ploughing action due to excessive wear of pin surface

6.3.4 SEM observation of worn surfaces

SEM micrographs of the worn out pins after conducting the wear test on PoD apparatus are represented in Figures 6.13-6.18. During the part manufacturing in FDM process, the layers are deposited one above the other at relatively high temperatures. Due to this phenomenon, there is a local heat transfer among the filaments in the layer and between the adjacent layers. This causes increase in their temperature resulting in re-melting of the already deposited filaments and hence the diffusion will occur between the filaments and the layers as well. This in-turn results in increase in effective area there by strength. Figure 6.13 is taken from the parts with minimum orientation, low operating disc speed with high load while Figure 6.14 is taken from the pin with orientation along with operating disc speed at center values with high load. The wear of the specimen mentioned in Figure 6.13 configuration resulted in abrasive wear since the orientation of filaments did not result in good bonding. While in Figure 6.14, since the orientation of the parts have resulted in better strength, the wear is not as much as when compared to that of in Figure 6.13. Sufficient time for bonding is the reason for the better strength which resulted in minimum wear. This is also evident from the earlier discussions on responses affecting friction and wear rate detailed in the earlier sections. Figure 6.15 depicts the wear condition where the layers are laid perpendicular to the build platform of the FDM machine. During this configuration, the layers get separated uniformly once the disc rotates past the layer due to which layer de-bonding takes place. This may be because of higher sliding speed of the disc past the pin with lower loads. This can be compared with the Figure 6.13 where the disc speed is at its center value and with higher loads. On close observation, one can observe the wear is occurring quite uniformly which is more desirable. Figure 6.16 depicts the condition where the layers are laid at an orientation of center value (45^0 to the FDM build table) with the PoD parameter settings

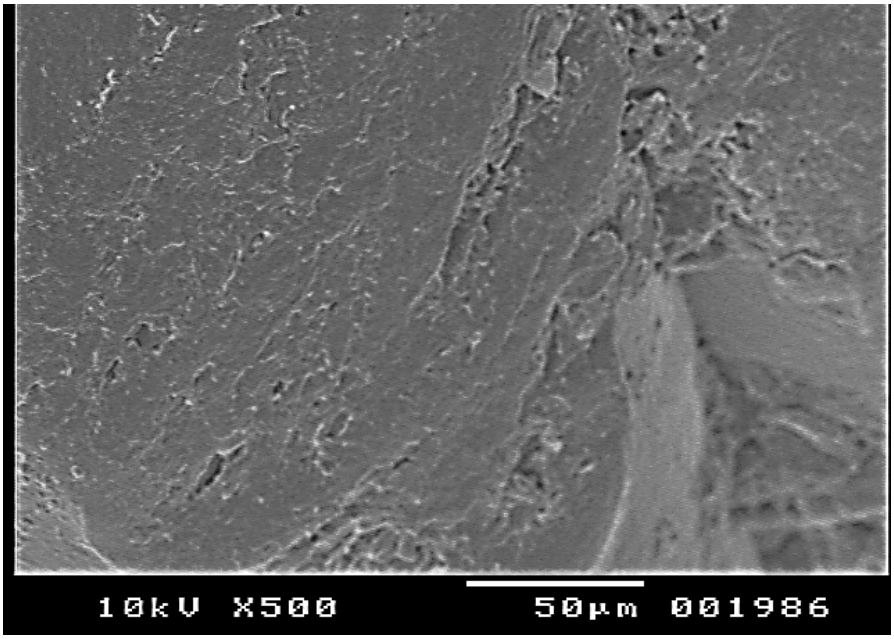

Fig. 6.13 SEM micro-graph of pin at A=1, B=0 and C=-1

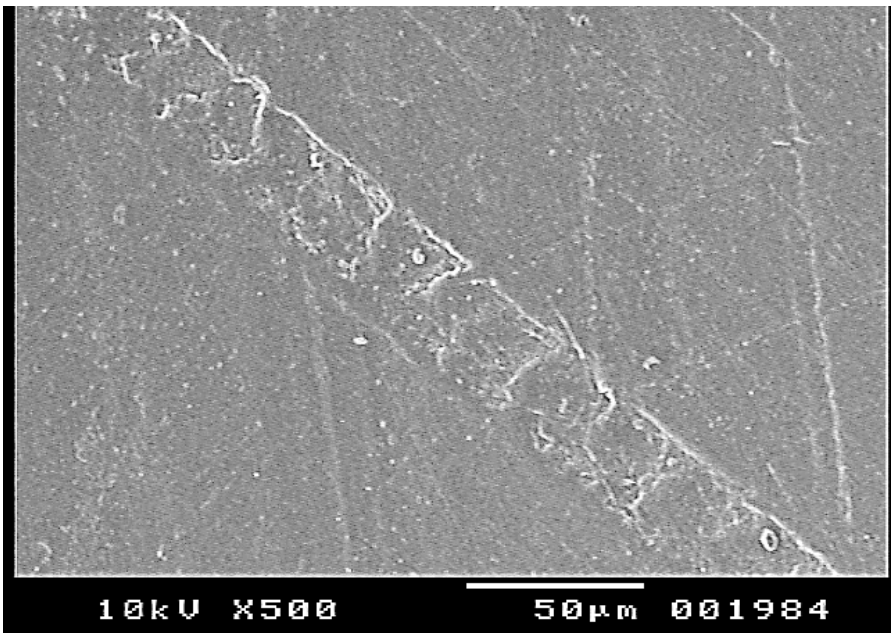

Fig. 6.14 SEM micro-graph of pin at A=1, B=0 and C=0

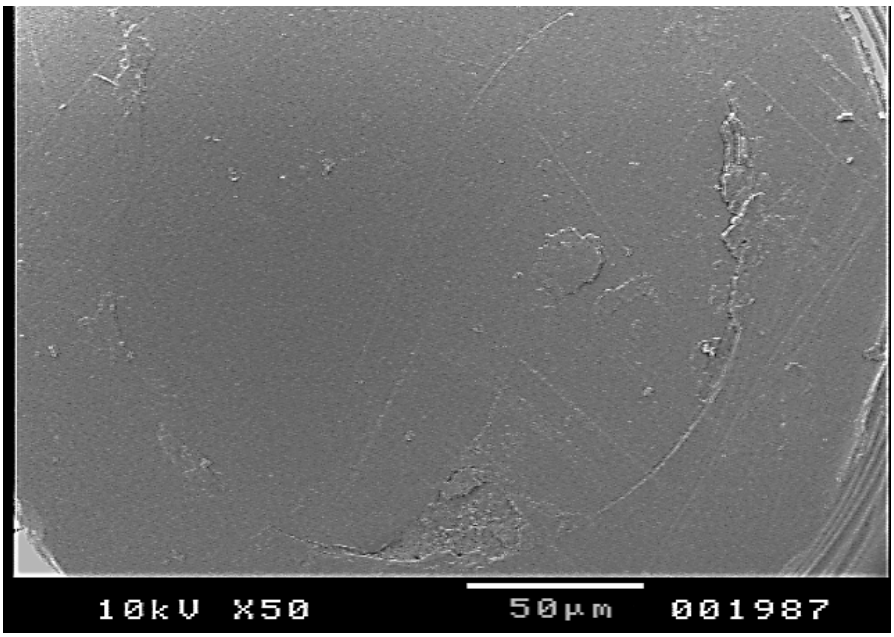

Fig. 6.15 SEM micro-graph of pin at A=-1, B=1 and C=1

as high disc speed and low load. It may be due to the fact the solid ABS during the test, may result into powder. This powder may act as a lubricant between the pin and the disc. The powder getting embedded on the surface of the pin is shown in Figure 6.16. This is evident from the Figures 6.10-6.11 that the wear rate is optimum with orientation settings at the mid value. Figure 6.17 shows the condition of specimens tested at high load, high disc speed and low orientation angle of the part during its manufacture in FDM where cracks are formed. Figure 6.18 shows the condition of specimens tested at low load, high disc speed and low orientation angle of the part during its manufacture in FDM machine. Cracks are formed between the filaments of the specimen but comparing the worn surfaces of both the figures highlighted in Figures 6.17 and 6.18, it can be concluded that with given conditions of high sliding speed and lower orientation of the filaments, cracks are more intense at high load. From the above discussions, we can conclude that the orientations in combination with sliding speed and the applied load plays a very important role in determining the friction and the wear rate of the parts manufactured by FDM.

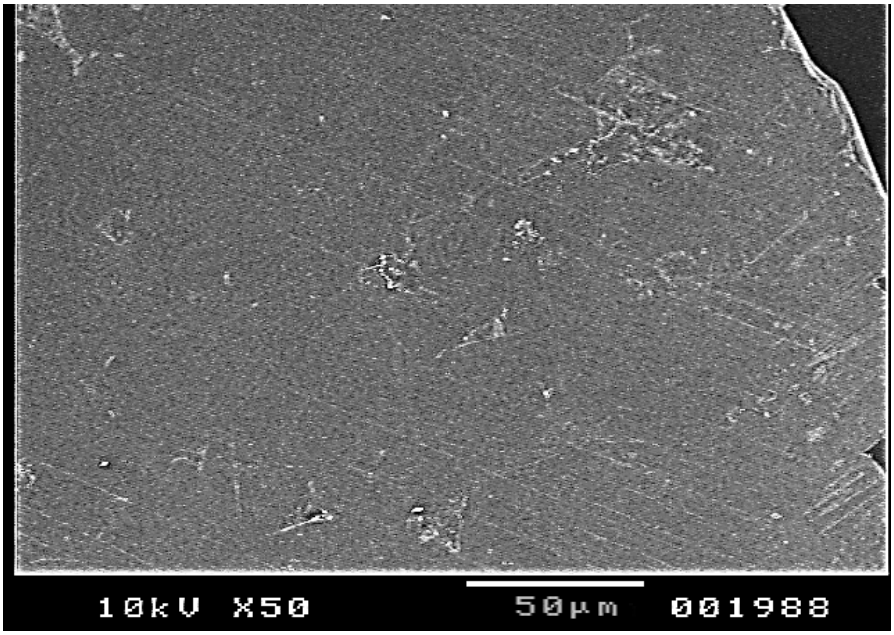

Fig. 6.16 SEM micro-graph of pin at A=-1, B=1 and C=0

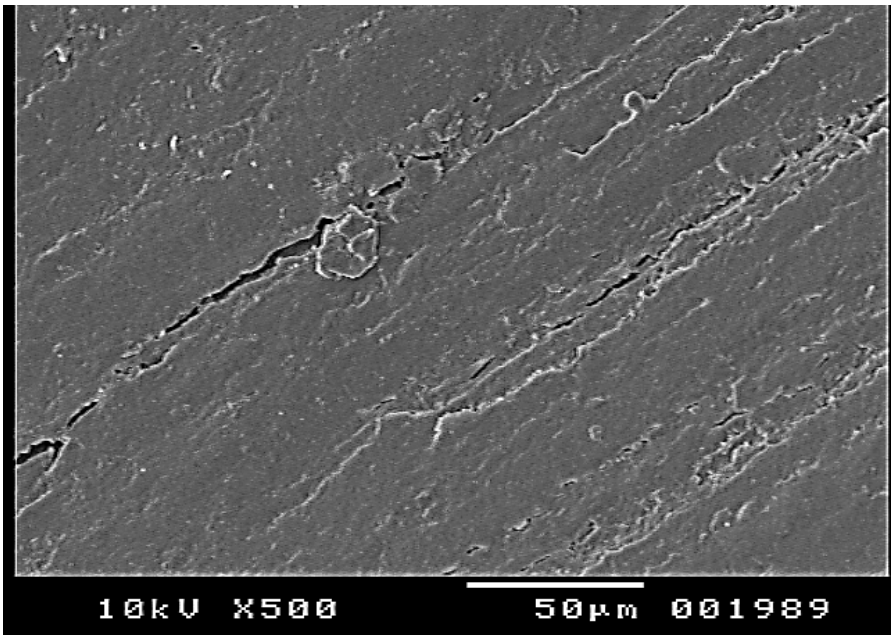

Fig. 6.17 SEM micro-graph of pin at A=1, B=1 and C=-1

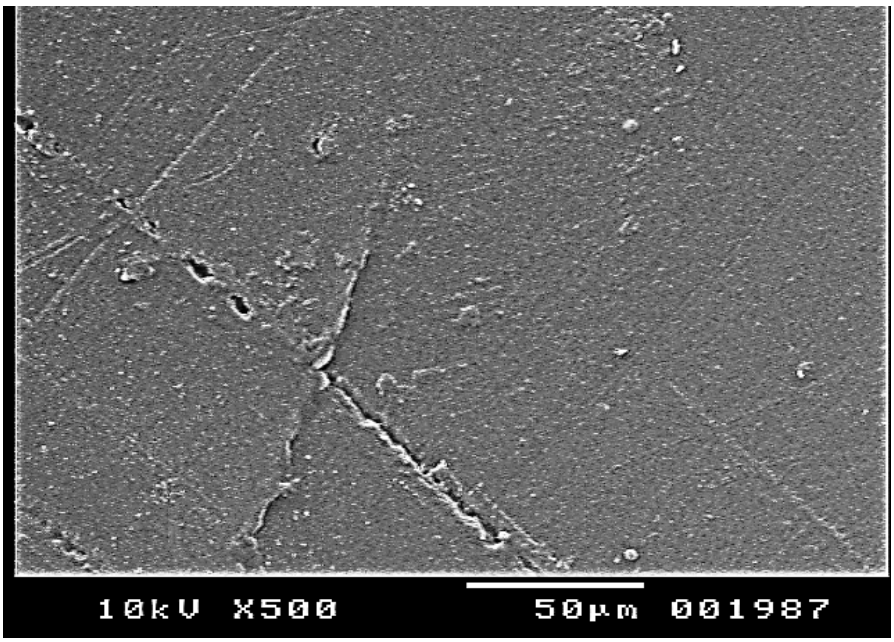

Fig. 6.18 SEM micro-graph of pin at A=-1, B=1 and C=-1

6.4 Summary

Estimation of the effect of the parameters from both the Pin-on-Disc experiment settings and FDM setting was carried out for polymer parts manufactured by FDM machine. It has been observed that out of the three parameters, the interaction of sliding speed with orientation and load with orientation have an effect on friction coefficient. It can be concluded that as the orientation decreases, with an applied load, the sliding speed of the disc moves past a section of filaments, causing more friction. It can also be concluded that as the load increases, cracks formed between the filaments. Similarly wear of pins are also observed to be affected predominantly during the interaction of sliding speed that is applied during the test and the orientation of the filaments during the manufacture of pins using FDM process. Also normal load on interaction with orientation affect the wear as much as observed in friction coefficient. For the wear condition, the desirable conditions are optimum orientation followed by filaments deposited in vertical direction followed by horizontal direction for lower loads. From the above

work, it can be concluded that the friction coefficient and wear are greatly affected by the orientation on interaction with applied load and sliding speed of the disc on the part that is manufactured using FDM process. The current work suggests building the part with optimum build angles and operate at lower load and optimum sliding speed for lower friction. The study also suggests lower load with high speed and medium angles of orientation for uniform wear condition. This is because the layers at lower orientations will be along the plane of the build platform. It also indicates that orientation not only affect the bulk properties like strength and dimensional accuracy but also the surface properties such as friction coefficient and wear. These results are important for increasing use of FDM parts as machine elements that are undergo intense tribological conditions.

And finally the next chapter concludes by providing summary, conclusions and specific contributions of the entire thesis along with future scope of work that can be extended to the current thesis.

Chapter 7

Conclusions

7.1 Introduction

Fused deposition modeling processed parts provide many advantages to the day-to-day industrial requirements in-terms of final finished products and more specifically prototypes. Advent of CAD with additive manufacturing technologies has an edge over the traditional manufacturing and prototyping in industries in-terms of easy of manufacturing, tool and die less manufacturing, quick product realization and many more. Despite its unique advantages, the challenges still persist and the need of the hour is to address various quality related issues pertaining to FDM process. Out of many such quality parameters, strength is one among the prime quality characteristics both as bulk strength and surface surface strength. With this as the main objective, the present thesis emphasizes on the understanding of neck growth, which is of prime importance to understand quality characteristics namely the strength along with volumetric shrinkage and tribological properties like friction coefficient and wear rate has been investigated. Mathematical model along with statistical techniques have been adopted to understand the dependence of neck growth on these responses. FEM models are developed to understand the evolution of neck growth. The process specific

parametric characterization has been done to understand the affect of these parameters on various responses like strength, volumetric shrinkage, friction and wear have been investigated. A multi-objective optimization has been performed based on the objectives formulated using the DOE, ANOVA and RSM methodologies. Based on the close observations and investigations carried out theoretically, experimentally and statistically, the present chapter highlights the summary of the findings of the current thesis, followed by conclusions of the thesis. Also a section on specific contributions that have been made based on the research work carried out has been highlighted. The chapter ends highlighting the future scope that could be extended for further study has been documented.

7.2 Summary of the findings

1. In the present thesis, in order to understand the manufacturing of part through FDM process, neck growth was modeled between the filaments. Mathematical expressions relating the evolution of neck growth was derived through the principles of sintering operation. The energy gained by surface reduction is dissipated by viscous flow, which sets the time scale for sintering.

2. The neck growth was established considering the balance of the work of surface tension and work of viscous dissipation while neglecting the effect of gravity and various other external forces.

3. Neck growth contributes to the strength. This phenomenon was undertaken by obtaining the effective area of neck growth between the two filaments in a sample test piece.

4. Theoretical strength has been evaluated by considering the strength of the specimen along with the effective area as obtained from the mathematical modeling. To validate the mathematical strength obtained, experiments

were conducted to evaluate the strength of the test specimens.

5. The strength as obtained due to neck growth was studied using two different orientations. The observations were recorded and compared with that of the theoretical strength as obtained by mathematical model. Agreement between theoretical and experimental ultimate tensile load indicates that the strength of the FDM part is primarily a consequence of intra-layer bonding and inter-layer bonding of filaments.

6. Scanning electron microscope (SEM) generated micro-graphs of the fractured surface of the specimen indicate that the part strength can be attributed to the necks between filaments.

7. The effect of necking resulted in the contribution of strength of the part. However, it has also been observed that there was certain change in dimension, and hence resulted in volumetric shrinkage of the parts due to the neck formation.

8. The FDM process parameters like model material, vertical direction and horizontal direction were chosen to understand the responses like strength and volumetric shrinkage. Statistical tools like DOE along with the ANOVA were employed in arriving at the most critical process parameters that affect the responses and arrive at objective functions that are required to maximize the strength and minimize the volumetric shrinkage, simultaneously. RSM was employed to understand the interrelationship between the factors and express the parameters in the form of response surfaces.

9. A similar study of parametric appraisal has been done on tribological properties like wear rate and friction. Load applied on the specimen along with the sliding speed are the two process parameters considered from pin-on-disc experiment and the orientation of the build material of FDM process

has been chosen.

10. It has been observed that out of the three process parameters, the interaction of orientation with sliding speed and also with load has an effect on both friction and wear rate. In FDM processed parts, at the minimum value of orientation, the normal load is taken by the inter-layers while at maximum value, the load is taken by the intra-layers.

7.3 Conclusions

Based on the research carried out in the present thesis, the following are the list of conclusions that have been made.

1. In FDM process, the time required for the two adjacent cylindrical filaments for finally coalescing completely into one single filament is not available before complete solidification and cooling to the chamber temperature occurs. Hence it can be concluded that not every pair of adjacent filaments builds the same size of the neck. In fact, some of the pairs of filaments may not build any necks at all.

2. The neck formation results in increase in strength as well as change in dimensions. From the SEM micro-graphs, it is clear that the cylindrical filaments convert into elliptical cross-section filaments after solidification.

3. From the experimental study, it can be concluded that the specimen loaded in the building direction fractured similar to brittle fracture as in metals whereas the failure of the specimen loaded in the transverse direction, the fracture occurred over the plane at an angle roughly equal to 45^0 to the loading direction.

4. From the experimental studies, it can also be concluded that the process

parameters bear a conflicting relation with the responses chosen namely strength and volumetric shrinkage.

5. From the Pareto's plot, it can be concluded that the best possible strength that can be obtained using any of the combinations is found to be 35.83 MPa. Also any improvement in the shrinkage cannot be obtained beyond 0.77 %.

6. From the tribological studies, it can be concluded that cracks are formed in the specimens when the specimens are tested at high load, high speed and low orientation angle of the part during its manufacture using FDM process.

7. For uniform wear, the layers are to be deposited vertical to the build platform of the FDM system so that the intra-layer bonds take the maximum load.

7.4 Specific Contributions of the Research Work

Based on the research carried out in the present thesis, the following are the specific contributions made.

1. Mathematical model for sintering of two successive cylindrical filaments has been derived and successfully computed to predict the neck growth between them.

2. In the literature, there is no finite element model of any kind to predict the neck growth. This was probably not done due to the complexity of the process. In the present work, both visco-elastic and viscoplastic finite element models have been developed in COMSOL Multi-physics software and the predicted neck growth is comparable to that in mathematical model as well as the experimental SEM micro-graphs.

3. NSGA-II has been successfully applied on predicting the Pareto optimal solution to the multi-objective optimization problem involving strength and volumetric shrinkage.

4. In the literature there are hardly any tribological studies to characterize the surface strength of FDM processed parts. In this present work, comprehensive tribological study on standard pin-on-disc experimental set-up has been conducted and friction and wear rate behavior has been characterized.

7.5 Scope for Future Work

From the research work carried out in this thesis, work in the following areas is suggested for further improvement.

1. Given the success of the methodology, these methods can be applied to practically more widely applicable metal additive manufacturing process such as Direct Metal Laser Sintering (DMLS) and Selective Laser Melting (SLM)

2. The multi-objective optimization has been successively carried out using face centered-central composite design in the present work. Application of Artificial Neural Networks (ANN) may also give additional insights.

3. The proposed methodologies of statistical methods along with the multi-objective optimization requirements has huge potential to be applied in the bio-engineering applications like prostheses, implants etc.

References

[1] Ahn, D., Kweon, J. H., Kwon, S., Song, J., and Lee, S. (2009). Representation of surface roughness in fused deposition modeling. *Journal of Materials Processing Technology*, 209(15-16):5593–5600.

[2] Ahn, S. H., Montero, M., Odell, D., Roundy, S., and Wright, P. K. (2002). Anisotropic material properties of fused deposition modeling abs. *Rapid Prototyping Journal*, 8(4):248–257.

[3] Aijun, L., Zhuohui, Z., Daoming, W., and Yang, J. (2010). Optimization method to fabrication orientation of parts in fused deposition modeling rapid prototyping. In *International Conference on Mechanic Automation and Control Engineering (MACE)*, pages 416–419.

[4] Ang, K. C., Leong, K. F., Chua, C. K., and Chandrasekaran, M. (2006). Investigation of the mechanical properties and porosity relationships in fused deposition modelling-fabricated porous structures. *Rapid Prototyping Journal*, 12(2):100–105.

[5] Anitha, R., Arunachalam, S., and Radhakrishnan, P. (2001). Critical parameters influencing the quality of prototypes in fused deposition modelling. *Journal of Materials Processing Technology*, 118(1–3):385 – 388.

[6] Babur, O., Alper, O., and Erhan, D. (2010). Influence of injection parameters and mold materials on mechanical properties of abs in plastic injec-

tion moulding. *International Communications in Heat and Mass Transfer*, 37(1):1359–1365.

[7] Bagchi, T. P. (2003). Multiobjective Robust Design by Genetic Algorithms. *Materials and Manufacturing Processes*, 18(3):341–354.

[8] Baraskar, S. S., Banwait, S. S., and Laroiya, S. C. (2013). Multiobjective optimization of electrical discharge machining process using a hybrid method. *Materials and Manufacturing Processes*, 28(4):348–354.

[9] Bellehumeur, C., Li, L., Sun, Q., and Gu, P. (2004). Modeling of bond formation between polymer filaments in the fused deposition modeling process. *Journal of Manufacturing Processes*, 6(2):170–178.

[10] Bellini, A. and Güçeri, S. (2003). Mechanical characterization of parts fabricated using fused deposition modeling. *Rapid Prototyping Journal*, 9(4):252–264.

[11] Bellini, A., Shor, L., and Guceri, S. I. (2005). New developments in fused deposition modeling of ceramics. *Rapid Prototyping Journal*, 11(4):214–220.

[12] Brajlih, T., Valentan, B., Balic, J., and Drstvensek, I. (2011). Speed and accuracy evaluation of additive manufacturing machines. *Rapid Prototyping Journal*, 17(1):64–75.

[13] Byun, H. S. and Lee, K. H. (2005). Determination of optimal build direction in rapid prototyping with variable slicing. *The International Journal of Advanced Manufacturing Technology*, 28(3-4):307–313.

[14] Cheng, W., Fuh, J., Nee, A., Wong, Y., Loh, H., and Miyazawa, T. (1995). Multi-objective optimization of part building orientation in stereolithography. *Rapid Prototyping Journal*, 1(4):12–23.

[15] Chhabra, M. and Singh, R. (2011). Rapid casting solutions: A review. *Rapid Prototyping Journal*, 17(5):328–350.

[16] Chockalingam, K., Jawahar, N., Ramanathan, K., and Banerjee, P. (2006). Optimization of stereolithography process parameters for part strength using design of experiments. *Internatioanl Journal of Advanced Manufacturing Technology*, 29(1):79–88.

[17] Choi, S. and Cheung, H. (2007). Multi-material virtual prototyping for product development and biomedical engineering. *Computers in Industry*, 58(5):438–452.

[18] Chou, K. and Zhang, Y. (2008). A parametric study of part distortion in fused deposition modeling using three dimensional element analysis. *Proceedings of the Institution of Mechanical Engineers, Part B: Journal of Engineering Manufacture*, 222(1):959–967.

[19] Chua, C. K., Teh, S. H., and Gay, R. K. L. (1999). Rapid prototyping versus virtual prototyping in product design and manufacturing. *The International Journal of Advanced Manufacturing Technology*, 15(8):597–603.

[20] Comsol (2013). User guide version 4.3b.

[21] Dearn, K., Hoskins, T., Petrov, D., Reynolds, S., and Banks, R. (2013). Applications of dry film lubricants for polymer gears. *Wear*, 298-299(1-12):99–108.

[22] Deb, K. (2002). *Multi Objective Optimization using Evolutionay Algorithms*. John Wiley and Sons, Singapore.

[23] Deb, K. and Pratap, A. (2002). A fast and elitist multiobjective genetic algorithm: NSGA-II. *Evolutionary Computation, IEEE Transactions on,*, 6(2):182–197.

[24] Deb, K. and Saxena, D. K. (2005). On finding pareto-optimal solutions through dimensionality reduction for certain large-dimensional multi-objective optimization problems. Technical report, Indian Institute of Technology, Kanpur.

[25] Deb, K., Sundar, J., Udaya Bhaskara Rao, N., and Chaudhuri, S. (2006). Reference Point Based Multi-objective Optimization Using Evolutionary Algorithms. In *International Journal of Computational Intelligence Research*, pages 635–642. Springer-Verlag.

[26] Durgun, I. and Ertan, R. (2014). Experimental investigation of FDM process for improvement of mechanical properties and production cost. *Rapid Prototyping Journal*, 20(3):228–235.

[27] Equbal, A., Sood, A. K., Toppo, V., Ohdar, R. K., and Mahapatra, S. S. (2010). Prediction and analysis of sliding wear performance of fused deposition modelling-processed ABS plastic parts. *Proceedings of the Institution of Mechanical Engineers, Part J: Journal of Engineering Tribology*, 224(12):1261–1271.

[28] Es-Said, O. S., Foyos, J., Noorani, R., Mendelson, M., Marloth, R., and Pregger, B. (2000). Effect of layer orientation on mechanical properties of rapid prototyped samples. *Materials and Manufacturing Processes*, 15(1):107–122.

[29] Franklin, S. (2001). Wear experiments with selected engineering polymers and polymer composites under dry reciprocating sliding conditions. *Wear*, 251(1-12):1591–1598.

[30] Frenkel, F. (1945). Viscous flow of crystalline bodies under the action of surface tension. *Journal of Physics*, 9(1):385–395.

[31] Galantucci, L., Lavecchia, F., and Percoco, G. (2008). Study of compression

properties of topologically optimized fdm made structured parts. *CIRP Annals - Manufacturing Technology*, 57(1):243–246.

[32] Gibson, I., Rosen, D. W., and Stucker, B. (2010). *Additive Manufacturing Technologies:Rapid Prototyping to Direct Digital Manufacturing*. Springer, New York, USA.

[33] Gill, S. S. and Kaplas, M. (2009). Comparative study of 3d printing technologies for rapid casting of aluminium alloy. *Materials and Manufacturing Processes*, 24(12):1405–1411.

[34] Goldberg, D. E. (1989). *Genetic algorithms in search, optimization, and machine learning*. Addison-Wesley, United Kingdom.

[35] Iftikhar, A., Khan, M., Alam, K., Imran Jaffery, S. H., Ali, L., Ayaz, Y., and Khan, A. (2013). Turbine blade manufacturing through rapid tooling (rt) process and its quality inspection. *Materials and Manufacturing Processes*, 28(5):534–538.

[36] Ippolito, R., Iuliano, L., and Gatto, A. (1995). Benchmarking of rapid prototyping techniques in terms of dimensional accuracy and surface finish. *CIRP Annals - Manufacturing Technology*, 44(1):157–160.

[37] James, M. M. (2006). *Engineering Plastics Handbook*. McGraw-Hill, New York.

[38] Jia, B. B., Li, T.-S., Liu, X. J., and Cong, P. H. (2007). Tribological behaviors of several polymer–polymer sliding combinations under dry friction and oil-lubricated conditions. *Wear*, 262(11-12):1353–1359.

[39] Kanagarajan, D., Karthikeyan, R., Palanikumar, K., and Davim, J. P. (2007). Optimization of electrical discharge machining characteristics of WC/Co com-

posites using non-dominated sorting genetic algorithm (NSGA-II). *The International Journal of Advanced Manufacturing Technology*, 36(11-12):1124–1132.

[40] Karunakaran, K. P., Vivekananda, P. S., Sanjay, J. J., Bhadauria, P., and Pandey, A. (2000). Rapid prototyping of metallic parts and moulds. *Journal of Materials Processing Technology*, 105(3):371 – 381.

[41] Kirk-Othmer (2004). *Encyclopedia of Chemical Technology*. John Wiley and Sons, New York.

[42] Kondayya, D. and Gopala Krishna, A. (2012). An integrated evolutionary approach for modelling and optimization of laser beam cutting process. *The International Journal of Advanced Manufacturing Technology*, 65(1-4):259–274.

[43] Krause, F., Ciesla, M., Stiel, C., and Ulbrich, A. (1997). Enhanced Rapid Prototyping for Faster Product Development Processes. *CIRP Annals - Manufacturing Technology*, 46(1):93–96.

[44] Kruth, J., Leu, M., and Nakagawa, T. (1998). Progress in additive manufacturing and rapid prototyping. *CIRP Annals - Manufacturing Technology*, 47(2):525–540.

[45] Kulkarni, P. and Dutta, D. (1999). Deposition strategies and resulting part stiffnesses in fused deposition modeling. *Journal of Manufacturing Science and Engineering*, 121(2):93–103.

[46] Kulkarni, P. M., Anne, and Dutta, D. (2000). A review of process planning techniques in layered manufacturing. *Rapid Prototyping Journal*, 6(1):18–35.

[47] Kumar, P., Ahuja, I., and Singh, R. (2012). Application of fusion deposition modelling for rapid investment casting - a review. *International Journal of Materials Engineering Innovation*, 3(3):204–227.

[48] Lan, H. (2009). Web-based rapid prototyping and manufacturing systems: A review. *Computers in Industry*, 60(9):643–656.

[49] Lee, B., Abdullah, J., and Khan, Z. (2005). Optimization of rapid prototyping parameters for production of flexible ABS object. *Journal of Materials Processing Technology*, 169(1):54–61.

[50] Levy, G. N., Schindel, R., and Kruth, J. (2003). Rapid manufacturing and rapid tooling with layer manufacturing (lm) technologies, state of the art and future perspectives. *CIRP Annals - Manufacturing Technology*, 52(2):589–609.

[51] Li, L. and Sun, Q. (2002). Investigation of bond formation in fdm process. In *Symp., Austin, TX*, pages 400–407.

[52] Liao, H. T. and Shie, J. R. (2007). Optimization on selective laser sintering of metallic powder via design of experiments method. *Rapid Prototyping Journal*, 13(3):156–162.

[53] Liu, Q., Leu, M., and Schmitt, S. (2005). International Journal of Advanced Manufacturing Technology. *International Journal of Advanced Manufacturing Technology*, 29(1):317–335.

[54] Masood, S. and Song, W. (2004). Development of new metal/polymer materials for rapid tooling using Fused deposition modelling. *Materials and Design*, 25(7):587–594.

[55] Minitab (2013). User guide version 14.

[56] Mitra, K., Majumder, S., and Runkana, V. (2009). Multiobjective pareto optimization of an industrial straight grate Iron ore induration process using an evolutionary algorithm. *Materials and Manufacturing Processes*, 24(3):331–342.

[57] Montgomery, D. (2003). *Design and Analysis of Experiments*. John Wiley and Sons, Singapore.

[58] Munguía, J., Ciurana, J. D., and Riba, C. (2008). Pursuing successful rapid manufacturing: a users' best-practices approach. *Rapid Prototyping Journal*, 14(3):173–179.

[59] Nassif, N., Kajl, S., and Sabourin, R. (2005). Optimization of HVAC control system strategy using two-objective genetic algorithm. *HVAC&R Research*, 11(3):459–486.

[60] Noorani, R. (2005). *Rapid Prototyping-Principles and Application*. John Wiley and Sons, New Jersey, USA.

[61] Onuh, S. O. and Yusuf, Y. Y. (1999). Rapid prototyping technology: applications and benefits for rapid product development. *Journal of Intelligent Manufacturing*, 10(3-4):301–311.

[62] Oxman, N. (2011). Variable property rapid prototyping. *Virtual and Physical Prototyping*, 6(1):3–31.

[63] Pandey, P. M., Thrimurthulu, K., and Reddy, N. V. (2004). Optimal part deposition orientation in FDM by using a multicriteria genetic algorithm. *International Journal of Production Research*, 42(19):4069–4089.

[64] Pedro, V. V., Jorge, L. F., Antonio, M. B., and Neto, R. J. (2006). Tribological behaviour of epoxy based composites for rapid tooling. *Wear*, 260(1):30–39.

[65] Pereira, A., Perez, J., Dieguez, J., Pelaez, G., and Ares, J. (2008). Design and manufacture of casting pattern plates by rapid tooling. *Archives of Materials Science*, 29(1-2):525–540.

[66] Pérez, C. (2002). Analysis of the surface roughness and dimensional accuracy capability of fused deposition modelling processes. *International Journal of Production Research*, 40(12):2865–2881.

[67] Pham, D. T. and Dimov, S. S. (2001). *Rapid Manufacturing: The technologies and applications of rapid prototyping and rapid tooling*. Springer, United Kingdom.

[68] Pokluda, O., Bellehumeur, C., and Vlachopoulos, J. (1997). Modification of frenkel's model for sintering. *American Institute of Chemical Engineers Journal*, 43(12):3253–3256.

[69] Ramesh, C. and Srinivas, C. (2009). Friction and wear behavior of laser-sintered iron–silicon carbide composites. *Journal of Materials Processing Technology*, 209(14):5429–5436.

[70] Ramesh, C., Srinivas, C., and Channabasappa, B. (2009). Abrasive wear behaviour of laser sintered iron–SiC composites. *Wear*, 267(11):1777–1783.

[71] Reddy, B. V., Reddy, N. V., and Ghosh, A. (2007). Fused deposition modelling using direct extrusion. *Virtual and Physical Prototyping*, 2(1):51–60.

[72] Regalla, S. P. (2010). *Computer Aided Analysis and Design*. IK International Publishers, New Delhi.

[73] Robert, O. E. (2000). *Polymer Science And Technology*. CRC Press, New York.

[74] Rochus, P., Plesseria, J., Van Elsen, M., Kruth, J., Carrus, R., and Dormal, T. (2007). New applications of rapid prototyping and rapid manufacturing (rp/rm) technologies for space instrumentation. *Acta Astronautica*, 61(1-6):352–359.

[75] Rodríguez, J. F. (2000). Characterization of the mesostructure of fused-deposition acrylonitrile-butadiene-styrene materials. *Rapid Prototyping Journal*, 6(3):175–185.

[76] Rodríguez, J. F. (2001). Mechanical behavior of acrylonitrile butadiene styrene (abs) fused deposition materials. experimental investigation. *Rapid Prototyping Journal*, 7(3):148–158.

[77] Rodríguez, J. F., Thomas, J. P., and Renaud, J. E. (2003). Mechanical behavior of acrylonitrile butadiene styrene fused deposition materials modeling. *Rapid Prototyping Journal*, 9(4):219–230.

[78] Rosochowski, A. and Matuszak, A. (2000). Rapid tooling: the state of the art. *Journal of Materials Processing Technology*, 106(1-3):191–198.

[79] Rymuza, Z., Kusznierewicz, Z., Solarski, T., Kwacz, M., Chizhik, S., and Goldade, A. (2000). Static friction and adhesion in polymer–polymer microbearings. *Wear*, 238(1):56 – 69.

[80] Santos, E. C., Shiomi, M., Osakada, K., and Laoui, T. (2006). Rapid manufacturing of metal components by laser forming. *International Journal of Machine Tools and Manufacture*, 46(12-13):1459–1468.

[81] Singh, R. (2011). An overview of three dimensional printing for casting applications. *International Journal of Precision Technology*, 2(1):93–116.

[82] Singh, R. (2012). Mathematical modeling for surface hardness in investment casting applications. *Journal of Mechanical Science and Technology*, 26(11):3625–3629.

[83] Singh, R. (2013). Some investigations for small sized product fabrication with fdm for plastic components. *Rapid Prototyping Journal*, 19(1):58–63.

[84] Singhal, S., Jain, P. K., Pandey, P. M., and Nagpal, A. (2009). Optimum part deposition orientation for multiple objectives in SL and SLS prototyping. *International Journal of Production Research*, 47(22):6375–6396.

[85] Smith, W. F., Hashemi, J., and Prakash, R. (2008). *Materials Science and Engineering*. McGraw-Hill, New Delhi.

[86] SolidWorks, D. S. (2009). Solidworks user guide version 1.1.

[87] Sood, A. K., Equbal, A., Toppo, V., Ohdar, R., and Mahapatra, S. (2012a). An investigation on sliding wear of FDM built parts. *CIRP Journal of Manufacturing Science and Technology*, 5(1):48–54.

[88] Sood, A. K., Ohdar, R., and Mahapatra, S. (2009). Improving dimensional accuracy of Fused Deposition Modelling processed part using grey Taguchi method. *Materials & Design*, 30(10):4243–4252.

[89] Sood, A. K., Ohdar, R., and Mahapatra, S. (2010). Parametric appraisal of mechanical property of fused deposition modelling processed parts. *Materials & Design*, 31(1):287–295.

[90] Sood, A. K., Ohdar, R. K., and Mahapatra, S. S. (2012b). Experimental investigation and empirical modelling of FDM process for compressive strength improvement. *Journal of Advanced Research*, 3(1):81–90.

[91] Sreenathbabu, A. and Karunakaran, K. P. (2006). Hybrid adaptive layer manufacturing: An intelligent art of direct metal rapid tooling process. *Robotics and Computer-Integrated Manufacturing*, 22(2):113 – 123.

[92] Srinivas, N. and Deb, K. (1994). Muiltiobjective optimization using nondominated sorting in genetic algorithms. *Evolutionary Computation*, 2(3):221–248.

[93] Stat-Ease, I. (2010). Design expert user guide version 8.

[94] Stratasys (2010). Fused deposition modeling uprint user guide version 1.1.

[95] Stuart, B. B., Kwon, H. K., and Anand, L. (1989). An internal variable

constitutive model for hot working of metals. *International Journal of Plasticity*, 5(1):95–130.

[96] Subashini, G. and Bhuvaneswari, M. C. (2012). Comparison of multi-objective evolutionary approaches for task scheduling in distributed computing systems. *Sadhana*, 37(6):675–694.

[97] Sun, Q., Rizvi, G. M., Bellehumeur, C. T., and Gu, P. (2008). Effect of processing conditions on the bonding quality of fdm polymer filaments. *Rapid Prototyping Journal*, 14(2):72–80.

[98] Tong, K., Joshi, S., and Amine Lehtihet, E. (2008). Error compensation for fused deposition modeling (fdm) machine by correcting slice files. *Rapid Prototyping Journal*, 14(1):4–14.

[99] Too, M. H., Leong, K. F., Chua, C. K., Du, Z. H., Yang, S. F., Cheah, C. M., and Ho, S. L. (2002). Investigation of 3d non-random porous structures by fused deposition modelling. *The International Journal of Advanced Manufacturing Technology*, 19(3):217–223.

[100] Tromans, G. (2003). *Developments in Rapid Casting*. Professional Engineering Publishing, London, UK.

[101] Vaidyanathan, R., Walish, J., Lombardi, J. L., Kasichainula, S., Calvert, P., and Cooper, K. C. (2000). The extrusion freeforming of functional ceramic prototypes. *JOM*, 52(12):34–37.

[102] Venkata Rao, R. (2011). *Advanced Modeling and Optimization of Manufacturing Processes*. Springer-Verlag, London.

[103] Wang, S., Makinouchi, A., Okamoto, M., Kotaka, T., and Nagagawa, T. (1999). Viscoplastic modelling of abs material under high strain rate uniaxial elongation deformation. *Journal of Materials Science*, 34(1):5871–5878.

[104] Wang, S., Miranda, A. G., and Shih, C. (2010). A study of investment casting with plastic patterns. *Materials and Manufacturing Processes*, 25(12):1482–1488.

[105] Wang, T., Xi, J., and Jin, Y. (2006). A model research for prototype warp deformation in the FDM process. *The International Journal of Advanced Manufacturing Technology*, 33(11-12):1087–1096.

[106] Wiedemann, B. and Jantzen, H. (1999). Strategies and applications for rapid product and process development in Daimler-Benz AG. *Computers in Industry*, 39(1):11–25.

[107] Yan, Y., Li, S., Zhang, R., Lin, F., Wu, R., Lu, Q., Xiong, Z., and Wang, X. (2009). Rapid prototyping and manufacturing technology: Principle, representative technics, applications, and development trends. *Tsinghua Science and Technology*, 14(6):1–12.

[108] Zeng, W., Lin, F., Shi, T., Zhang, R., Nian, Y., and Zhou, T. (2008). Fused deposition modelling of an auricle framework for microtia reconstruction based on CT images. *Rapid Prototyping Journal*, 5(14):280–284.

[109] Zhang, Y. and Chou, K. (2006). Three-dimensional finite element analysis simulations of the fused deposition modelling process. *Proceedings of the Institution of Mechanical Engineers, Part B: Journal of Engineering Manufacture*, 220(10):1663–1671.

Appendix A

Simulated ultimate tensile load of the tensile test specimen

Table A.1 Simulated ultimate tensile load of the tensile test specimen

S. No	Dimensionless time t	Ultimate Tensile Load	S. No	Dimensionless time t	Ultimate Tensile Load
1	0	0	19	0.15	0.34
2	0	0.02	20	0.16	0.36
3	0.01	0.04	21	0.18	0.38
4	0.01	0.06	22	0.19	0.4
5	0.02	0.08	23	0.21	0.41
6	0.02	0.1	24	0.22	0.43
7	0.03	0.11	25	0.24	0.45
8	0.04	0.13	26	0.26	0.47
9	0.04	0.15	27	0.27	0.49
10	0.05	0.17	28	0.29	0.51
11	0.06	0.19	29	0.31	0.53
12	0.07	0.21	30	0.33	0.54
13	0.08	0.23	31	0.35	0.56
14	0.09	0.25	32	0.37	0.58
15	0.1	0.27	33	0.39	0.6
16	0.11	0.28	34	0.41	0.62
17	0.12	0.3	35	0.43	0.63
18	0.14	0.32	36	0.45	0.65

continued ...

... continued

S. No	Dimensionless time t	Ultimate Tensile Load	S. No	Dimensionless time t	Ultimate Tensile Load
37	0.48	0.67	66	1.37	1.15
38	0.5	0.69	67	1.41	1.17
39	0.52	0.71	68	1.45	1.18
40	0.55	0.72	69	1.49	1.2
41	0.57	0.74	70	1.53	1.21
42	0.6	0.76	71	1.57	1.22
43	0.63	0.78	72	1.61	1.24
44	0.65	0.79	73	1.66	1.25
45	0.68	0.81	74	1.7	1.27
46	0.71	0.83	75	1.74	1.28
47	0.73	0.84	76	1.79	1.3
48	0.76	0.86	77	1.83	1.31
49	0.79	0.88	78	1.88	1.32
50	0.82	0.89	79	1.92	1.34
51	0.85	0.91	80	1.97	1.35
52	0.88	0.93	81	2.01	1.36
53	0.91	0.94	82	2.06	1.38
54	0.95	0.96	83	2.11	1.39
55	0.98	0.98	84	2.16	1.4
56	1.01	0.99	85	2.2	1.42
57	1.05	1.01	86	2.25	1.43
58	1.08	1.03	87	2.3	1.44
59	1.11	1.04	88	2.35	1.45
60	1.15	1.06	89	2.4	1.47
61	1.19	1.07	90	2.45	1.48
62	1.22	1.09	91	2.51	1.49
63	1.26	1.1	92	2.56	1.5
64	1.3	1.12	93	2.61	1.51
65	1.33	1.14	94	2.67	1.52

continued ...

. . . continued

S. No	Dimensionless time t	Ultimate Tensile Load	S. No	Dimensionless time t	Ultimate Tensile Load
95	2.72	1.54	123	4.44	1.79
96	2.77	1.55	124	4.51	1.79
97	2.83	1.56	125	4.58	1.8
98	2.88	1.57	126	4.65	1.8
99	2.94	1.58	127	4.72	1.81
100	3	1.59	128	4.8	1.82
101	3.05	1.6	129	4.87	1.82
102	3.11	1.61	130	4.94	1.83
103	3.17	1.62	131	5.01	1.83
104	3.23	1.63	132	5.09	1.84
105	3.29	1.64	133	5.16	1.84
106	3.35	1.65	134	5.24	1.85
107	3.41	1.66	135	5.31	1.85
108	3.47	1.67	136	5.46	1.86
109	3.53	1.68	137	5.54	1.86
110	3.59	1.69	138	5.62	1.87
111	3.65	1.69	139	5.77	1.87
112	3.72	1.7	140	5.85	1.88
113	3.78	1.71	141	5.93	1.88
114	3.84	1.72	142	6.01	1.88
115	3.91	1.73	143	6.09	1.88
116	3.97	1.74	144	6.17	1.89
117	4.04	1.74	145	6.25	1.89
118	4.11	1.75	146	6.33	1.89
119	4.17	1.76	147	6.5	1.89
120	4.24	1.76	148	6.58	1.9
121	4.31	1.77	149	6.67	1.9
122	4.38	1.78	150	6.75	1.9

Appendix B

ABS Properties

Mechanical Properties

Ultimate Tensile Strength:	33 MPa
Yield Tensile Strength:	8 MPa
Tensile Modulus:	2200 MPa
Tensile Elongation at Break:	6 %
Tensile Elongation at Yield:	2 %
Notched IZOD Impact:	106 J/m
Rockwell Hardness:	109.5

Thermal Properties

Heat Deflection:	96°C
Glass Transition Temperature (Tg):	108°C
Coefficient of Thermal Expansion:	$8.82 \text{x} 10^{-5}$ mm/mm/°C

Other Properties

Specific Gravity:	1.04
Dielectric Constant:	2.3-2.85 x 10^6 Hz
Dielectric Strength:	16 kV/mm

List of publications published from this thesis

List of Journal publications:

1. **Pavan Kumar Gurrala** and Srinivasa Prakash Regalla. (2014). Multi-objective optimization of strength and volumetric shrinkage of FDM parts. *Virtual and Physical Prototyping*, 9(2):127-138.

2. **Pavan Kumar Gurrala** and Srinivasa Prakash Regalla. (2014). Part strength evolution with bonding between filaments in FDM. *Virtual and Physical Prototyping*, 9(3):141-149.

3. **Pavan Kumar Gurrala** and Srinivasa Prakash Regalla. (2012). Optimization of support material and build time in fused deposition modeling (FDM). *Applied Mechanics and Materials*, 110-116:2245-2251.

4. **Pavan Kumar Gurrala** and Srinivasa Prakash Regalla. (2014). DOE based parametric study of volumetric change of FDM parts. *Procedia Material Science*, 6:354-360.

5. **Pavan Kumar Gurrala** and Srinivasa Prakash Regalla. DOE based experimental study of the effect of build orientation on tribological properties of ABS polymer parts. *Under Review.*

List of Conference publications:

1. **Pavan Kumar Gurrala** and Srinivasa Prakash Regalla. Friction and wear behavior of ABS polymer parts made by Fused Deposition Modeling (FDM). International Conference on Advances of Tribology *(ICAT)* , $21-24^{th}$ February 2014, NIT Calicut, Kerala, India. *(Won the best paper award).*

2. **Pavan Kumar Gurrala** and Srinivasa Prakash Regalla. Prediction of neck growth due to inter and intra layer bonding for high strength parts in additive manufacturing, 4^{th} International and 25^{th} All India Manufacturing Technology, Design and Research Conference *(AIMTDR)* , $14-16^{th}$ December 2012, Jadavpur University, Kolkata, India.

3. **Pavan Kumar Gurrala** and Srinivasa Prakash Regalla. Optimization of support material and build time in Fused Deposition Modeling (FDM) using Central Composite Design Methodology. 26^{th} International Conference of CAD / CAM, Robotics and Factories of Future *(CARS & FoF)* , $26 - 28^{th}$ July 2011, Kuala Lumpur, Malaysia.

Biography of the Candidate

Pavan Kumar Gurrala obtained ME from BITS Pilani, Pilani campus in Design Engineering and he is currently pursuing Ph.D in the department of Mechanical Engineering. He is also working as a Lecturer in the Mechanical Engineering department at BITS Pilani, Hyderabad Campus. His research interests include 3D Printing/Additive Manufacturing, Design of Experiments and optimization.

Biography of the Supervisor

Srinivasa Prakash Regalla obtained Ph.D. from IIT Delhi in Mechanical Engineering and M.Tech. from IIT Kanpur in Manufacturing Science and Engineering. He is currently a Professor in the Mechanical Engineering department and Associate Dean of Work Integrated Learning Programmes at BITS Pilani, Hyderabad Campus. His current research areas include 3D Printing and Additive Manufacturing for engineering products as medical implants and prosthetics, sheet metal forming, micro-manufacturing, MEMS, advanced manufacturing processes for automobile vehicles.